Advancing Transportation Climate Vulnerability Assessment

Across Infrastructure and Travel Behavior

by

Rui Li

A Dissertation Presented in Partial Fulfillment
of the Requirements for the Degree
Doctor of Philosophy

Approved July 2022 by the
Graduate Supervisory Committee:

Mikhail V. Chester, Chair
Ariane Middel
David M. Hondula
Ram Pendyala

ARIZONA STATE UNIVERSITY

August 2022

ABSTRACT

Infrastructure systems are facing non-stationary challenges that stem from climate change and the increasingly complex interactions between the social, ecological, and technological systems (SETSs). It is crucial for transportation infrastructures—which enable residents to access opportunities and foster prosperity, quality of life, and social connections—to be resilient under these non-stationary challenges. Vulnerability assessment (VA) examines the potential consequences a system is likely to experience due to exposure to perturbation or stressors and lack of the capacity to adapt.

Post-fire debris flow and heat represent particularly challenging problems for infrastructure and users in the arid U.S. West. Post-fire debris flow, which is manifested with heat and drought, produces powerful runoff threatening physical transportation infrastructures. And heat waves have devastating health effects on transportation infrastructure users, including increased mortality rates. VA anticipates the potential consequences of these perturbations and enables infrastructure stakeholders to improve the system resilience. The current transportation climate VA—which only considers a single direct climate stressor on the infrastructure—falls short of addressing the wildfire and heat challenges. This work proposes advanced transportation climate VA methods to address the complex and multiple climate stressors and the vulnerability of infrastructure users. Two specific regions were chosen to carry out the progressive transportation climate VA: 1) the California transportation networks' vulnerability to post-fire debris flows, and 2) the transportation infrastructure user's vulnerability to heat exposure in Phoenix.

DEDICATION

I dedicate this dissertation to my mom, Yan.

Yan means Geese in Chinese.

As a daughter, I've wished countless times that she could be braver, flying out of the thorn cage that has trapped her.

As a daughter, I'm living a life that could have been hers.

ACKNOWLEDGEMENT

I want to express my gratitude to my advisor Dr. Mikhail Chester for the opportunities to work on the infrastructure resilience projects. I am grateful for Dr. David M. Hondula, Dr. Ariane Middel, and Dr. Jennifer K. Vanos for the comments and discussions on the personal heat exposure work. I am also thankful for Dr. Alysha M. Helmrich for great suggestions on the PhD life and proofreading my work.

This study was made possible through fundings received by the University of California Institute of Transportation Studies from the State of California via the Public Transportation Account and the Road Repair and Accountability Act of 2017 (UC-ITS-2020-38), United States National Science Foundation award CMMI-1635490 (A Simulation Platform to Enhance Infrastructure and Community Resilience to Extreme Heat Events), and CMMI-1942805 (CAREER: Human Thermal Exposure in Cities - Novel Sensing and Modeling to Build Heat-Resilience).

Last but not least, I would like to thank my two cats for accompanying me through the pandemic.

TABLE OF CONTENTS

Page

CHAPTER Page

LIST OF TABLES

Table Page

LIST OF FIGURES

Figure Page

LIST OF EQUATIONS

CHAPTER 1

INTRODUCTION

1.1. Background and Motivation

1.1.1. Out of the Envelope Climate Stress and Infrastructure Vulnerability

Transportation infrastructure was designed with a focus on functionality and safety, which is rather the infrastructure would try to avoid failure (Kim et al., 2017; Meyer, 2008). The infrastructure's climate interface, such as the location of the infrastructure, the drainage, for a long time, is designed based on 'design standards' (Meyer, 2008), or the text-book envelope of design (Hollnagel et al., 2006). The design standards, which are established to provide guidance to the engineers, have been accepted by the community as 'safe and defensible' and usually address the historically observed climate perturbations, such as flood, earthquake, or wind speed (Meyer, 2008). However, those text-book envelopes fell short to cover the unexpected, and uncertain environmental change (Hollnagel et al., 2006; Meyer, 2008), such as wildfires, sea level rise, post-fire debris flow, and extreme heat events etc. Climate change is expected to shift local weather patterns and increase the extreme weather events which fall out of the design standards or the text-book envelope (Hollnagel et al., 2006; Meyer, 2008).

While the traditional design codes do not consider the out of design envelope perturbations, vulnerability assessment could fill the gap by identifying the susceptibility and consequences when perturbation happens, and the system lacks the capacity to adapt. Vulnerability, defined as the 'propensity or predisposition to be adversely affected', encompasses elements such as 'susceptibility to harm' and 'lack of capacity to cope and

adapt' (Pörtner et al., 2022). Vulnerability assessment was widely used to estimate the risk of infrastructures, or a community's susceptibility to certain hazard/s. In Hollnagel (2009) the four cornerstones of resiliency (Figure 1.1), vulnerability assessment provides anticipations on the potential consequences of perturbations. The technological systems vulnerability assessment stems from critical infrastructure identification (Berdica, 2002; Church et al., 2004; Ibrahim et al., 2011; Taylor, 2017). While 'susceptibility to harm' is always presented in the vulnerability definition, there is general recognition that vulnerability consists of the exposure and sensitivity to climatic perturbations, and the resilient capability to deal with these perturbations (Adger, 2006; Ford et al., 2018; Pörtner et al., 2022). As anthropogenic climate change is expected to increase the intensity and frequency of these extreme climate events, vulnerability assessment addresses the exposure, susceptibility, and the adaptability of the system when outside of performance envelope shocks happen and provide opportunities to build resilience.

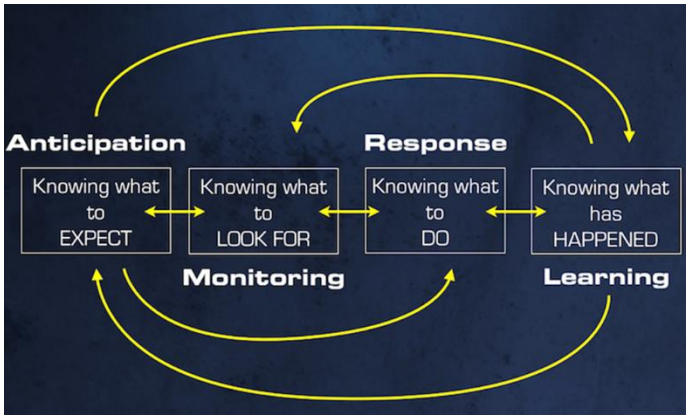

Figure 1.1. Four Cornerstones of Resiliency (Redraw from Hollnagel, 2009)

1.1.2. Vulnerability Assessment for Transportation Infrastructures.

Transportation infrastructure vulnerability assessment studies have two distinct traditions: the topological vulnerability analysis and the system-based serviceability loss from perturbation (Adger, 2006; Mattsson & Jenelius, 2015). The topological vulnerability assessments use the abstract network to present the transportation system, and the vulnerability is measured as the change of network characteristics, such as the centrality, or connectivity, before and after the perturbation (Grubesic et al., 2008; Mattsson & Jenelius, 2015; Murray et al., 2008). The system-based vulnerability assesses the accessibility lost due to the perturbation, which requires prediction of travelers' response to the disruption (Mattsson & Jenelius, 2015). While transportation climate vulnerability assessments focused on the external threats from adverse weather and climate disasters on infrastructure, few attempted to address the development of the disruptions, especially estimating the probability of disruptions (Mattsson & Jenelius 2015). More climate perturbations need to be studied, and the vulnerability assessment framework for transportation infrastructures should couple human-environment systems.

1.1.3. Transportation Infrastructure Vulnerability from Post-fire Debris Flow

In the arid U.S. west, wildfires and heat represent particularly challenging problems for infrastructure and users (Pierce et al., 2018a; Stocker et al., 2014; Westerling et al., 2011). A wildfire can cause billions of dollars in property damage and life lost (Kean et al., 2019; Molly Mowery et al., 2019). The direct damage from wildfires to roadways is unlikely since local transportation authority frequently practice vegetation control—such as prescribed fire or carry out vegetation management near the road—to prevent wildfires from spreading to infrastructure (Minnesota Department of

Transportation, 2021). However, wildfires cause extreme changes in the hydrologic, hydraulic, and geomorphologic characteristics in the burned watersheds (e.g., Cannon et al., 2008; Kean et al., 2019). These changes lead to the drastic increase (i.e., 3 to 90 times) in the runoff volume and post-fire debris flow in and downstream of the burned basin (e.g., Elliott et al., 2004; Verdin et al., 2012). The post-fire debris flow risk can last for several years and constantly threaten the roadway infrastructures—where streams cut through—until the burned basin returns to pre-fire conditions (Fraser et al., 2020; Valentin & Stormont, 2019). It typically takes about five years for a watershed to return to its pre-fire conditions (Ice et al., 2004) and common precipitation events (defined as return periods of up to 10 years) are capable of producing 1000-year floods after an intense fire (Gartner et al., 2008).

While transportation infrastructure in general has fire mitigation strategies such as use prescribed fire to clean up the fuel (vegetation) near the infrastructures, post-fire debris flow produces greater damage since the location where post fire debris flow happens can be outside of the burned area, and can last longer. Residents and stakeholders are in general prepared for fires but not the post-fire debris flood. The existing transportation climate vulnerability assessment, which overlays the climate stressor map on top of the infrastructure network, falls short to address the post-fire debris flow problem.

1.1.4. Transportation Infrastructure Users Vulnerability from Extreme Heat

Environmental heat has a direct impact on human health, especially when people carry out outdoor activities. Outdoor trips may significantly increase traveler's heat

exposure in hot climates because they occur simultaneously with physical exertion (Hoehne et al., 2018; Karner et al., 2015). Personal preference for walking and biking trips is a function of individual attitudes, preference, transportation network connectivity, and the available transportation infrastructure (Karner et al., 2015; Saelens et al., 2003). The outdoor build environment on a different route influences the metabolic performance, core temperature, and heat exposure for city-dwellers (Xiao et al., 2020). Transportation infrastructures such as asphalt and concrete pavement, and parking lots are associated with high air temperature (Aniello et al., 1995; Markolf et al., 2019; Milošević et al., 2017). However, replacing the impervious transportation infrastructure surfaces with a high ratio of irradiance reflected to absorbed (albedo) or green parking surface can reduce the micro environmental temperature (Onishi et al., 2010; Qin & Hiller, 2014). Despite the inherent connection between microclimate around the transportation infrastructure, residents' travel behavior, and the personal heat exposure, the state-of-art human heat vulnerability assessment still focused on the fixed-point measurements of outdoor temperature and little is known about the real-time thermal discomfort people experience in their daily life (Karner et al., 2015). And heat waves have devastating health effects, including increasing mortality rates (Anderson & Bell, 2011; Kovats & Hajat, 2008). And cities have been motivated to deploy mitigation strategies—such as community awareness program, establishing networks of cooled public spaces, and increase tree planting (Mesa, 2014; Phoenix, 2021; Tempe, 2019). Yet, how to balance the limited budget and heat mitigation effort is still not answered.

1.2. Research Question and Objectives

Transportation vulnerability assessment has developed from the pure technological system (TS) centered on critical subset identification, to ecological and technological systems (ETSs) linked perturbation and consequences prediction. As one of the cornerstones in the resiliency, transportation climate vulnerability assessment helped stakeholders to identify the hierarchy of vulnerable sections and the consequences from climate perturbations, and to implement mitigation strategies to increase SETSs resilience.

The wildfire and heat are challenging climate problems for the transportation infrastructure and urban residents using the infrastructure. Although direct damage from wildfire on the roadway is unlikely, fire tends to change the watershed features and combined with the precipitation generate powerful debris-flow that put the roadway at risk, even those outside of the burned scar. Higher temperature can cause pavement to soften and expand, but the most paramount threat is on the infrastructure users who may have life-threatening health problems from excessive heat exposure. The current transportation climate vulnerability assessment is insufficient to address the most crucial problem that wildfire and heat pose. Here, I propose to advance the transportation climate vulnerability assessment approaches, by including the social system into the study. The approach would expand the climate perturbation by considering the complex mechanisms of wildfire, precipitation, and other environmental mechanisms. It would also address the delicate and complex travel behavior transportation infrastructures posed to personal heat exposure. The advanced transportation climate vulnerability assessment will serve to address the following problems and research questions:

- Transportation climate vulnerability is often framed as a spatial coincidence of a future hazard with today's infrastructure. Where hazards exist or increase there is a tendency to say that the assets are vulnerable. But the infrastructure is robust, and their failure processes are complex. How do we understand the vulnerability of roadways to wildfires and post-fire debris flows considering fire risk, geology, vegetation, hydrology, future climate conditions, and infrastructure configuration?
- Our understanding of personal extreme heat exposure is often based on a home address. Yet how people interact with their environments is complex, involving travel activities, air-conditioned spaces, and exposure to shade and reflective heat surfaces. Can we use advanced meso-scale travel simulations to provide new insights into traveler exposure considering travel behavior and infrastructure form?
- How do strategies to protect travelers change when heat exposure considers travel behavior and urban form?

Two specific regions were chosen to carry out the advanced transportation climate vulnerability assessment: 1) the California transportation networks' vulnerability to post-fire debris flows, and 2) the transportation infrastructure user's vulnerability to heat exposure in Phoenix.

CHAPTER 2

VULNERABILITY OF CALIFORNIA ROADWAYS TO POST-WILDFIRE DEBRIS-FLOWS

2.1. Introduction

Characterizing the vulnerability of infrastructure to climate change represents an important new frontier in theory, research, and practice. Infrastructure systems—the human engineered structures that deliver basic and critical services, such as transportation, power, and water—are caught between design processes that largely emphasize historical weather and those that emphasize future climate uncertainty (Chester et al., 2020). As infrastructure managers are increasingly required to confront climate change in order to ensure the reliability of services into the future, new methods are needed for understanding risks and vulnerabilities, as well as adaptation options.

Wildfires represent a particularly challenging problem for infrastructure. Although their direct damaging of roadways is unlikely (MacArthur et al., 2012), wildfires tend to present as a concurrent hazard, manifesting with heat and drought, and producing powerful post-fire debris flows. These debris flows represent significant hazards for infrastructure in general, but areas where landslides, debris movement, and exacerbated water flows cut across roadways are particularly vulnerable. It typically takes about five years for a watershed to return to its pre-fire conditions (Ice et al., 2004) and common precipitation events (defined as return periods of up to 10 years) are capable of producing 1000-year floods after an intense fire (Gartner et al., 2008). However, few rigorous methods exist for exploring the relationships between climate change, wildfires,

post-fire debris flows, and transportation infrastructure. With climate forecasts generally showing that extreme events lead to significant and relatively fast changes, there is cause for an immediate examination into how our critical services (which are generally supported by long-lifetime infrastructure) are vulnerable, and what can be done to protect them.

When it comes to transportation and wildfires, work tends to focus on evacuation strategies and hazard mapping, and there are few efforts to understand post-fire flows risk and how that translates to roadway vulnerability. The evacuation literature is rich and has been pursued for decades. This includes evacuation order strategies (Cohn et al., 2006; Cova et al., 2013; Wolshon & Marchive, 2007) and logistics (i.e., Camp et al., 2013; Dijst et al., 2013; Morton et al., 2003). Several studies have established a precedent for more rigorous vulnerability assessments, with researchers noting the potential for increased landslides and loss of control systems (De Graff et al., 2015; MacDonald & Larsen, 2008; Wu, 2001). However, only one existing study that systematically assesses the relationships between fires, precipitation, geological and vegetative conditions, hydrology, and roadway infrastructure has been identified. Fraser et al. (2020) developed a model using Arizona's forested region to assess post-fire debris flow-risk to roadways. The study assessed how soil, topography, precipitation, current wildfire potential, watersheds, and hydrologic analyses effect roadway infrastructure, also considering the importance of various links in the network (betweenness centrality). Fraser et al.'s findings were confirmed as they showed high-risk assets where recent fires and subsequent post-fire debris flows and roadway washouts had occurred. However, the

work did not consider future climate change (and its fire and precipitation uncertainty). Furthermore, the study was conducted in a relatively small region, raising questions around how state or regional variations in geology, vegetation, hydrology, climate, and infrastructure may affect a large infrastructure system and an agency's prioritization for mediating risk.

In contrast, for our study we developed a roadway vulnerability assessment method for the entire state of California, considering climate change (and its uncertainty). In this way, several important methodological advancements were made over the approaches developed by (Fraser et al., 2020). First, the inclusion of climate forecasts (for wildfires and precipitation) required assessment of current and future risk using consistent methods. Second, state-wide assessments within California presented several major computational challenges in terms of commensurate data inputs (data are sometimes regionalized and inconsistent) and scalability of computation. Third, because the relationship between post-fire flows and roadways is complicated, our study required new methods. Flows are expected to impact roads following stream paths so new hydrologic methods were developed to characterize how individual roadway links (as they intersect stream paths) are vulnerable. These methods embrace the uncertainty inherent in the work, in terms of climate change scenarios, wildfires, precipitation, and post-fire debris flows.

In the following sections we describe our data processing, methodological assessments, and results. We conclude with a discussion focused on the significance of the work for decisionmakers, emphasizing the need to help infrastructure managers

prioritize limited resources towards high-risk areas. The code and all documentation we used are available to the general public on our project website: wildfires.resilientinfrastructure.org.

2.2. Methodology

Transportation vulnerability is mostly defined by two factors: the risk of hazardous events and consequences of the system when hazards happen (Taylor, 2017). Here, the hazardous event is the post-fire debris flow—which is measured as the frequency (recurrence) of the 15-min rainfall threshold (i.e. TH_{i15}) to result in a 90% chance of post-fire debris movement. The consequences are measured by loss of critical roadways. The criticality of roadways are characterized as the betweenness centrality. Climate change is expected to worsen the wildfire and polarize the extreme precipitation intensity in California (Pierce et al., 2018a; Westerling, 2018). Since post-fire debris flow is a combined hazard related to both fire and rainfall, evaluating transportation vulnerability under climate change scenarios could help stakeholders identify changing future hotspots that may be overlooked by present-day analyses. Therefore, a novel approach was developed to address the debris risk and infrastructure network connectivity through a state-of-the-art post-fire debris model, downscaled climate projections, and network criticality assessment (Figure 2.1).

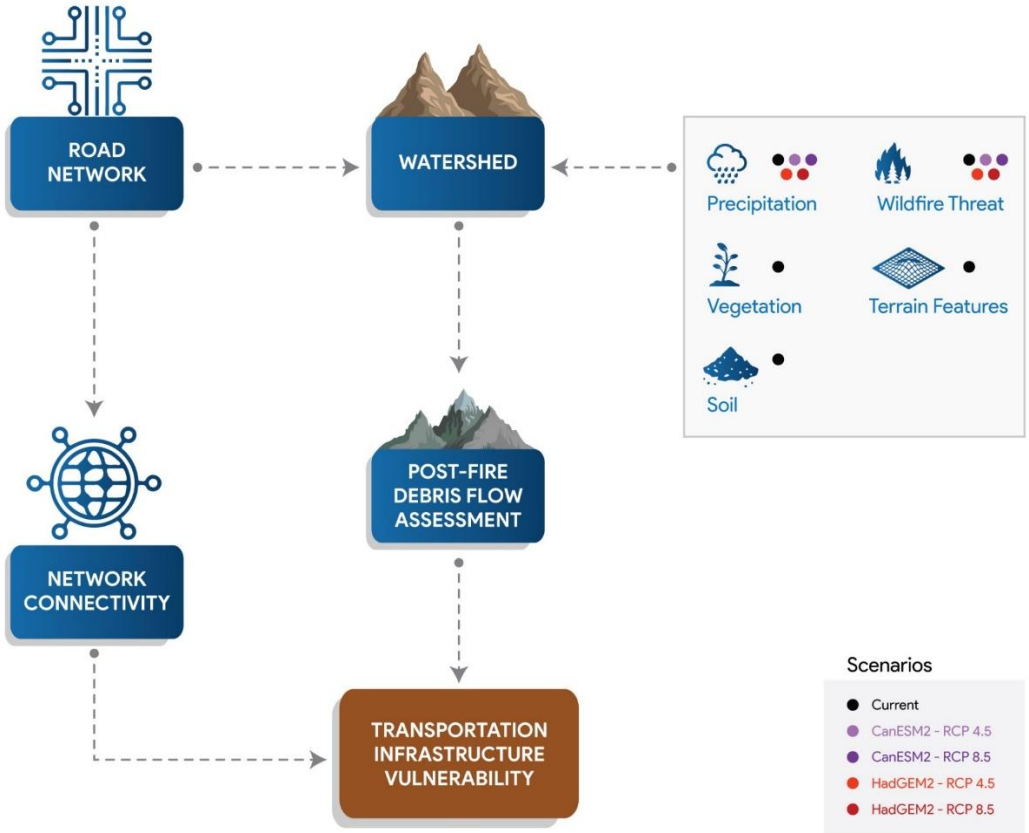

Figure 2.1. Methodology Overview

2.2.1. Post-fire Debris Flow Risk Assessment

The post-fire debris flow risk is defined as the frequency (recurrence) of the rainfall threshold that results in high likelihood of post-fire debris movement. As per Staley et al.(2017), the 15-min duration rainfall threshold (TH_{i15}) of a debris flow event is estimated with Equation *2.1*:

$$TH_{i15} = \frac{log\left(\frac{P}{1-P}\right) + 3.63}{0.41X_1 + 0.67X_2 + 0.7X_3} \qquad \text{Equation 2.1}$$

P ranges between 0% and 100%, representing a statistical likelihood of post-fire debris flow occurrence. X_1, X_2, and X_3 represent the steepness and burn severity,

vegetation burned ratio, and soil erosion characteristics in the watershed. Additional detail as well as data sources are shown in Table 2.1. We calculated the rainfall threshold (TH_{i15}) by assuming P equals 90% in order to represent a high likelihood of post-fire debris flow.

Table 2.1. Parameters Definition and Data Source for TH_{i15} Estimation

Parameter	Detail	Data Source
X_1	Proportion of basin area burned at high or moderate severity with gradients ≥ 23°	burn severity was derived from the Cal Fire 2014 threat map (FRAP, 2017); gradients was calculated from 30-meter resolution digital elevation (DEM) models for California (USGS, 2017, p. 201)
X_2	Average differenced normalized burn ratio (dNBR)	dNBR was simulated from the 2018 LandFire EVT (LANDFIRE, 2018), and Weibull distribution parameters for each category were obtained from (Staley et al., 2018)
X_3	Average value of soil erosion factors in the watershed	Soil erosion factor was extracted from STATSGO database(Schwartz & Alexander, 1995)
P	debris flow likelihood	

Among the parameters, soil erosion factor (X_3) could be obtained prior to a fire. But basin burned severity, and differenced normalized burn ratio (dNBR)—which were used to calculate X_1, X_2 in Equation 1—can only be retrieved after the fire form the Burned Area Emergency Response's (BAER) land survey. A proper approximation of these fire related parameters is needed for TH_{i15} calculation. And a proper estimation should consider of basin fire threat, and the vegetation presented in the watershed. The current fire threat map (FRAP, 2017) classifies fire risk in six levels: very low, low, medium, high, very high, and extreme. Here assumes regions where fire threats exceed

medium level are going to have medium to high level burn severity. (Staley et al., 2018) simulated the difference normalized burn ratio (dNBR) by considering the existing vegetation type (EVT) as per Equation *2.2*.

$$dNBR_{sim} = \lambda[-ln(1 - P_{dsim})]^{1/k} \times 2000 - 1000 \qquad \text{Equation 2.2}$$

In Equation 2.2, k and λ are the shape and scale parameters of the historical dNBR fitting Weibull Cumulative Distribution Functions (CDFs) for different types of vegetation (Staley et al., 2018). The EVT data was obtained from LandFire EVT (LANDFIRE, 2018). P_{dsim}, which is the cumulative percentile of the Weibull CDF, simulates the frequency of fire severity. For instance, P_{dsim} = 0.5 represents a moderate frequency and medium fire burn severity while P_{dsim} = 0.9 represents a less frequent but higher severity wildfire. We used the current fire threat map to determine the value of P_{dsim}. It is assumed that P_{dsim} is 15% when the fire threat level is very low, and P_{dsim} increasing incrementally by 15% each time the fire risk increases. As such, regions with high to extreme fire risk are assumed to burn with medium to high severity, while regions that have a low fire threat are assumed to burn at low severity.

USGS Landslide Hazards Program uses Staley's model (i.e. USGS, 2018) and BAER burned severity assessment to estimate the post-fire debris flow hazard after a fire got contaminated. We retrieved 40 post-fire debris flow assessments carried out by USGS between 2017 to 2020 (Kean & Staley, 2018). The locations and sizes of the 40 fires are shown in Figure 2.2.a. We validate each variable in Equation *2.1* and the simulated TH_{i15} by calculating the standardized difference between the simulated and the observed value for each modelled watershed in the 40 previous fire regions.

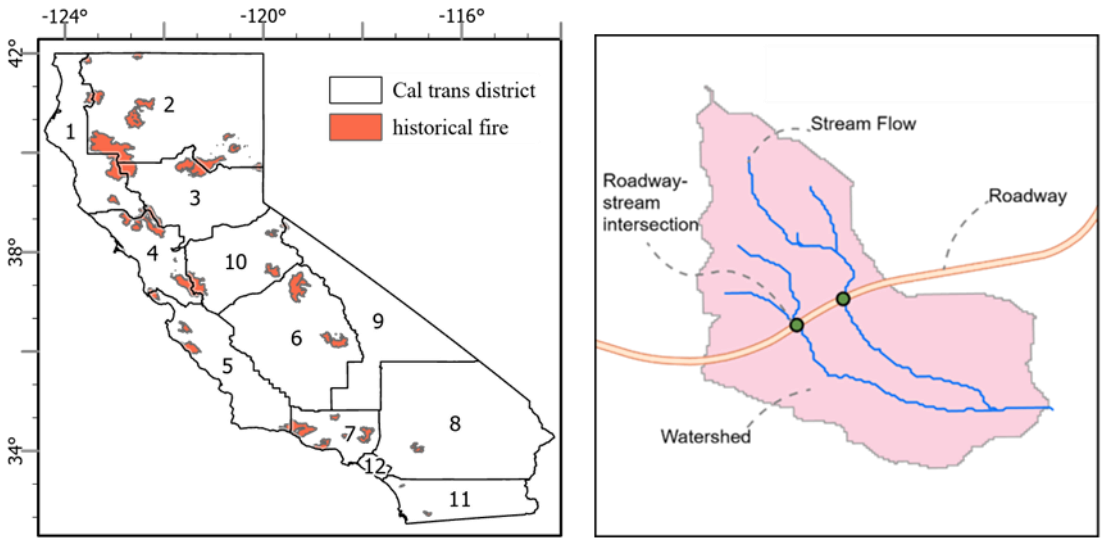

a. Historical wildfires used for validation b. Roadway and Streamflow Intersections

Figure 2.2. Historical Wildfires Used for Validation and Roadway and Streamflow Intersections

The post-fire debris flow risk is represented as the frequency (recurrence) of the threshold rainfall compared to design storms. The calculated TH_{i15} can be compared with the design storm intensity to check how frequent the estimated threshold would be. For instance, a 2-year design storm is more frequent than a 10-year design storm. As such, the risk of post-fire debris flow is higher when a TH_{i15} is between 2 to 10-year occurrence (more frequent), compared with a TH_{i15} over 10-year design storm occurrence (less frequent). The post-fire debris flow risk level is classified by 10, 50, and 100-year design storm. If the TH_{i15} happens at least once every 10-years, the corresponding watershed/roadway is defined as *high* risk. If a TH_{i15} happens at least once every 50-years but no more than once every 10-years, it is defined as *moderate* risk. If a $TH_{i15}$is more frequent than a 100-year design storm but less than 50-year design storm, it is defined as *low* to *moderate* risk. And when TH_{i15} is less frequent than a 100-year design

storm, it is defined as a *low* risk. The current design storm intensity, which is used to classify the TH_{i15} frequency, was obtained from the National Oceanic and Atmospheric Administration (NOAA) precipitation frequency estimation service (Bonnin et al., 2006).

The location where post-fire debris flow occurs is assumed to be the roadway and stream intersections. It is also assumed that: 1) roadway sections with no streamflow interactions would not experience debris flow, and 2) roadways would have the same degree of risk as the catchment areas at their intersections with the streamflow (Figure 2.2. b). As such, while post-fire debris flow risk was calculated for each watershed where corridors passed through, roadway risk was assigned to be equal to the watershed's risk. Watershed shape, location, and streamflow's were obtained from NHDPlus HR data (Viger et al., 2016). The Caltrans district map (Figure 2.2. a) was introduced to describe the analysis results.

2.2.2. Climate Change Uncertainty

Climate change is expected to change the profile of wildfire and extreme precipitation hazards. To estimate the climate change effects on the post-fire debris flow risk, future scenarios were considered. Future scenarios were defined by two greenhouse representative concentration pathways (RCP), 4.5 and 8.5, and two Global Climate Models (GCM). RCP 4.5 represents a scenario in which greenhouse gas (GHG) emissions are stabilized and begin to decline in the middle of the twenty-first century. RCP 8.5 describes a scenario in which GHG emissions increase rapidly until the end of the century. To capture the uncertainty of climate change, two GCMs were chosen for each scenario. There are many climate models and the California Energy Commission

(CEC) provides guidance on selecting appropriate GCMs for each scenario (Pierce et al., 2018a). The CanESM2 and HadGEM2-ES models are used. CEC simulated 10 climate change models and found that all showed substantial warming. Compared to other models, CanESM2 is identified by the CEC as being an average future while HadGEM2-ES is characterized as being a 'warmer and drier' future. The combination of two models and two RCPs resulted in four future scenarios.

To apply the climate change predictions into the post-fire debris flow risk assessment, transformations of the fire-burned severity, dNBR, and design storm intensity are applied as per Equation *2.3* and Equation *2.4*.

$$TH_{i15} = \frac{log\left(\frac{P}{1-P}\right) + 3.63}{(\varphi_f + 1) \times 0.41X_1 + (\varphi_f + 1) \times 0.67X_2 + 0.7X_3} \qquad \text{Equation 2.3}$$

$$future\_i15_p = current\_i15_p \times (\varphi_i + 1) \qquad \text{Equation 2.4}$$

where φ_i is the percentage increase of future design storm intensity, and φ_f is the percentage increase of future wildfire burned area. $current\_i15_p$ is the current 15-minutes design storm intensity at a given recurrence interval p, and $future\_i15_p$ is the estimated future 15-minutes design storm intensity at a given recurrence interval p. φ_i and φ_f are derived from the 6 km resolution LOCA downscaled climate estimation obtained from (Cal-Adapt, 2017). In the LOCA downscaled dataset, the projected fire burned area or rainfall intensity from 2010 to 2099 are used to resemble the future while the simulated 1960 to 2009 data are used to represent the current. It's worth noticing that

the LOCA model estimates 24-hour design storm intensity under various recurrence intervals (Pierce et al., 2018b).We assumed the 15-minutes design storms intensity changing ratio would be the same as the 24-hour rainfall intensity changing ratio.

2.2.3. Roadway Criticality Assessment

Betweenness centrality—a measure of how important each link is to a network—is used to analyze the topological connectivity of networks. Criticality of roadways can also be measured as link capacity (Li & Ozbay, 2012)or traffic delay when disruption occurs (Dowds et al., 2017). But traffic data, while a useful measure of how intensively a roadway is used, does not capture dynamics related to how important a link is in the overall network (Dowds et al., 2017; Fraser et al., 2020; Yang et al., 2018). In addition, if a high traffic link is disabled and the traffic can be accommodated on nearby links at minimal to no cost, then the link should not necessarily be considered critical. Transportation resilience studies often rely on measures of betweenness centrality to describe network criticality (Kermanshah & Derrible, 2016; Zhang et al., 2015). Therefore, the roadway criticality was analyzed as being the roadway betweenness centrality. The *roadway network*, including interstates, highways, arterials, and service roads, was retrieved from (OSM, 2019). The betweenness centrality for each section of the corridors was estimated using the network analysis toolkit NetworkX (Hagberg et al., 2008). It was assumed that rank of roadway criticality would stay the same into the future.

2.3. Results

The results describe the post-fire debris flow risk and roadway vulnerability under current and future conditions. First, the current debris flow risk and validation with historical wildfires are presented. Second, the climate change spatial unevenness and its effects on the future post-fire debris flow risk are discussed. Third, the shifting trends of roadway vulnerability and the geographical distribution of highly vulnerable corridors under different climate scenarios are demonstrated.

2.3.1. Current Risk and Validation

The fire burned severity estimation, soil erosion susceptibility, and the regional rainfall intensity affect the post-fire debris flow risk estimation. We estimated the burned severity on steep slopes (i.e., X_1 in Equation *2.1*) and the vegetation burned dNBR (i.e., X_2 in Equation *2.1*). The estimated medium to high-level burn severity on steep slopes concentrated at mountain forests in Caltrans Districts 1-8 and 10. These regions are also estimated to have high dNBR, as vegetation is fuel for the fire. The susceptibility of soil erosion (i.e., X_3 in Equation *2.1*) is higher in west California than in the east portion of the state. The rainfall intensity is high in the Sierra Nevada Mountains seen in Caltrans District 2, 3, 6, and 10. The values of X_1, X_2, and X_3 concurrently decide the regional TH_{i15}. A watershed is in high post-fire debris flow risk when the regional 10-year design storm intensity exceeds the estimated TH_{i15}. In such a case, a common precipitation event could result in the highly susceptible post-fire debris flow when the watershed is burned.

Watersheds with high post-fire debris flow risk cluster in forests along the coast and Sierra Nevada Mountains. The Central Valley and the Mojave Desert have low to

medium post-fire debris flow risk (Figure 2.3.a). Coastal and mountain forests in Caltrans District 4, 5, 7, and 8 (deep blue color in Figure 2.3.a) have high simulated dNBR, medium to high-level burn severity on steep slopes, high soil erosion susceptibility, and intense precipitation for common rainfall events (i.e., 10-year recurrence design storm). The debris flow risks in these districts are high. In the west part of Cal-trans District 2 adjacent to section 1, the simulated dNBR and burned severity are both high, but the soil is relatively stable. In such a case, precipitation intensity determines the debris-flow risk. Only a portion of this region has a high post-fire debris flow risk. high-risk areas are associated with very intense 10-year design storms. Meanwhile, Caltrans District 8 and 9 in the Mojave Desert and District 3, 6, and 10 in the Central Valley have low post-fire debris flow risk. These low-risk regions have little fire threat and low vegetation. The estimated high-risk areas overlap with the wildland-urban interface (WUI) (Radeloff et al., 2017) in the Sierra Nevada Mountains, Shasta-Trinity National Forest north of Redding, mountain regions in Santa Barbara, and Angeles National Forest and San Bernardino National Forest near Los Angeles. (Radeloff et al., 2017) identified other WUI regions near the San Francisco Bay Area and east of San Diego. These WUIs are currently under medium to low post-fire debris flow risk.

Most roadways passing through high-risk watersheds tend to be service or recreational roads, but some crucial highways are also identified. The service roads connect cities—such as Los Angeles, San Diego, and metropolitan areas in Central Valley—with the WUIs. These highways include Interstate-5 at Redding in District 2, Interstate-80 between Colfax and Blue Canyon in District 3, and Highway 101 in Ventura

and Santa Barbara counties in Caltrans District 5 and 7. The high-risk roadways identified align with the previous post-fire debris flow records (Figure 2.3.a). The 2017-2018 Thomas Fire debris flow hit Santa Barbara and Ventura counties after a 50-year recurrence storm triggered the event. The debris flow contributed to an inundation zone more extensive than the once in 100 years floodplain in Montecito and created a 500-meter-wide flow path across Highway 101(Kean et al., 2019).

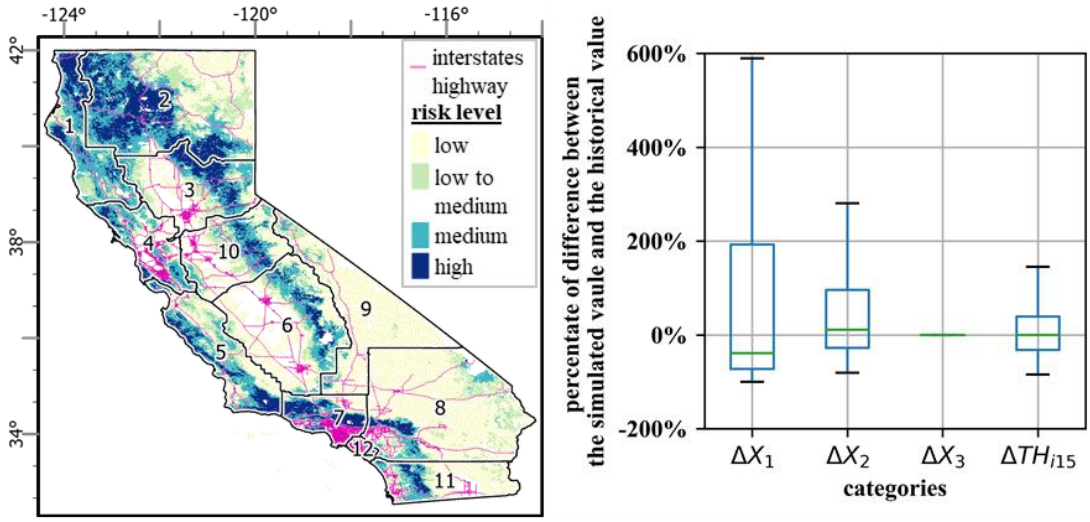

a. Roadways' post-fire debris flow risk under current climate conditions

b. Validation results for current climate condition

Figure 2.3. Current Post-fire Debris Flow Risk and Validation With Historical Wildfires

Validation results show that our model tends to overestimate the risk at the burned scar's outskirts in the selected 40 previous fire burned regions but underestimate the risk near the center of the burned area. The performance of the model is measured by comparing our estimated TH_{i15} with the TH_{i15} calculated from USGS. 16,000 watersheds in the 40 previous wildfire regions were used to validate the simulation and the historical wildfire events. Figure 2.3.b shows the percentage difference between simulated variables and the historical measures. Nearly half of the sample data had their TH_{i15}

overestimated, and one-third of the samples have TH_{i15} underestimated. Overestimating TH_{i15} in our study means we underestimated the post-fire debris flow risk in the watershed compared with USGS, and vice versa. The estimation of slope and burn severity of the basin (i.e., X_1), dNBR (i.e., X_2), and soil erosion characteristics (i.e., X_3) affects the accuracy of the TH_{i15} assessment. Validation results show that X_3—which could be retrieved prior to the fire event—is consistent with the sample data. The average difference between the estimated and historical measured X_3 is less than 0.3%. But X_1 and X_2—simulated based on fire and vegetation assumptions—show discrepancy with the historical fire records. The percentage difference between the simulated and the historical X_1 ranges between -90% to 600%. Two-thirds of the 40 historical samples have their X_1 under-predicted. Meanwhile, the percentage difference between simulated and historical X_2 ranges between -45% to 255%. About 15% of the watersheds have the simulated X_2 matching with the historical data. 53% of the simulated X_2 over-estimated the watershed X_2. The inconsistency between the simulated and historical X_1 and X_2 comes from the difficulty to predict the fire behavior. Compared with X_1 and X_2, simulated TH_{i15} shows less disparity with the historical value in the 40 fire regions which were selected for the validation.

Even though there are disparities between the simulation and historical wildfire data, we still suggest using the proposed method to estimate post-fire debris flow risk. This is because the proposed model represents the state-of-art post-fire debris flow assessment methods and appears to reasonably estimate risk where actual events are taking place.

2.3.2. Climate Unevenness and Future Post-fire Debris Flow Risk

Climate change is expected to increase the total fire burn size and change rainfall event intensity, while downscaled climate models show the unevenness of climate change effects in California. In some locations, precipitation and wildfire are expected to worsen, while in other places, they are expected to improve. For example, under the HadGEM2-ES RCP 8.5 scenario, climate change could lead to up to a 4600% increase in fire burn area at the mountain forest regions of Caltrans Districts 1-3, 6, and 10 (Figure 2.4.a). The expanding wildfire burn area is associated with the higher temperatures, increasing droughts, and more subsequent insect-induced tree mortality in montane forests (California Energy Comission, 2021). Most parts of California will experience an increase in design storm intensity as we move into the future. For example, in the HadGEMM2-ES RCP 8.5 scenario, the design storm intensity is expected to increase in mountain regions and along the coast. Still, the design storm intensity are expected decrease in parts of the Central Valley by the end of the century Figure 2.4.b). The unevenness of future precipitation changes results from rising global temperatures which are expected to increase evaporation and result in more frequent and intense storms in storm tracks, but decrease precipitation in areas far from the storm tracks (NASA, 2021; Pierce et al., 2018a).

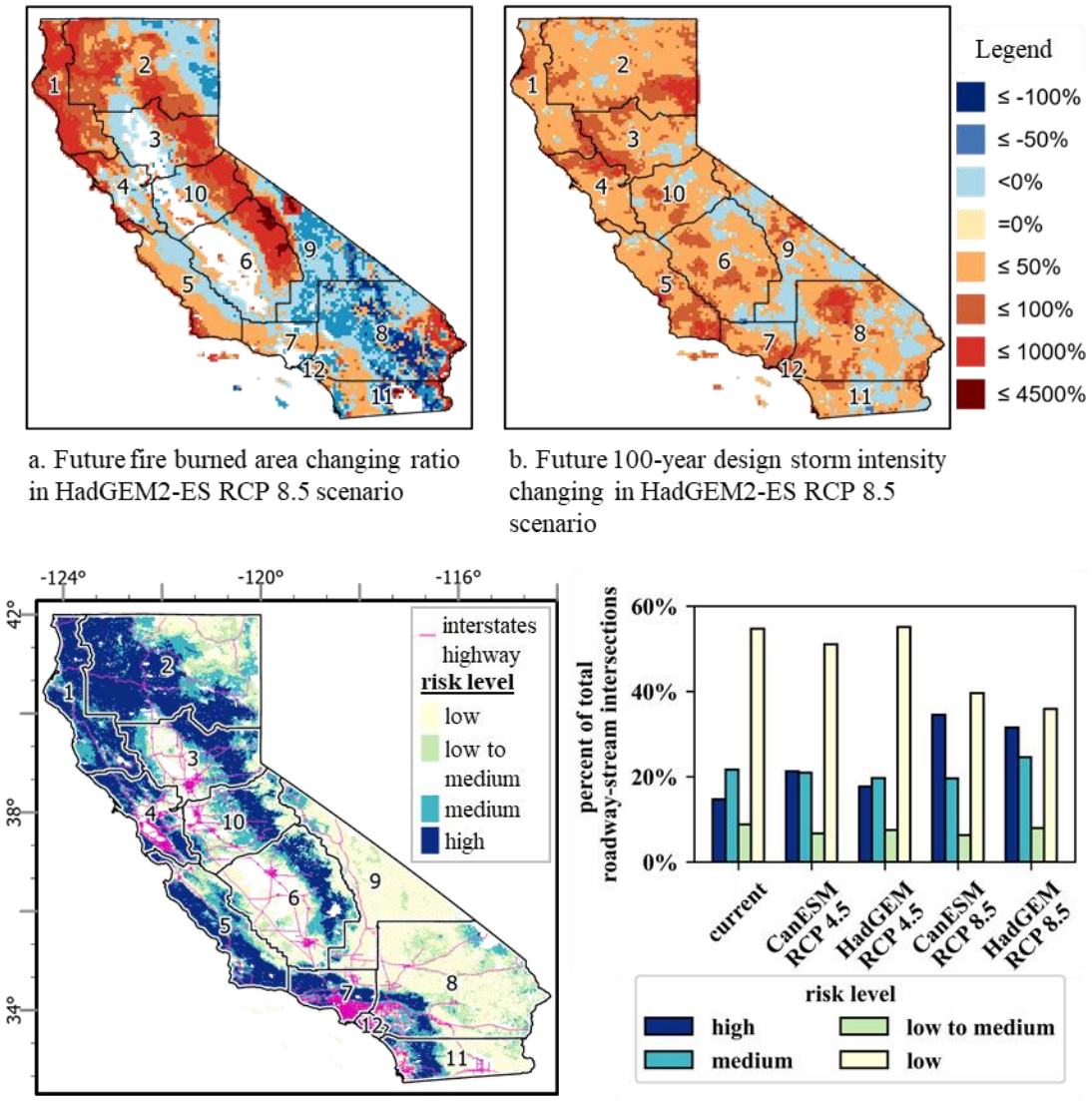

a. Future fire burned area changing ratio in HadGEM2-ES RCP 8.5 scenario

b. Future 100-year design storm intensity changing in HadGEM2-ES RCP 8.5 scenario

c. Post-fire debris flow risk under HadGEM2-ES RCP 8.5 scenario

d. Percent of roadways under different levels of post-fire debris flow risk

Figure 2.4. Climate Unevenness and Impacts on Post-fire Debris Flow Risk

Debris flow risk is expected to increase in watersheds where either precipitation intensity or wildfire size is projected to go up. The increase in wildfire size is expected to result in decreased TH_{i15}. Meanwhile, the common recurrence precipitation event (i.e., 10-year recurrence) would become fiercer as storm intensity increases. As a result, more watersheds will have their regional 10-year design storm exceed the TH_{i15}. For instance,

the mean 10-year design storm is 51.1 mm/hr currently. The mean 10-year design storm intensity is expected to increase 10% to 20% in the RCP 4.5 scenario and 20% to 30% in the RCP 8.5 scenario. The mean TH_{i15} is anticipated to decrease from 53.7 mm/hr currently to around 50 mm/hr in the RCP 4.5 scenario, and 47 mm/hr in the RCP 8.5 scenario. As a result, more watersheds would expect to have an increased risk level since their 10-year design storm is more likely to exceed the TH_{i15}. The increase of post-fire debris-flow risk happens in the current risky region along the mountain forest and coastal line in Caltrans districts 1-7 and 10 (Figure 2.4.c). In such regions, the future fire burn size (Figure 2.4.a) and the storm intensity (Figure 2.4.b) are expected to increase.

The number of roadway-stream intersections under high post-fire debris flow risk will dramatically increase as we move into the future, especially under the RCP 8.5 scenario (Figure 2.4.d). About 14.7 % of roadways are currently under high post-fire debris flow risk. The roads under high post-fire flooding threat could increase by between 17.7% and 21.3 % in the RCP 4.5 scenario and between 31.6 % and 34.5 % in the RCP 8.5 scenario. The increased risky roadways are mainly concentrated in and around currently problematic areas. In the meantime, the ratio of low-risk roadways will decrease as we move from current climate to the future climate scenarios. Approximately 55% of roadways have low post-fire debris risk in current climate condition. The ratio of low-risk roadways is expected to be stabilized around 51% to 55% in RCP 4.5 scenario but decrease to 35.9% to 39.6% in RCP 8.5 scenario. The increasing 100-year design storm intensity and the decreasing TH_{i15} creates more roadways that have debris flow risk increasing from low to medium.

2.3.3. Vulnerability and District Priority

Roadway vulnerability considers its spatial criticality and its post-fire debris flow risk. The highly vulnerable corridors are those with high betweenness centrality (i.e. the top 10% betweenness centrality) and high post-fire debris risk (i.e. TH_{i15} is smaller than a 10-year design storm intensity). The betweenness centrality ranges from 0 to 1, and 10% roadways have values above 0.28. As such, the identified roadways are all spatially critical (i.e. top 10%) to the network with many parts of the system dependent on them, and they are also vulnerable to post-fire debris flow when rainfall occurs. Table 2.2 shows the number and percentage of highly vulnerable corridors in the system. Currently, 0.97% of the total roadways have high post-fire debris flow risk and are critical in the roadway network. The number of highly vulnerable roadways is forecast to increase by 1.92-4.27 times in the future. Under the RCP 4.5 scenarios, the number of highly vulnerable roadways will increase 92% to 131%, and could rise to between 251% and 327% in the RCP 8.5 scenarios.

Table 2.2. Trends of Highly Vulnerable Roadways From Current to Future

	current	RCP 4.5		RCP 8.5	
		HadGEM2-ES	CanESM	HadGEM2-ES	CanESM
number of highly vulnerable roadways	925	2138	1774	3949	3246
% of highly vulnerable roadways in the system	0.97%	2.25%	1.87%	4.15%	3.41%
(% change vs. current)		131%	92%	327%	251%

As climate change will affect the future fire burn areas and precipitation heterogeneously, the vulnerability profile of the Caltrans districts will change. Currently, more than 70% of the highly vulnerable corridors are in Caltrans District 2, 5, 7, and 11

(Figure 2.5.a). It is worth noting that in future scenarios, more vulnerable roadway hotspots are anticipated to appear in Southern California and along the West Coast. For comparison, the debris flow vulnerability ranking chart in Figure 2.5.b shows Caltrans districts based on the number of hotspots in each region. Districts 3, 9, and 10 are ranked as the least vulnerable, while Districts 2 and 7 are expected to have the most perturbations in both current and future scenarios. Half of the districts have vulnerability profile shifts between different climate scenarios. Districts 1 and 6 are anticipated to see an increase in their vulnerability rankings. The risk ranking of District 8 is expected to decrease because other districts will become riskier. The changing ranking could signal a shift in the distribution of roadway impacts from post-fire flows, warranting consideration of how resources are invested between different districts.

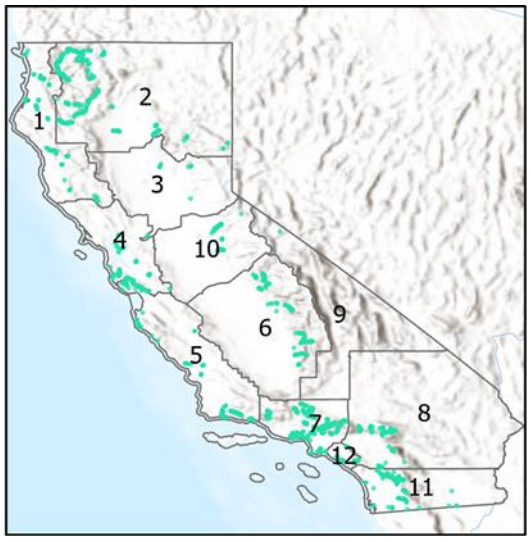

a. Spatial distribution of highly vulnerable roadways under current climate conditions.

District	Current	RCP 4.5		RCP 8.5	
		HadGE M2-ES	CanESM	HadGE M2-ES	CanESM
1	8	6	3	6	6
2	2	1	1	1	2
3	11	11	11	11	11
4	7	8	9	9	9
5	3	4	5	3	4
6	5	5	6	4	3
7	1	2	2	2	1
8	6	7	8	7	8
9	12	12	12	12	12
10	10	10	7	8	7
11	4	3	4	5	5
12	9	9	10	10	10

b. Post-fire Debris-flow Vulnerability Ranking by Caltrans District

Figure 2.5. Spatial Distribution of Highly Vulnerable Roadways and Caltrans District Vulnerability Ranking

2.4. Discussion

2.4.1. Policy Implications

Post-fire debris flows create great risk for transportation infrastructure, since the location and intensity of the debris movement is hard to predict, and the threats could last for several years until the watershed is restored back to pre-fire conditions. The current hazard warning system estimates the debris flow risk in the burned scar by comparing the upcoming precipitation events (detected by radar) with the rainfall threshold estimated for the burned scar (USGS, 2018). The current approach gives transportation infrastructure managers and stakeholders little time and resources to react to the imminent threat.

This research demonstrates a method to proactively estimate transportation infrastructure post-fire debris flow risk and the system's vulnerability prior to wildfire. Both current and future climate conditions are considered when estimate watershed post-fire debris flow risk and roadway system vulnerability. Several key takeaways emerge that warrant discussion: 1) to identify, reinforce, and fortify the highly vulnerable roadway infrastructures, 2) to prioritize watersheds fire mitigation treatment, and 3) to assist future transportation infrastructures site selection.

Reinforcement and fortifications can be done on the identified highly vulnerable roadways to increase infrastructures' resilience to post-fire debris flow. Currently, the estimated highly vulnerable roadways are concentrated along coastal regions in SoCal, Northern California, and the west rim of the Sierra Nevada Mountains. In these regions, resources could be used to reinforce the highly vulnerable roadway system. Engineering techniques to increase roadways' resilience include expending culvert capacity, installing

lateral berms, building debris flow basin, and planning extra routes to increase redundancy.

The mitigation of post-fire debris flow risk can be done by prioritizing fire reduction treatment on watersheds where highly vulnerable roadways pass through. Post-fire debris flow is the result of concurrent wildfire and heavy precipitation hazards. Watershed treatment and preventing the fire from happening or reducing the fire burning severity, can mitigate the post-fire debris flow from roots. Watersheds-which have highly vulnerable roadway sections within them, can be prioritized for future fire reduction treatment. In this way, the fire mitigation would reduce the system mobility lost from debris flow by preventing the post-fire debris flow from happening on top of critical infrastructure.

Transportation planning efforts can use the results to assist site selection. The roadway network was assumed to be static through end-of-century, and planning efforts should minimize the expansion of critical infrastructure where heavy debris flow risk is estimated.

2.4.2. Limitations

The limitations come from the uncertainties embedded in the empirical debris-flow risk model, network simplifications, and the exclusion of non-direct hazards. The debris-flow risk model was regressed based on historical wildfire records in Southern California (Staley et al., 2018). When implementing this model for the whole California state, we assumed the model would fit for the entire state. The regression model's performance might decrease when been used outside of the regression regions.

Assumptions of vegetation and soil burn severity were introduced when implementing the model before wildfires. These assumptions introduced more uncertainty into the model application result. Because of the computational challenges of calculating the network criticality for every roadway in California, we simplified the transportation infrastructure. We only considered the divided highways, arterials, and parts of non-major routes. The final limitation is that only location of the direct physical disruptions was considered. The direct physical disturbances on transportation infrastructure from post-wildfire hazards include but are not limited to roadway washout, flash flooding, bridge scour, debris flows, culvert flood with debris, and mudslide (Valentin & Stormont, 2019). But there also have indirect impacts of post-fire hazards on roadway infrastructure including the deterioration of roadway embankments and pavement foundations, and eventually pavement and roadway damage (Vennapusa et al., 2013). Both direct and indirect hazards can create critical damages to the roadway system. But because of the absence of models to estimate the indirect impacts, we only considered the direct physical disruptions from post-fire debris hazard.

2.4.3. Resilience Strategies

The findings have broad implications for how California approaches resilience of roadways to post-wildfire debris flows. As California and other communities develop strategies for preparing infrastructures for climate change, they must confront a concurrent set of challenges that affect their ability to deploy solutions (Chester & Allenby, 2019). This includes limited (and possibly insufficient) funding, large uncertainty about where and how climate impacts will manifest, and limited insights into

the radically changing landscape regarding how we will use transportation services in the future. These forces are emerging and appear to contradict the state-of-the-art design and operation principles of infrastructure which remain rooted in certainty and intentionally long design lifetimes. In an uncertain future, the rigidity of our systems and our emphasis on predictability are potentially problematic (Chester & Allenby, 2019). Reconciling future conditions with current ones with an emphasis on how infrastructure is designed and operated is paramount to adapting for resilience (Chester et al., 2020).

Resilience in transportation has often emphasized approaches rooted in armoring and strengthening. These may be sufficient at some scale but are likely fall short as systemic solutions (Markolf et al., 2019) . Traditional approaches for protecting infrastructure from hazards focus on controlling or holding back the hazard. Stormwater systems channelize or pipe away intruding flows up to a particular intensity, and retaining walls push back intruding land. Much of our engineered infrastructure is designed to control or push back the environment (Chester et al., 2019), and the uncertainty inherent in climate change raises serious questions about the efficacy of this approach as we move into the future. To what future intensity event should roadways be able to withstand given the uncertainty of climate futures? Can California afford to upgrade roadway assets that are able to withstand a chosen intensity? Would upgrading assets result in infrastructure that is unacceptably intrusive to communities (e.g., a massive open culvert that bisects a neighborhood?) Given that infrastructure design may scale non-linearly with changes in the hazard, these questions raise serious questions regarding the implementation of present-day state-of-the-art thinking. As such, California should deploy a multi-tiered

strategy to addressing post-fire debris flow roadway adaptation. Hardening assets (through armoring or strengthening) have their place, most likely at the asset level, but systemic strategies that consider failure as inevitable and give alternative ways of satisfying function are also needed (Markolf et al., 2019). First, California should consider how mobility and accessibility can be extended in the face of surprise. Instead of simply focusing on hardening the roadway system in anticipation of a particular intensity event, California should also create conditions for mobility and accessibility needs to be met when the system is overwhelmed. Put simply, California should view the transportation network through a lens of it being capable to adapt to handling surprise events. This might include shifting from physical to virtual connectivity through investments in high bandwidth cybertechnologies, or rapid and large-scale mode shifting as particular assets go offline. Given the long lifetimes of the infrastructures and the organizations that manage them, California should also begin to consider the conditions necessary for sustained adaptation into the future, i.e., the expected rapid change in how we demand and supply services (Chester & Allenby, 2019). The coming century is expected to be characterized by change at rates and scales that neither California, nor anywhere else, has ever experienced (Steffen et al., 2015). To assume that the technologies and processes that supply transportation services, and the ways in which we demand transportation services will remain similar to today, or even predictable, is therefore problematic. Instead, California must recognize that the transportation system, the technologies that define it, and what we ask of it, is going to have to adapt more rapidly into the future, and, because of the uncertainty of climate hazards, it warrants

approaches committed to sustained adaptability. Sustained adaptability is the commitment to perpetual change, the continuous reassessment of the conditions, hazards, needs, and technologies that form the foundations of our systems' designs (Woods, 2015). California's leaders should recognize that the changing conditions in environment (climate and otherwise) represent a fundamental challenge to rigid design approaches. Instead, they should embrace agility and flexibility in how they design, operate, and govern their transportation systems (Chester & Allenby, 2019). California's leaders should establish processes and governance models that commit to the reassessment of the conditions and needs that surround infrastructure, and a willingness to change systems rapidly as the environment changes. This, in many ways, contrasts completely with the models of infrastructure design today (Chester et al., 2019).

Focusing back on climate change, it is critical to recognize that that there is inherent complexity in the confluence of several uncertainties in infrastructure design. Upgrading roadway infrastructure across California's entirety in order to better manage future post-fire debris flows is a very long undertaking and a massive financial commitment. Any strategy that can prioritize limited resource investments will be critical. Infrastructure exists at the confluence of past and future uncertainty (Chester et al., 2020) The majority of California's infrastructure was built in the past century. Environmental sensor networks that detect, for example, precipitation events, were first deployed in the middle of the twentieth century. At this time, infrastructure design was informed by relatively limited data streams as sensor networks were still in their infancy. As such, there may have been significant uncertainty around the frequency and intensity

of local events. Guidelines that specified return periods by which to design infrastructure assets (e.g., a 50-year event) may have over- or under-estimated these critical events, leading to assets that were over- and under-designed. While under-designed assets may have been corrected over the past decades, this has not been universally true, and over-designed assets also exist. Today, climate change represents an additional layer of uncertainty, in which conditions in some regions worsen and in other regions improve. The confluence of these uncertainties can be characterized by four domains that can aid decisionmakers to surgically invest limited resources (Chester et al., 2020). The three domains are as follows: the severe domain, the guarded domain, the elevated domain. In the severe domain, infrastructure has already experienced conditions that surpass its design. Climate change is expected to worsen the severity of this. Here, a roadway designed to withstand a low intensity post-fire flow may experience much more intense flows, and climate change is forecast to elevate flow risk. For this reason, roadways in the severe domain should be top priority. At the other end of the spectrum is the guarded domain. Assets in this domain are the lowest priority assets since they include roadways which were overdesigned for what they experienced. When it comes to these roadways, climate change is expected to lessen the hazard. The most difficult and troubling assets are found in the elevated domains, where either the asset is experiencing conditions that are less severe than those they were designed for and climate change is worsening the hazard, or the asset is experiencing more severe conditions than those they were designed for, and climate change is weakening the hazard. These domains are problematic because they do not provide a clear picture of robustness of the asset in the future. Assets in these

domains require new knowledge and insights to be able to make decisions regarding their future. As California looks to prepare its roadways against post-fire debris flows, taking stock of past design conditions relative to future climate becomes critically important for deciding how to prioritize investments.

Given the uncertainties of future climate, the massive investments required to adapt infrastructure, and the long lifetimes of assets, California should consider safe-to-fail strategies. Infrastructure has been and continues to be designed as fail-safe, being constructed, for example, to withstand a particular intensity shock, and when failure happens, the impacts are generally externalized. Safe-to-fail is a resilience framework that calls for the impacts of failure to be internalized in the design process, towards minimizing and better managing failure consequences (Kim et al., 2017). Infrastructure failure under climate change may be inevitable, and as such, planning for its eventuality is prudent. In planning for failure, California must rethink the ways in which failures occur, identifying novel ways of avoiding or compensating for such failures. Given the remoteness and low use of some post-fire flow-vulnerable roads, for example, the state may allow such roads to fail rather than investing in keeping them functional when climate strikes. However, since this will inevitably mean certain services being inaccessible, it may be prudent to identify alternatives to these services. Such graceful extensibility may be cheaper in the long-term than traditional robustness-centric approaches (Kim et al., 2017; Woods, 2015). Safe-to-fail is not about uncontrolled failure, but the acceptance that failure is inevitable and should always be planned for in design.

Adapting California's roadways to withhold future post-fire debris flows will likely require extensive planning and novel investment strategies for the diverse conditions and needs of the state. A one-size-fits-all approach may not be prudent; what works in the Mojave Desert may be fundamentally different than what works in the high forested High Sierra. Adaptation strategies should therefore embrace agility and flexibility, recognizing that diverse and rapidly changing conditions are not conducive to rigid and single vision strategies (Chester & Allenby, 2019). Preparing roadways for future post-fire debris flows will require new outlooks, innovative financing models, and possibly improved governance models that embrace agility and flexibility.

CHAPTER 3

REPURPOSING MESOSCALE TRAFFIC MODELS FOR INSIGHTS INTO TRAVELER HEAT EXPOSURE MITIGATION: ICARUS AND THE CASE OF PHOENIX

3.1. Introduction

Climate change and rapid urbanization have posed heat-related health challenges for urban residents. Vehicles have high Greenhouse Gas (GHG) emissions embedded in their life cycle (Chester et al., 2010) . Increasing non-vehicle trips and reducing travelers' dependence on cars have been proved to reduce GHG emissions (Nazelle et al., 2010), mitigate city congestion (FlLOW Project, 2016), and improve residents' physical health (Hamer & Chida, 2008). Despite the positive outcomes of active trips, there are concerns that the combined effect of increasing urban heat and climate change will contribute to adverse health outcomes for outdoor trips (Eisenman et al., 2016; D. M. Hondula et al., 2014). Many heat-related health risks proportionately impact populations with low socioeconomic status who face inequitable distribution of coping resources (Karner et al., 2015). Cities have carried out heat exposure mitigation initiatives, such as planning for cooling shelters or increasing shading along sidewalks, to combat the increasing heat-related illness and discomfort among residents (City of Mesa, 2014; Phoenix, 2021). Further research on personal- and population-scale heat exposure could assist cities in more optimal planning for and investing in heat mitigation strategies without creating new future challenges.

Previous heat exposure studies have focused on the population scale and personal scale. Many heat exposure studies have also provided insights into the relationship between heat and adverse health outcomes at the population-scale (e.g., Bao et al., 2015; D. Hondula & Davis, 2012; Reid et al., 2009). Select studies have examined how the heat-caused adverse health outcomes are associated with certain demographic features among residents (Chow et al., 2012; Karner et al., 2015). However, the population-scale "heat" exposure studies are often limited to proxy variables like land surface temperature, which do not reflect the full temporal and spatial variation of the heat load or travel behavior that greatly influence exposure (Bao et al., 2015; Bernhard et al., 2015; Kuras et al., 2017). Heat exposure at the scale of human bodies - personal heat exposure - provides a more precise understanding of individual experience with heat among heterogeneous city environments (Glass et al., 2015; Kuras et al., 2015, 2017). However, it is challenging to generate population-scale heat exposure findings as the personal heat exposure studies are often limited to small sample sizes and short time periods of measurement. Thus, research on personal heat exposure connected behavior and the built and natural urban environment is still in its infancy.

The advancements of ambient (air) temperature simulations and the advanced mesoscale travel models provide unique opportunities to update methods in personal heat exposure research within heterogeneous city environments across a population. However, air temperature (T_{air}), which is most commonly measured within previous heat exposure studies (e.g., Chow et al., 2012; Johnson et al., 2018), does not fully capture the full individual thermal experience (of heat exposure) in urban environments (Kuras et al.,

2015, 2017; Middel & Krayenhoff, 2019). To quantify the total heat load on a human, we must also incorporate mean radiant temperature (T_{MRT}), wind speed, and humidity (Budd, 2008; McGregor & Vanos, 2018; Middel & Krayenhoff, 2019). However, these parameters are often more difficult to measure or model, with wind speed and radiation changing dramatically in time and space throughout urban areas compared to T_{air} and humidity.

New advanced approaches exist to generate T_{MRT} from deep learning Google Street View images (Middel et al., 2017) to estimate patterns of exposure across space and time at fine-scales (10-meters resolution). The T_{MRT} is an important variable used to calculate the wet bulb globe temperature (T_{WBGT}), which is an empirical model developed to estimate heat stress in working populations (ACGIH, 2019; Budd, 2008). In combining these models with activity or mobility patterns, the spatiotemporal pattern of an individual's heat load can be derived.

Activity-based model (ABM) - a Mesoscale travel model with personal daily travel and activity schedules - has been used to study personal air pollution exposure (Yoo et al., 2015). Karner (et al., 2015) used the simulated ABM output to study the personal heat exposure for active trips in the Bay area with the consideration of the travel schedule and the air temperature corresponding to the trip origin. However, neither the specific travel pattern (path) nor the ambient temperature variability along the transportation infrastructure were considered in their study.

The current research examines the use of advanced mesoscale travel simulations to provide new insights into personal heat exposure by leveraging individual travel

behavior, infrastructure, and fine-scale microclimate data. The simulation platform - Icarus - was built to estimate a traveler's heat exposure at both personal and population scales at the interface of travel behavior, microclimate, and the built environment. Icarus joins state-of-the-art Activity-based travel Model (ABM) output with fine-scale measures of spatiotemporal temperature data, parcel characteristics, household characteristics, and travel characteristics. In Icarus, a transportation network with spatiotemporal meteorological information is constructed. Agents from the mesoscale travel model data are used to provide the demographic information and trip-activity schedule of each person/agent. Each agent is then routed on the transportation network with spatiotemporal information to estimate their heat exposure.

Icarus is applied to the Phoenix metropolitan region as a case study. Metro Phoenix is a particularly appropriate case study given the extremely high frequency of extreme heat, rapid urbanization and population increase, and heavy car dependency. Further, climate change is expected to increase the extreme heat in both intensity and duration—thus, Metro Phoenix is a harbinger of the future for other cities. Findings from this study can guide urban planning, public health policymaking, and heat stress mitigation strategies in Metro Phoenix and potential further cities in future applications.

3.2. Methods

Figure 3.1 illustrates the major parts of this study, including the core processes of Icarus and the Metro Phoenix case study. Icarus consists of two core processes: core data ingestion and simulation. During the core data ingestion process, Icarus will take critical datasets, such as network data, ABM output, and environmental temperature data, with

certain assumptions and store them in a database (Icarus SQL Server I in Figure 3.1). From this database, Icarus will build a transportation network with spatiotemporal temperature information, population group, and travel schedule for each agent to start the simulation. The simulation platform estimates personal travel patterns and heat exposure based on agents' daily travel schedule. The simulation result will be stored in a second database (Icarus SQL Server II in Figure 3.1) for final analysis, such as estimating the sub-group and the locations with high heat stress. The details of input data, data parsing techniques, heat exposure calculator, and hot trips identification are explained in the following section.

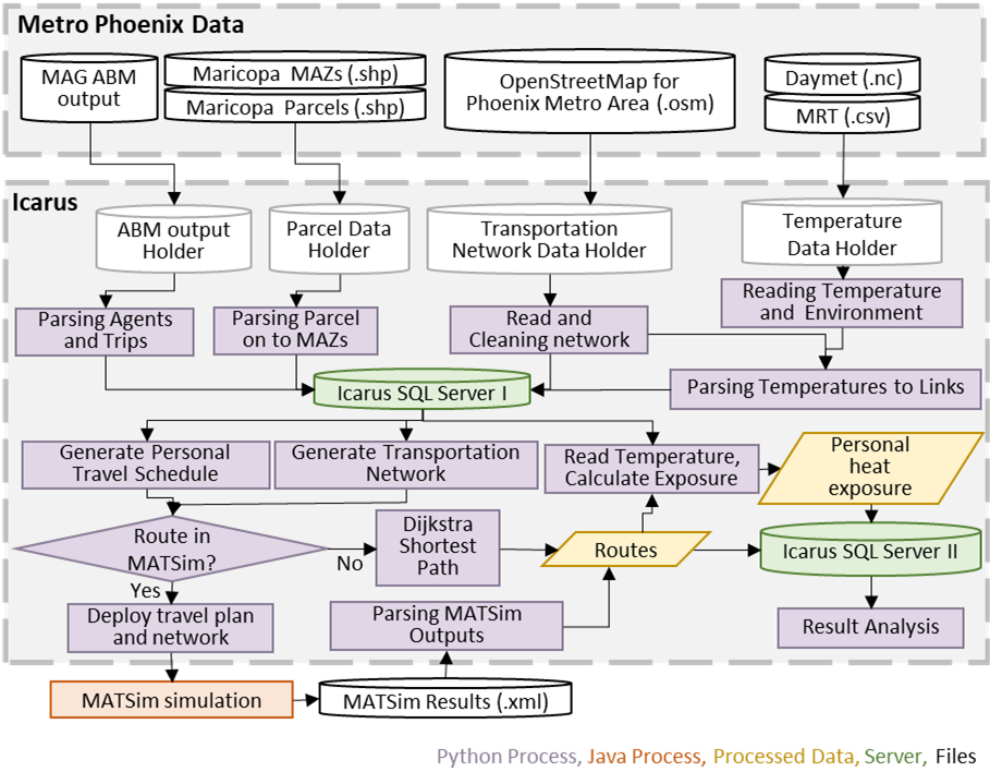

Figure 3.1. Icarus Framework

3.2.1. Icarus

Icarus is an open-source Python package for the agent-based personal heat exposure simulation, intended for transportation planning, urban planning, and policy research use. Agents with complimentary information (e.g., age, gender) are the primary simulation object in Icarus. Icarus simulates the heat exposure that an agent is experiencing by tracing the daily travel and activity schedule. Icarus ingests the agent's daily travel and activity schedule and the geolocation of the activities. At the personal scale, Icarus simulates the individually experienced temperatures by considering the time and ambient temperature (outlined below). Multiple datasets are needed to achieve the function of Icarus, and essential functions have been built to ensure that data in different formats can be loaded into the same simulation environment.

3.2.1.1. Core Data Ingestion

Parsing and unifying common urban-related data sources are a critical first step in Icarus. The core datasets ingested are described in Table 3.1 and detailed in the following subsections. Data requirements include ABM output, parcel data, transportation network data, temperature profiles, and environmental data. The ABM and parcel data are used to extract travel schedules and locations. ABM are state-of-the-art simulations used by metro regions to estimate travel characteristics of individuals and households for long-term planning focusing on an estimated – or synthetic – population. Icarus does not generate ABM; Icarus uses the ABM output, usually generated by the regional transportation planning agency, to extract the household and activity's location, agents' travel schedule, and agents' demographic characters to generate trip plans. Second, land parcel data that describe buildings and their uses are also ingested. Furthermore,

transportation networks and fine-scale heat exposure measures are needed to route the trips and estimate temperature metrics (including T_{air}, T_{MRT}, and T_{WBGT}) along the roadway coinciding with activities. Towards improving the scalability of Icarus, publicly available datasets are retrieved from OpenStreetMap (for the transportation network) (OpenStreetMap Contributors, 2015) and NOAA (for T_{air}).

Table 3.1. Core Input Data, Format, and Source for This Project

Data name	**Data format**	**Data Source**
Activity-based model output (ABM)	.csv, .db	City or regional planning organization
Land Parcel data	.shapefile, or .csv file with locations	City or county assessor database
Transportation network data	.osm or .shp	OpenStreetMap or Tiger shapefile
Temperature data	.net4 or .csv file with location information	NOAA or regional MRT estimation

3.2.1.1.1. Activity-Based Model (ABM) Output

The Emerging ABM output is a core input to Icarus towards estimating fine-scale movements of individuals. Using travel surveys and complementary datasets, ABMs generate a synthetic population capturing individual actors and their daily travel plans. ABMs describe the specific needs and demographics of a region's population, including

travel for work or groceries, the vehicles used, and how households and agents make decisions to take specific tours to maximize the achievement of their needs with the given resources (Davidson et al., 2010). In general, ABM data contain agent, household, activities, and trip information. Agent information includes education, age, gender, and job type. The trip information consists of each trip's origin and destination (described through either Traffic or Micro Analysis Zones), travel mode, travel time, duration, trip purpose, and the person who carried out the trip. Metropolitan Planning Organizations across the U.S. are developing ABMs and thus their output is becoming increasingly accessible.

3.2.1.1.2. Land Parcel Data

Land parcel data is introduced to improve the locations described in ABM output. The locations in ABM are at the Micro Analysis Zones (MAZ) or Traffic Analysis Zones (TAZ) level, but Icarus needs the exact origin and destinations (O/D), such as the buildings and parcels, to initiate the routing and assess environmental exposure profiles. An MAZ contains dozens to hundreds of parcels. For buildings, parcels, and land use, Icarus relies on county assessor databases, a generally publicly available spatial dataset that describes parcel location and properties. To downscale the O/D for each from MAZ to a specific parcel inside the MAZ, Icarus applies a random selection algorithm. The parcel data is spatially joined with the MAZ boundaries. By analyzing MAZ bounds and parcel use codes, households and activity locations are randomly assigned to parcels in the zone. Parcel data would also be used to estimate if AC is present during the activity.

3.2.1.1.3. Roadway Network Data

Trips are routed in Icarus on distance- or temperature-weighted shortest paths and thus require roadway inputs, especially the biking/walking network. These are sourced from OpenStreetMap (OSM). OSM contains rich information about the roadway network for active trips, including length and allowed travel mode. Icarus includes a module to load, parse, and store OSM data into the simulation environment. In the data loading process, Icarus uses the Python module Osmium (Hoffmann, 2021) to read the OSM as arcs (links) and vertices (nodes). Considering the agility of walking and biking trips, the single-direction arcs, which overlap with each other but have the same set of end nodes, are simplified as one bidirectional arc. Extra nodes are added at the intersection of arcs if the crossing edges are checked, and no nodes exist at the intersection point. The parsed network is stored as a Networkx Graph (Hagberg et al., 2008) in the simulation environment, and allows for walking and biking routing.

3.2.1.1.4. Temperature Metrics Data

The activities and trips can be carried out with and without AC. In studying heat exposure, agents taking in-vehicle trips or having activities in the AC-cooled parcels are assumed to have significant heat reprieve. Biking and walking trips are assumed to be carried out with no temperature control. Activities on no AC-cooled parcels are also assumed to be carried out under the given environmental temperature. As there are many measures of environmental temperature, radiation, and personal comfort, flexibility is provided in Icarus for considering different types of heat exposure metrics. T_{air}, T_{MRT}, and T_{WBGT} are each considered.

T_{air} measures how hot/cold the air is without considering other effects such as wind, radiance, and humidity effect on temperature. T_{air} in Icarus is obtained from the Daymet dataset, which describes the daily temperature lows and highs at 1km*1km grid, available from 1980 over continental North America (Thornton et al., 2021). Assuming the minimum temperature (T_{min}) occurs before dawn (t_{dawn}), the maximum temperature (T_{max}) occurs in the early afternoon (t_{peak}), then the hourly air temperature function can be interpolated using a sinusoidal function per Equation 3.1. Since near-surface air temperature measurements are the primary input for Daymet data (Thornton et al., 2016), it is safe to assume the T_{air} is equal to the Daymet temperature.

$$T_t = \begin{cases} T_{min} * \cos\left(\pi * \dfrac{t_{dawn} - t}{24 + t_{dawn} - t_{peak}}\right) & t < t_{dawn} \\ T_{min} * \cos\left(\pi * \dfrac{t_{peak} - t}{t_{peak} - t_{dawn}}\right) & t_{dawn} \le t < t_{peak} \\ T_{min} * \cos\left(\pi * \dfrac{24 + t_{dawn} - t}{24 + t_{dawn} - t_{peak}}\right) & t \ge t_{peak} \end{cases} \quad \text{Equation 3.1}$$

T_{MRT} is a measure of the total incident shortwave and longwave radiation on the human body (Middel & Krayenhoff, 2019). T_{MRT} data can be obtained through observations or modeling (Crank et al., 2020; Zhang et al., 2015). In our Icarus implementation, we use T_{MRT} simulated from Google Street View images using a deep learning image segmentation approach (Lukasczyk et al., 2016; Middel et al., 2017). Since the resulting data are limited to roads where street view images are present, Icarus assumes a default T_{MRT} value for missing locations that equals spatially averaged T_{MRT} with a 0-10% tree shading ratio. Since the T_{MRT} readings represent environmental radiance, especially the sun's radiance flux for outdoor environments, it is safe to assume

the T_{MRT} is equal to T_{air} before sunrise and after sunset, or in indoor environments (Kántor & Unger, 2011).

T_{WBGT} is a widely used index of heat stress to measure worker heat stress by considering humidity, sun, and wind in addition to air temperature (Budd, 2008; OSHA, 2015). T_{WBGT} can be obtained from measurement (Budd, 2008) or empirically developed models (OSHA, 2015; Stull, 2011; Vanos et al., 2021). As citywide T_{WBGT} is less common, Icarus uses functions from OSHA (2008), Vanos (et al., 2021) and Stull (2011) to calculate T_{WBGT} when both T_{air} and T_{MRT} are presented. The OSHA manual (2015) offers Equation 3.2 and Equation 3.3 for T_{WBGT}:

$$T_{WBGT} = 0.7 * T_W + 0.2 * T_G + 0.1 * T_{air} \quad \text{Equation 3.2}$$

Where T_w is the Nature Wet-Bulb Temperature, and T_G is the Globe Temperature. Icarus adapts the T_w calculation from Stull (2011) showing in Equation 3.3:

$$T_w = T_{air} atan[(RH + 8.314)^{0.5}] + atan(T_{air} + RH) - atan(RH - 1.676) + 0.004(RH)^{1.5} atan(0.0231RH) - 4.686 \quad \text{Equation 3.3}$$

Where RH is the relative humidity.

For indoor, or outdoor environments without solar load, T_G equals to T_{air}. For an outdoor environment with solar load, T_G in Equation 3.2 and Equation 3.3 is calculated by solving for T_G in the formula (Equation 3.4) from Vanos et al.(2021):

$$T_{MRT} = \sqrt[4]{(T_G + 273.15)^4 + (0.24 + 2.08v_a^{0.5} + 1.14v_a^{0.667})(T_G - T_{air}) * 1} \quad \text{Equation 3.4}$$

-273.15

Where v_a is the wind velocity.

The ingested temperature and environmental data can be in different formats, spatial resolutions, and temporal resolutions. Icarus interpolates the min and max T_{air} to the same temporal resolution as T_{MRT} using the sinusoidal function. Further, the temperature data in different spatial resolutions are spatially joined with the roadway network. A spatially averaged value of each temperature profile is retrieved for a 30-meter buffer radius around roadway links. As such, Icarus built a transportation network with the spatiotemporal temperature information for the personal heat exposure simulation.

3.2.1.2. Simulation

After the core data ingestion, Icarus runs the simulation by first extracting the trip and activity schedules from ABM output, allocating the location of activities and O/D of trips to the parcels, then routing the trips on the roadway network loaded in the simulation environment. After routing, the trip path and activity locations would be used to estimate the personal heat exposure and heat stress. Lastly, trips where the agent may have a challenge gaining reprieve from the heat, even after agents rest in an AC-cooled environment, are assessed. The following sections will discuss the details and assumptions of each step in the simulation process.

3.2.1.2.1. Routing

The active trips from the ABM output are extracted to carry out the routing. Icarus can accommodate two simulation engines: a Dijkstra shortest pathfinder, or a

MatSIM travel simulation. The Dijkstra shortest path algorithm finds the route for each trip in a weighted roadway network. Icarus users can weigh the network by distance or by both distance and temperature. With a distance-only weighted network, the Dijkstra algorithm returns the shortest path between the origin-destination (OD) pair. With distance-temperature weighted networks, cooler but slightly longer routes are selected (Middel et al., 2017). The shortest pathfinder returns the nodes and links on trips' routes. Routes of in-vehicle trips would not affect the temperature measures that an agent experiences as they are constantly under AC. Hence, the model does not route personal car and public transport trips. MatSIM is the start-of-art open-source agent-based simulation platform for transportation planning. Icarus can generate the transportation network, agent plans, and the simulation configuration file required by MatSIM. While computationally equivalent to Dijkstra, MatSIM can be used to adjust travel schedules with modifications to the underlying utility function. For the proof-of-concept case study, Dijkstra shortest pathfinder is used in this paper.

3.2.1.2.2. Heat Exposure Calculation

Heat exposure measures — T_{air}, T_{MRT}, and T_{WBGT} — estimate the given environmental temperature that trips and activities are likely to experience at the time when agents carry out these events. Assuming all activities happen in an indoor environment, which is always under shading, the T_{air} exposure of activities would be equal to T_{MRT} (Kántor and Unger, 2011). The default T_{air} in an AC-cooled environment is set as 26.6 °C (80 °F) in Icarus. As such, for in-vehicle trips and activities under AC, their T_{air} exposure is constantly 26.6 °C (80 °F) and T_{MRT} is equal to T_{air}. For activities in

parcels without AC, the T_{air} is equal to Daymet readings at the parcel location. Heat exposure for active trips is calculated in Equation 3.5,

$$T_{i,j} = \frac{\sum_{r \in R}(L_r * T_r)}{\sum_{r \in R} L_r} \quad \text{Equation 3.5}$$

where $T_{i,j}$ is the ambient temperature for a person i, in trip j. $T_{i,j}$ can be either T_{air}, T_{MRT}, or T_{WBGT}. R is the collection of links on the route for a trip j. Link r should always be in R. T_r is the temperature (T_{air}, T_{MRT}, or T_{WBGT}) at the link r when trip j happens. L_r is the length of link r. The calculated trip and activity heat exposure can then be used for heat stress classification.

3.2.1.2.3. Heat Stress Classification

Icarus provides three heat stress classification matrices to rank the active trips heat exposure level, recognizing the variety of temperature measures and little consensus on the relevant heat exposure metrics for predicting health outcomes. The WBGT work/rest table is introduced to rank the trip heat exposure using T_{WBGT} and trip duration. Further, a four-level rating scheme based on the quartile of calculated T_{MRT} and T_{air} for the simulated agents in ABM output is used to rank the trip heat exposure from *cool* to *very hot*.

Heat stress level identification with WBGT Work/Rest table

The WBGT work/rest table (W/R table) is widely used to provide guidance on the work and rest duration for workers (ACGIH, 2019; Epstein & Moran, 2006; Sutherland, 2015). The W/R table suggests the work-rest cycles a person should follow under different environmental temperatures, considering their time in that environment, the

clothing they wear, their workload, and acclimation to heat (ACGIH, 2019; Iverson et al., 2020). Icarus adapts the W/R table designed by Oklahoma Mesonet Agriculture program (Sutherland, 2015) with assumptions to classify the potential heat stress level for each trip. Assuming that all agents in ABM output are acclimated, wearing long sleeve shirts and pants, the adjusted W/R table used in Icarus is shown in Table 3.2. Icarus uses the trip-activity cycles to analogize the work-rest cycle in the W/R table. Walking and biking are classified as moderate and heavy workload according to their metabolic equivalent of task (MET) level (National Cancer Institute, 2002; Tudor-Locke et al., 2009). Based on duration and T_{WBGT}, the heat stress levels of trips include *no risk*, *low risk*, *moderate risk*, *high risk*, *extreme risk* as shown in Table 3.2. Besides the listed stress levels, Icarus introduces a *violation of the W/B* level to categorize the trips that contravene the suggested work-rest cycle.

Table 3.2. WBGT Work/Rest Table (Adapted From Sutherland, 2015)

risk level	WBGT		trip/activity duration (minutes)	
	(C°)	(F°)	Walking (moderate work)	Biking (heavy work)
no risk	25.6-25.9	78-79.9	continuous	50/10
low	26-28.9	80-84.9	50/10	40/20
moderate	29-30.9	85-87.9	40/20	30/30
high	31-31.9	88-90	30/30	20/40
extreme	>32	>90	20/40	10/50

Heat exposure level identification with T_{MRT} and T_{air} quartiles

Icarus introduces the heat stress level classification schemes based on the trips T_{MRT} and T_{air} quartiles, considering the limitations of the WBGT W/R table. There is no standard threshold to distinguish low to high heat exposure using T_{MRT}, and T_{air}, hence

trip exposures are grouped based on the quartiles. From the low to high temperature, trips are grouped as *cool* (lowest 25%), *warm* (25-50%), *hot* (50-75%), and *very hot* (highest 25%) based on the four temperature groups binned by quartiles. For each quartile, the demographic group that carried out the trips was also studied.

3.2.1.2.4. Reprieve of Trips Heat Exposure during the Activity

If trip-destinations are activities where AC is equipped, agents carrying out these activities and trips might be able recover from the excessive heat exposure. On the contrary, agents may not recover from heat if their activities are in no AC-cooled parcels. Trips are in two general categories: in-vehicle trips and active trips. To determine the portion of trips that cannot be reprieved after outdoor active trips, we categorize the trips and their reprieve conditions based on Figure 3.1 and as follows. For in-vehicle trips, as the temperatures are assumed constantly under AC, the heat exposure during the trip would not necessarily be reprieved from the activity follow. Active trips may *not be reprieved* from excessive heat if the activity followed happens in a parcel without AC and with a high environmental temperature, or the duration of activity in the AC-cooled environment is too short. As such, whether a trip can be reprieved in the AC-cooled parcel is determined by how long an agent stays in the AC-cooled room after travel outside. Equation 3.6 is used to determine cumulative heat exposure for trips and activities following the trip:

$$E_i = -t_{act,i} * 26.6°C + t_{trip,i} * T_{trip,i} \qquad \text{Equation 3.6}$$

Where $t_{act,i}$ and $t_{trip,i}$ are the duration of activity and trip, $T_{trip,i}$ is the air temperature of the trip. If E_i is larger than 0, then the time an agent stays in the AC-

cooled room is long enough to get a reprieve. Otherwise, the trip cannot get reprieved indoors since the time one stays in the AC is too short. Figure 3.2 demonstrates the detail of how to define if a trip can reprieve its heat exposure or not.

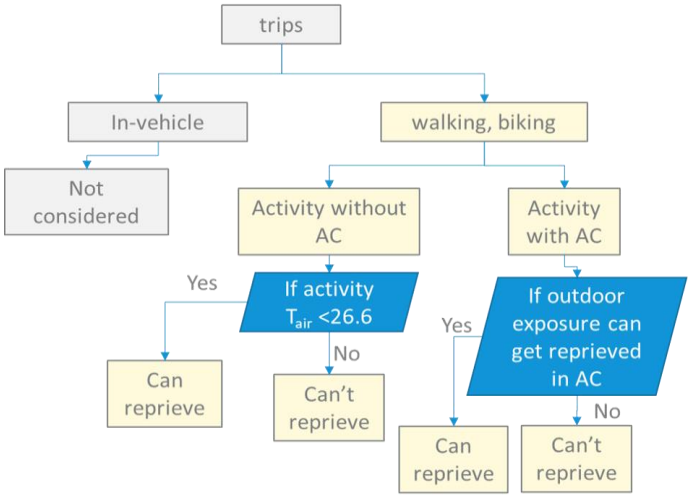

Figure 3.2. Decision Tree for Trips Heat Reprieve Assessment

3.2.2. Metro Phoenix Case Study

The implementation and testing of Icarus have focused on a case study of the Phoenix metropolitan region in Arizona. The Phoenix metropolitan region is an ideal case study area as it is located in the hot and arid Sonoran Desert (D. M. Hondula & Kuras, 2021) and has a population of 4.85 million people in 2020 https://www.zotero.org/google-docs/?6G8mmM(US Census Bureau, 2022). Metro Phoenix has an average of 175 days a year with a daily maximum air temperature above 32°C (90 °F) (Lawrimore et al., 2016). The extreme temperature is expected to increase as a result of climate change. Despite these extreme temperatures, Metro Phoenix has been one of the fastest-growing cities in the country since the 1950s, and the population is projected to grow to 8.04 million by 2050 (State of Arizona, 2018). The high

temperature combined with the large population created a significant amount of heat-related mortality in Metro Phoenix. In 2020 Metro Phoenix attributed 191 heat-associated deaths, and those aged 50-64, and 75+ had the highest rates of heat-associated death (Maricopa County Public Health, 2017, 2020). The increase in temperature has a direct but nonlinear relationship with heat death (Eisenman et al., 2016). It is vital to understand the heat exposure during outdoor travel for residents in Metro Phoenix.

For the case of Metro Phoenix, the simulation is run for a synthetic population of 3.8 million travelers on June 30th, 2017, the middle of summer. The synthetic population and their activities/trip schedules, which is generated from the 2010 household survey for the whole of Maricopa County, are obtained from the ABM output developed by the Maricopa Association of Governments (MAG) (Vovsha et al., 2011). The MAG ABM output contains 18.6 million trips, with 93.61% (17.41 million) in-vehicle trips, 5.6% (1.05 million) walking trips, and 0.79% (148,541) biking. The simulation assumes the population and travel pattern will remain the same in 2017, although the ABM was based on the 2010 survey. The ABM output gives the activity location in MAZs. The 2018 assessor database was used to assign the activity locations, which will be used as the O/D for trips (Maricopa County Assessor's Office, 2018). For instance, if an activity's purpose is *groceries,* Icarus will assign a non-residential parcel located in the given MAZ to the activity location. The details of activity types and parcels assigned are listed in Appendix A. Households are assigned to distinct residential parcels. However, multiple households can be assigned into the same parcel if the number of residential parcels is smaller than the total household number in a MAZ. When a MAZ contains no residential

parcels, households are assigned non-residential parcels randomly. Since trips are the travel chain that links the activities, the parcels selected will be used as the origin and destination of the trips. The assessor database is also used to estimate the AC at the parcel level. For non-residential parcels, Icarus assumes the following land-use categories would not have AC: barns, farm storages, garages, car wash, and pavilions. Details of the non-residential parcel types and AC assumptions are listed in Appendix B. For residential parcels, if the dataset provides the AC information for each record, Icarus would follow these records. Otherwise, Icarus would assume all residential parcels are equipped with AC.

The weather of the simulation day was hot and dry, with the lowest T_{air} between 13.26 °C (55.9 °F) to 25.29 °C (77.5 °F) before sunrise and the hottest temperature between 28.82 °C (83.9 °F) to 43.15 °C (109.7 °F) around 15:00h. Icarus also applies the T_{MRT} during daytime derived from Google Street View in the Metro Phoenix case study (Middel et al., 2017). The T_{MRT} only provides temperature information after sunrise and before sunset. The T_{MRT} before sunrise and sunset is estimated to be equal to T_{air}. The wind velocity is assumed to be a fixed speed of 3.2 m/s (7mph), which is the average wind speed in June observed at Phoenix Sky Harbor station (Lawrimore et al., 2016). The relative humidity (RH) is assumed to be 20%, considering the monsoon season humidity in Phoenix. T_{air}, T_{MRT}, wind speed, and RH will be used in calculating T_{WBGT}.

3.3. Results

The results show heat exposure of individuals across the population, heat stress by demographic groups, and spatially explicit outcomes – focusing on walking and biking –

to identify potential demographic disparities in heat stress. A statistical summary of the Icarus simulation results—including the travel speed, trip duration, and distance—is discussed to validate the simulation results. Following, heat exposure in T_{air}, T_{MRT}, and $T_{WBGT,}$ and heat stress classifications across different demographic groups are demonstrated. Lastly, locations where travelers are likely to experience excessive heat exposure are discussed. As the heat mortality data highly correlate with age (Maricopa County Public Health, 2017, 2020), the discussion focuses on the travel patterns through the lens of different age groups.

3.3.1. Non-motorized Trips Travel Patterns and Icarus Simulation Statistics

From the ABM output, car driving is the dominant travel mode for residents in the Phoenix metro region. Over 87% of agents use cars as their only transportation mode, and less than 3% of people use walking and biking in their daily travel plan. There are 1.17 million active trips carried out by the 3.8 million agents. Icarus successfully simulated 96% of those active trips. The 4% of trips not simulated was because the origin and destination of the trip are the same or Icarus can't find a suitable route in the network. Table 3.3 shows summary statistics of Icarus simulation results. From the ABM output and simulation results, the active trips are short in duration and distance. The average walking and biking trip distances are 1.76 km (1.1 miles) and 3.17 km (1.98 miles) respectively. And the synthetic population spends 14.3 and 9.34 minutes on average on walking and biking trips. As the trip duration is given by the ABM output, the simulated trip speed can be estimated by dividing the simulation trip length by the trip duration. 90% of the simulated walking trips are within the speed range of 2.35 to 17.85 km/h (1.5

to 11.1 mph) and biking speed within 10.31 to 48.6 km/h (6.4 to 30 mph). The mean speed of running is around 27.27 km/h (17.22 mph) (Seidl et al., 2021). While bikers can maintain a speed of 35 km/h (22 mph) on flat surfaces (Whitehouse, 2019), electric bikes can reach 48.3km/h (30 mph) (Paulson, 2020). Considering the walking trips may also include running or even sprinting, bike trips might be complete with e-bikes, the simulated walking trips are in the reasonable speed range.

Table 3.3. Statistics of Icarus Simulation Results

Trip type	Number of trips[1]	Trip Duration[1] (minutes) *mean (5%, 95%)*	Trip Distance[2] (km) *mean (5%, 95%)*	Speed[2] (kph) *mean (5%, 95%)*
walking	1,030,014	14.3 (1.3, 14.04)	1.76 (0.4, 3.66)	8.4 (2.35, 17.85)
biking	147,142	9.34 (2.1, 21.3)	3.17 (0.6, 7.5)	23.35 (10.31, 48.6)
car driving	17,245,967	12.4 (1.2, 34.15)	N/A	N/A
public transit	142,869	78 (20.48, 142.05)	N/A	N/A

1. From ABM output
2. From Icarus output

Although active trips are of short durations in general, certain age groups tend to spend longer time on their trips compared to other groups (Table 3.4). People over age 64 tend to take shorter active trips compared with other age groups, as over 96% of their active trips are less than 20 minutes. Young kids (under 5) and people aged between 50 to 65 years old tend to have longer-duration active trips. According to ABM, the major travel purpose for people over 64 is to travel between home, shopping, and maintenance. The main purpose of young kids is to travel between home, school, and visiting relatives. According to the ABM output, these young population groups may not carry out the

outdoor activities by themselves but be escorted by teenagers or adults. The trip duration difference is likely to impact the heat stress identification when the heat stress index considers the event duration, such as the W/R table.

Table 3.4. Trip Duration for Different Age Groups

trip duration (min)	age group						
	0-5	5-20	20-35	35-50	50-65	65-75	75+
< 20	65.0%	87.9%	91.3%	71.2%	63.3%	96.0%	97.0%
20-30	23.2%	8.5%	6.2%	21.1%	26.6%	2.9%	2.9%
>30	11.8%	3.6%	2.4%	7.7%	10.1%	1.1%	0.1%
number of trips	47,655	290,874	239,908	234,062	184,756	75,110	47,603

Using multiple temperature metrics in the heat exposure study may result in a different exposure value for the same trip, which could make heat stress identification challenging. As shown in Figure 3.3, T_{WBGT} has the lowest temperature range, and T_{MRT} has the highest temperature range. Besides, the three temperature measures used in the Icarus, T_{air}, T_{MRT}, and T_{WBGT}, reach their maximum at different times of the day. While the highest T_{MRT} happens around noon when the sun-radiance reaches its maximum, the hottest T_{air} and T_{WBGT} happens around 15:00. The difference in time of the hottest temperature increases the uncertainty in identifying the personal heat exposure and heat stress classification. From ABM output, people aged between 5 to 20 have a high frequency to travel around 15:00 under the hottest T_{air} and T_{WBGT}. While for people older than 20, they have more active trips when the T_{MRT} is estimated to be the hottest of the day. Just looking at the temperature profile and travel patterns, people above 20-year old tend to have more *very hot* trips under T_{MRT} estimation while people younger than 20-year

old who have *very hot* trips under T_{air} and T_{WBGT} estimation. The details of heat exposure and demographics for very hot trips will be discussed in the next section.

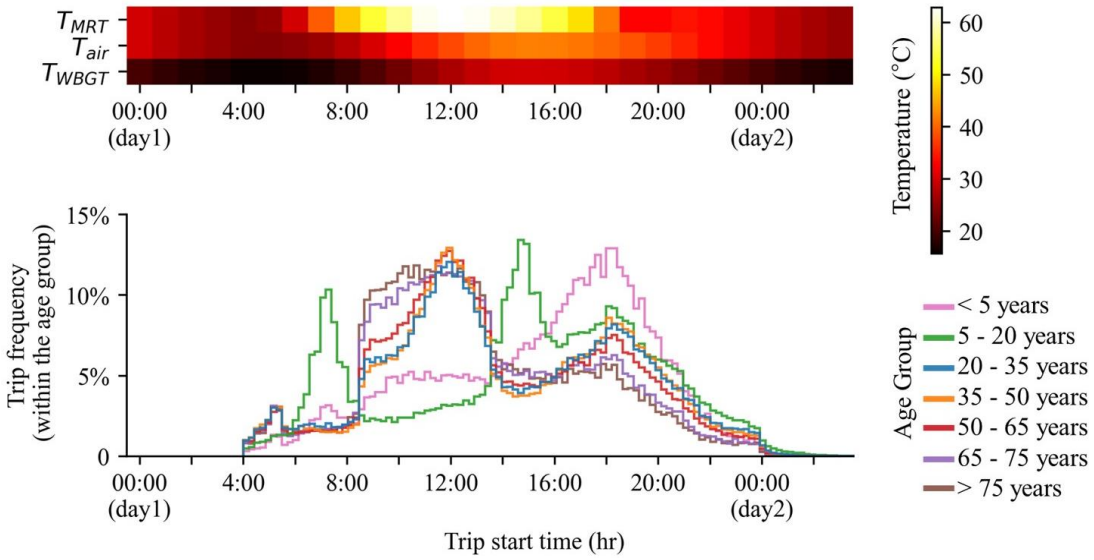

Figure 3.3. The Temperature Range (Top) and Trip Frequency for Each Age Group (Bottom) in the Simulation Day

3.3.2. Personal Heat Exposure

Personal heat exposure during active trips varies based on T_{air}, T_{MRT}, and T_{WBGT} measures. The simulation results show that for active trips, T_{MRT} ranges between 22.03 to 65.24°C (71.66 to 149.43°F), T_{air} ranges between 22.03 to 43.07°C (71.66 to 109.53°F). Trip exposure calculated from T_{MRT} shows a wider range, which may be associated with the high resolution and details of the build environment captured in the calculation of T_{MRT} data. T_{WBGT} ranges between 13.91 to 30.71°C (57.04 to 87.28°F) which is below the 30.71°C *high* risk threshold in the WBGT W/R table. Since the three temperature metrics are completely different physical concepts, the comparison of cross-metric is not proper.

The three temperature measurements would serve as different purposes for assessing the heat vulnerable trips.

3.3.2.1. Heat Stress Levels Across Different Age Groups

The temperature profiles of T_{air} and T_{MRT} t affect the trip temperature estimation considerably, wherein the proportion of trips under *very hot* temperature significantly shifts within each age group (Figure 3.4). The *very hot* trips, marked as red bar in Figure 3., are the 25% of trips with the highest T_{air} or T_{MRT}. When heat stress is classified with T_{air}, people under 20 years have over 35% of their trips classified as *very hot*. The same population group would only have 13% of trips ranked as *very hot* when ranked with T_{MRT}. For people aged between 5-20 years old, the ratio of *very hot* trips under T_{MRT} is 13%, much lower than the 37% *very hot* trips calculated using T_{air}. For the senior population, more *very hot* trips are identified when using T_{MRT} (Figure 3.4.b) compared to T_{air} (Figure 3.4.a). For instance, for people aged 75+, about 35% of their active trips are *very hot* under T_{MRT} and 14% are *cool*. If the temperature is estimated using T_{air}, the same age group would have fewer *very hot* trips (about 22%) and more *cool* trips (26%). This discrepancy is caused by the mismatch of the hottest time of the day in T_{air} and T_{MRT}, identified in the travel pattern and simulation statistics section.

Unlike T_{air} and T_{MRT}, heat stress classified by T_{WBGT} considers not only the temperature, but also the humidity, radiation, wind, and intensity of travel mode and trip duration. Comparing trips using T_{WBGT} and established walk/rest risks, 42% of them have *no risk* since their T_{WBGT} is under 26 °C (Figure 3.4.c). 29.5% of walking and biking trips were simulated to experience T_{WBGT} between 26°C to 29°C, which is classified as *low*

risk. And 22.8% of active trips are simulated to have moderate *risk*. Although most walking and biking trips have short durations and are carried out under moderate $T_{WBGT,}$ 10.5% of active trips violates work-rest cycles the W/R. When considering demographics, a higher ratio (16.9%) of toddlers (younger than 5) have trips that violate the W/R table. The ratio of trips from senior populations (older than 65+ years) that violate the WBGT W/R table is low (less than 0.3%) mainly because this demographic group has short duration trips.

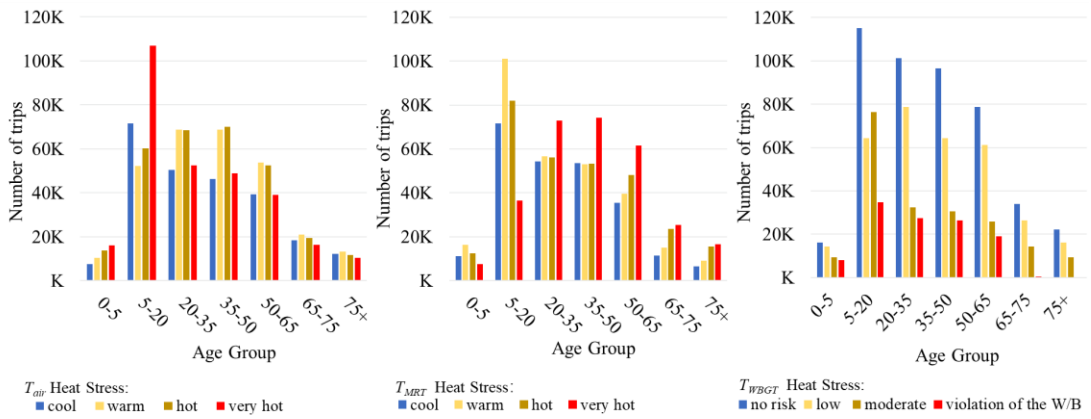

Figure 3.4. Trips Heat Stress Level by Age Groups under T_{air}, T_{MRT}, and T_{WBGT}

Ranking the trip heat stress by both the quartiles of T_{air} and T_{MRT}, or the WBGT *W/R* table, are all potential ways to identify people and travel under extreme heat stress. But the challenge comes with choosing the right temperature measure and heat stress index to identify the heat vulnerable trips and population. Using T_{WBGT}, the majority (71%) of trips are identified with *no* or *low* risk. People under 5 have the highest (16.9%) ratio of their trips that violate the WBGT W/R table. Meanwhile, people ages 75+ are identified as the least risky population as less than 0.2% of their trips violate the WBGT W/R table. Using T_{air}, people ages under 20 have 36% while the rest of the population

have 21% of their active trips identified as *very hot*. And about one fifth of trips carried out by people ages 65+ are identified as *very hot* T_{air}. Using T_{MRT}, over one third of trips from people over 50 years are under the very hot T_{MRT}. But people ages under 20 years find 13% of their trips under *very hot* T_{MRT}. Considering the reported heat-associated death from Maricopa County which finds those ages 75+ with the highest rates of heat-related death while children under 20 only made up less than 1% of the heat-death records (Maricopa County Public Health, 2017, 2020), using T_{air} and T_{WBGT} tend to overestimate the heat stress on young population but underestimate the heat exposure old demographic group may experience. The heat stress levels identified with T_{MRT} matches with the reported heat-associated mortality, where people ages 75+ have more and people younger than 20 have less *very high*-level heat stress.

3.3.2.2. Locations with High Heat Exposure

The link flow - or frequency of active trips passing through a link in the simulated day - for the city of Phoenix is shown in Figure 3.5. In the Phoenix metro region, the busiest link accommodates up to 7,657 trips per day. Most of the links are less traveled. The mean link flow in the network is 70 trips per day, while 95% of the links have less than 282 trips passing through. The most traveled 2% links - with their link flow greater than 500 - are mostly around shopping malls, business centers, city parks, and medical centers (e.g., Carl T Hayden Veterans Affairs Medical Center, Banner Estrella Medical Center).

A colored scheme is used in Figure 3.5 to show the ratio of trips with high heat stress ranking passing through the link. Figure 3.5.a and b show the ratio of *very hot* trips

while Figure 3.5.c shows the ratio of *violated W/R* table trips link flow compared with all trips link flow. To be convenient, the link flow ratio of *very hot* trips or trips that violate WBGT W/R tables are going to be written as the *Flow Ratio*. Demonstrating the *Flow Ratio* in the network could help the user of Icarus to identify the locations where trips with high heat stress are located. On average, about 31% to 33% of the flow on links is contributed by *very hot* trips under T_{air} and T_{MRT}, while 24% of the links flow from trips that violate the *WBGT W/R table*. This is because the number of *very hot* trips is more than twice of the *W/R violation* trips. *Very hot* trips under T_{air} tend to be evenly distributed across the network, as the *Flow Ratio is mainly* between 20% to 50% with little disparity (Figure 3.4.a). Locations with high *Flow Ratio* under T_{air} tend to be spread out among local collectors in the suburban region. Contradictory, *Very hot* trips under T_{MRT} tend to be concentrated near downtown Phoenix and major arterials (Figure 3.4.b) and contribute over 50% of the link flow in these regions. The suburban area shows low concentrations of *very hot* trips under T_{MRT}, as the *Flow Ratio* in suburban areas is mostly below 30%. The trips which have their T_{WBGT} violate the W/R table cluster near the downtown and major arterials (Figure 3.4.c). The *Flow Ratio* maps demonstrate the locations where high heat stress trips are likely to occur and create opportunities for planners to design heat mitigation strategies along the network. But the disparity of *Flow Ratio* maps from different temperature measures posed challenges for decision makers to nail down the locations to make the investment. The *Flow Ratio* maps from T_{MRT} and T_{WBGT} both find that the downtown and major arterials have more high heat stress trips

compared to the suburban region, but this finding still needs to be verified with more studies.

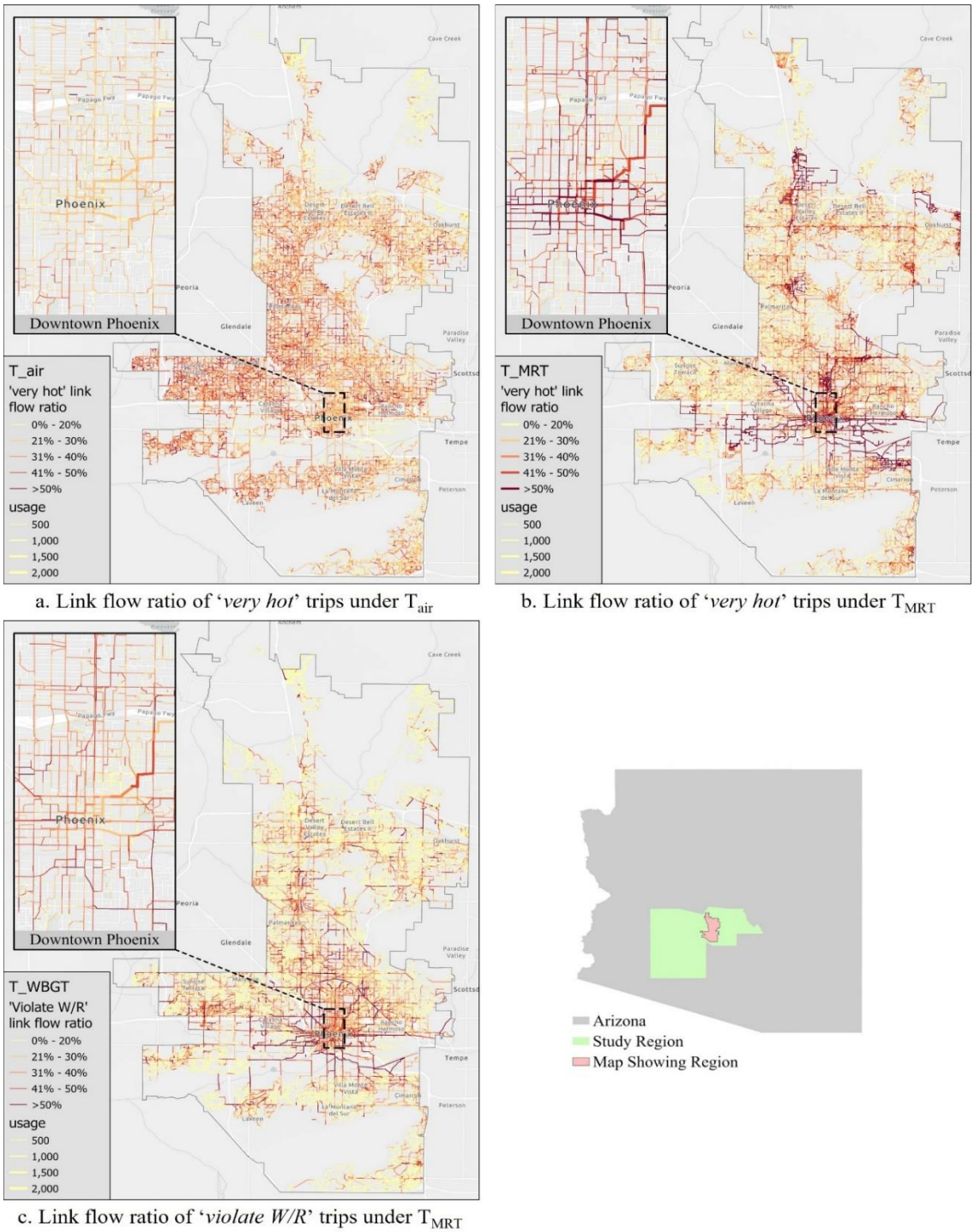

a. Link flow ratio of '*very hot*' trips under T_{air}

b. Link flow ratio of '*very hot*' trips under T_{MRT}

c. Link flow ratio of '*violate W/R*' trips under T_{MRT}

Figure 3.5. High Heat Exposure Trips Link Flow Ratio under Different Temperatures

3.3.3. Trips Cannot Reprieve During the Activity

Travelers who experience heat exposure may get a reprieve from AC during activities. The AC condition of activities is estimated from parcel data. Maricopa county, where the Metro Phoenix is located, has 1.56 million parcels with one fifth of them being non-residential parcels. 99.8% of residential parcels have a refrigerator AC system or wall cooling system installed (Maricopa County Assessor's Office, 2018). Assuming that garages, warehouses, golf courses, storage facilities, greenhouses, farms, carwashes, barns, and pavilions do not have AC installed, about 35% of the non-residential parcels in Maricopa County do not have AC. In the 1.13 million simulated active trips, 72.6% can reprieve from the excessive heat exposure as the agents destine in an AC-cooled parcel and stay at the parcel for enough length. 21.15% of the active trips end up on an AC-cooled parcel, but the duration of the activity was too short for these agents to reprieve from the excessive heat exposure. 5.79% of trips would stop at a parcel with no AC equipment with an above 26.6°C T_{air}. Lastly, 0.46% of trips end on a no AC-cooled parcel but there is no need for these trips to be reprieved from excessive heat, since both the trips and activities happen at a time when T_{air} is below 26.6°C.

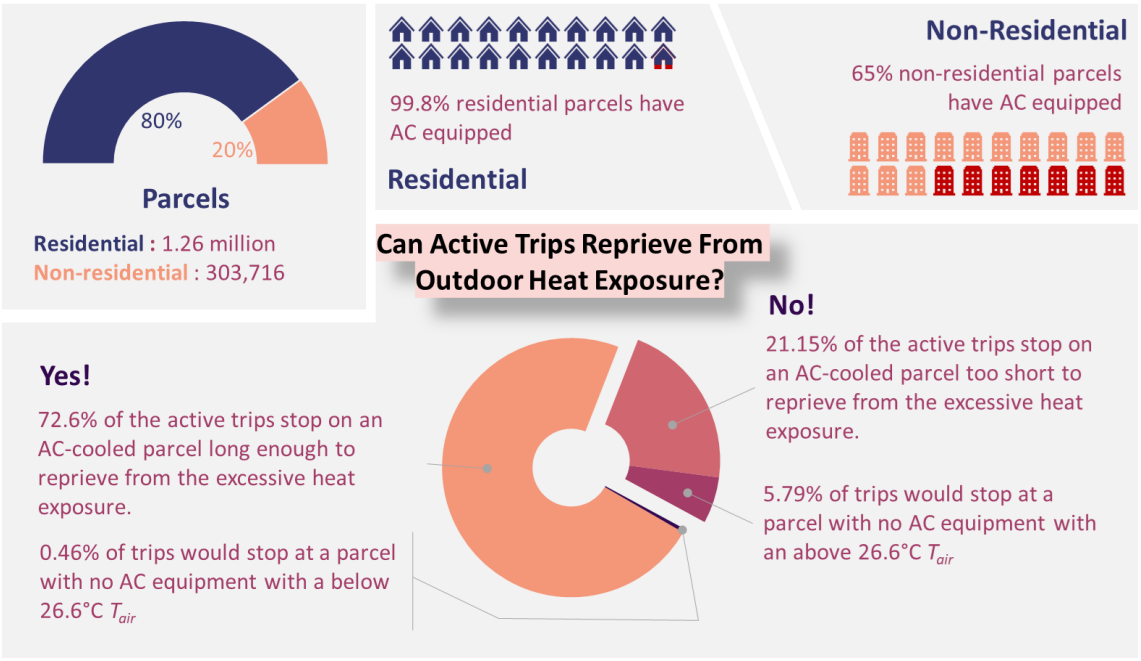

Figure 3.6. Infographic of Parcel, AC, and Trips Heat Reprieve

3.4. Conclusion and Discussion

Transportation policies are evolving to meet global sustainability goals, emphasizing shifts of travelers away from automobiles to more walking and biking to reduce the emission of greenhouse gasses and air pollutants. The Phoenix metro area has historically been heavily car-dependent, and there is a significant potential to motivate residents of the region to shift to active trips. However, the extreme summer temperatures may limit people's willingness to shift their transportation mode. This study demonstrates a way to understand the personal heat exposure of urban dwellers from the individual scale to the population scale and to identify the location where high heat exposure travels are likely to occur. This research contributes to the growing studies of personal heat exposure and provides a flexible framework - Icarus - to simulate personal heat exposure at the population scale. The analysis shows that travel patterns (such as trip duration and

the trip start time) for different demographic groups (age group in these circumstances) affect personal and population heat exposure.

3.4.1. Differences in Personal Heat Exposure are Revealed with Multiple Temperature metrics

In this case study, we found that the use of different temperature measures resulted in widely varying estimates of personal heat exposure. On a population scale, using T_{MRT} to calculate heat exposure, trips that happen around noon are more likely to experience the hottest temperature, while using T_{air} and T_{WBGT}, the hottest trips are more likely to happen around early afternoon. On a personal scale, people ages 65+ are more likely to experience *very hot* temperatures under T_{MRT}. In contrast, people younger than 20 are more likely to have *very hot* heat exposure under T_{air}. With T_{WBGT}, most of the population is classified as under moderate heat risk, and nearly all trips taken by senior residents were classified as safe. At the city scale, the locations where the high heat exposure trips are more likely to happen near city centers and major arterials under T_{MRT} and T_{WBGT}. But high heat exposure trips under T_{air} are identified near suburban areas. The inconsistency of heat exposure using the different temperature measurements raises the need for further studies to validate the temperature assessments and identify the most appropriate temperature metric for simulations. The most used heat stress identification index (the WBGT W/R table) has limitations in considering individual health conditions and may not be well suited for different demographic groups.

3.4.2. Novelty of Icarus

Icarus is novel in that it is the first of its kind to combine meteorological data on multiple scales with a transportation network into one platform to simulate the personal heat exposure at the population scale. On one hand, Icarus is designed to take the ABM output for population-scale heat exposure estimation. On the other hand, the modularized design of Icarus allows future users to change the input data based on the specific study region, or just focus on the personal heat exposure simulation if ABM data is not available. Icarus also efficiently utilizes computational resources and manages voluminous data, especially for large-scale analysis. For instance, it takes 30 minutes to simulate the personal heat exposure of 3.8 million agents with 1.17 million active trips in the Phoenix Metropolitan Area. The rich information in the Icarus output opens opportunities for the study of the population-scale heat risk and infrastructure planning that affect heat exposure. This study expands the method Karner (et al., 2015) used by routing the individuals in the spatial-temporal meteorologically attributed network. ABM output is used to estimate the heat exposure at the population scale in this study. Future researchers can use Icarus to assess the population heat exposure with travel survey data or GPS tracking data if the ABM data is not available. Icarus is different from previous personal heat exposure simulation models that considered human thermal response to heat (Glass et al., 2015) but did not consider the travel and activity behavior. However, the human heat balance model can be incorporated into Icarus in future updates to help identify the heat stress.

3.4.3. Limitation

The limitations of Icarus come from the simplification of the travel model and different temperature metrics while not deciding which one is better. Uncertainties were introduced into the model during the random selection of parcels in the MAZ and assuming the shortest path as the routes agents would choose. The parcel assignment algorithm introduces uncertainty as to the start, and end location may differ at the neighborhood scale from the actual, which affects the accuracy of routing and AC-cooled parcel assessment results. Traveler walking or biking path choice could be affected by safety, preference, or street perceptions and conditions (Marshall & Garrick, 2010; Titze et al., 2012). Downscaling the MAZ-based ABM to a more precise scale, such as the parcel level and active trip routing pathfinding, are active research topics beyond this study. The use of different temperature metrics complicates the result interpretation, as the high heat stress population and locations depend on the metric used for analysis. Previous studies pointed out that T_{air} is not a comprehensive indicator of personal heat exposure as it is only one of the several environmental factors (Hondula & Kuras, 2021; Kuras et al., 2017). While the T_{WBGT} is widely used to identify the heat stress risk, the WBGT W/B table has its limitations in identifying the heat stress for the senior population. More research needs to be done to identify the temperature metrics most suitable for personal heat exposure study.

Despite the limitations, Icarus creates immense value in person-based heat exposure simulation. By using ABM output to create a bottom-up picture of the heat exposure at a population scale, Icarus provides a more detailed look at exposure to extreme heat, which is often limited to proxy variables such as land surface temperature,

which do not reflect the entire temporal and spatial variation of temperature or travel behavior that greatly influence exposure (Bao et al., 2015; Bernhard et al., 2015; Kuras et al., 2017). Icarus could enhance our understanding of the relationship between exposure to extreme heat and social vulnerability and their role in influencing heat risk.

CHAPTER 4

URBAN HEAT VULNERABLE TRIPS IDENTIFICATION AND MITIGATION STRATEGIES: OPTIMIZE TREE PLANTING LOCATIONS USING ICARUS OUTPUT

4.1. Introduction

Climate change is expected to significantly increase urban heat, exacerbating heat-related health risks among urban dwellers. Maricopa County, AZ, reported 339 heat-associated deaths in 2021, a 5% increase from 2010, a 70% increase from 2019, and a 220% increase from 2011 (Maricopa County Public Health, 2021). Rising summer temperatures, extended heatwave durations, and increasing population density contribute to the city's increasing heat mortality (Hajat & Kosatky, 2010; O'Neill et al., 2017; Perkins-Kirkpatrick & Gibson, 2017). Encouraging active mobility and transit can produce co-benefits for residents by increasing physical activities and reducing chronic disease (Nazelle et al., 2010). Cities acknowledge that accommodating active mobility is necessary to curb urban heat island effects, and GHG emissions (City of Mesa, 2014). However, transportation planning in US cities has historically focused on car traveling. Promoting walking and biking without proper planning and transportation infrastructure to combat extreme heat exposure may cause more heat-related morbidity and mortality in the future.

Environmental cooling studies have shown that changing urban configurations can create cooling effects. Increasing tree canopy or installing cool roofs have been approved to reduce the neighborhood air temperature (Aminipouri et al., 2019; Middel et

al., 2014; Tan et al., 2017). In cities, geometric and surface cover combinations influence the temperature at screen height. Studies often use Local Climate Zone (LCZs) models to define the built environment, based on similar geometric and land cover patterns (Stewart et al., 2014). Knowing the cooling benefit of changing the built environment is helpful but not sufficient. The results in chapter 3 showed that active trips use only a small portion of the city street network in a highly car-dependent city. And the corridors with high heat exposure trips do not necessarily correspond to where people travel most. As cities with limited budgets aim to change the built environment to reduce heat island effects, there are lingering questions as to where to implement cooling strategies so that the most vulnerable populations receive the greatest benefit.

Personal heat exposure studies, which identify the populations with high exposure, are a relatively new but active area of research. The exposure estimates the ambient temperature a person experiences during a trip or a study period (D. Hondula & Davis, 2012, Chapter 3). Personal-scale heat exposure studies the thermal environment people experienced (Karner et al., 2015; Kuras et al., 2015, 2017). At population-scale, heat exposure studies review the sub-populational adverse health outcomes related to the high environmental temperature (Chow et al., 2012; Karner et al., 2015). Both personal and populational heat exposure commonly use the fixed-point weather stations temperature in the assessment, although studies have identified the environmental conditions people experience are heterogeneous (Hondula et al., 2021). Besides, different behavior could also affect personal heat stress (ACGIH, 2017).

This study developed a framework to estimate the effectiveness of personal heat mitigation at the nexus of environmental temperature, people's traveler behavior, and the urban built environment. The specific objectives in this paper are to 1) test if changing the built environment towards cooler configurations can significantly reduce heat exposure for travelers, 2) estimate if changing the travel behavior—rerouting people to cooler corridors—can reduce traveler heat exposure, and 3) find the marginal benefits of built environment and travel behavior change. To achieve these objectives, simulations of Phoenix metro area daily travel were conducted on Icarus—a personal heat exposure simulation platform—to test how changing environments and behavior could potentially reduce heat exposure.

4.2. Methodology

Three sets of simulations were conducted to assess the heat mitigation effects: the baseline, changing built environment, and changing travel behavior. The baseline simulation captures heat exposure of all Phoenix metro active (walking and biking) trips today, prioritizing the shortest travel distance. With a baseline simulation profiles current heat exposure and travel behavior, changing built environment, and behavior simulations are considered to compare their heat reduction benefits.

All simulations are conducted in Icarus developed in chapter 3, and combine publicly available street network data, spatial-temporal specific temperature data, environmental data, etc. for the Phoenix metro area to estimate residents' personal heat exposure. The details of the three simulations are described in the following subsections.

4.2.1. Simulation Platform and Setup

The simulations are conducted in Icarus designed in Chapter three. Icarus is a personal heat exposure simulation platform built in Python. It estimates the personal heat exposure with the consideration of an individual's activity and travel schedule, the transportation infrastructures, environmental temperature, and the indoor/outdoor environment. With the input data, Icarus first constructs a transportation network with the spatial-temporal temperature information, then extracts the daily travel and activity schedule for each person in the simulation, simulating the travel route of each person. Finally, Icarus calculates the personal heat exposure based on the environment temperature at the location where the activity and travel take place.

The heat mitigation benefits from changing environment and travel behavior have focused on a case study of the Phoenix metropolitan region in Arizona. The Phoenix metropolitan region is a rapidly growing city located in the hot and arid Sonoran Desert (Hondula & Kuras, 2021). The high temperature combined with the large population created a significant amount of heat-related mortality, for instance, in 2020 Metro Phoenix attributed 191 heat-associated deaths (Maricopa County Public Health, 2017, 2020). The simulation is run for a synthetic population of 3.8 million travelers on June 30th, 2017, the middle of summer. The synthetic population and their activities/trip schedules, which is generated from the 2010 household survey for the whole of Maricopa County, are obtained from the Activity Based Model (ABM) output developed by the Maricopa Association of Governments (MAG) (Vovsha et al. 2011). The MAG ABM output contains 18.6 million trips, with 93.61% (17.41 million) in-vehicle trips, 5.6% (1.05 million) walking trips, and 0.79% (148,541) biking. The simulation assumes the

population and travel pattern remains the same in 2017, although the ABM was based on the 2010 survey. The ABM output gives the activity location in MAZs. The 2018 assessor database was used to assign the activity locations and as the O/D for trips (Maricopa County Assessor's Office, 2018).

The weather of the simulation day was hot and dry. While many temperature measures exist and can be meaningful, Icarus applies the Mean Radiant Temperature (TMRT) – a measure of net effect of air temperature and radiation from surrounding surfaces – data provided by Middel et al. (2017) as the temperature profile. T_{MRT} captures the environmental radiation on human bodies. And T_{MRT} used in this study has a higher spatial and temporal resolution which captures the temperature differences within the street network. The T_{MRT} of the simulation ranges from 13.26 °C (55.9 °F) in early morning before the sunrise to 68°C (154.4 °F) at noon with the highest sun radiance and no shade. The T_{MRT} model only provides temperature information after sunrise and before sunset, and the values before sunrise and sunset are estimated to be equal to air temperature.

A network of 81,559 km extracted from OpenStreetMap (OpenStreetMap Contributors, 2015) was loaded in the simulation, which consists of arterials, local roads, and bike and pedestrian trails. As this study focuses on choosing the feasible routing for pedestrians and bicyclists, freeways are blocked for the path-finding algorithms.

4.2.2. Simulation 1 - Baseline of Personal Heat Exposure

The baseline simulation profiles the synthetic population's personal heat exposure and identifies where people are traveling in the current network. ABM data provides the

daily travel and activity schedule for the synthetic population in the Phoenix metro. Icarus simulated the walking and biking trips as they are constantly exposed to outdoor temperature. Although people chose paths based on multiple reasons, such as their preference for the environment, or safety concerns, in the baseline simulation, all active trips are assumed to travel on their shortest distance path and routing with a bi-direction Dijkstra algorithm (Hagberg et al., 2008). Beside active trips heat exposure, Icarus also estimated the frequently visited corridors in the baseline simulation. The temperature reading of the hottest 20% active trips in the baseline simulation are identified and used as the threshold to bin the hottest trips in the changing environment and travel behavior simulations.

4.2.3. Change Built Environment or Travel Behavior to Reduce Heat Exposure

With a baseline simulation, two heat-reduction simulations are developed to assess the potential heat exposure mitigation from changing built environment and travel behavior. Transforming the built environment by increasing the shading and pervious pavement may reduce the local temperature along the resident's travel path, which would eventually mitigate traveler heat exposure. To compare the different levels of heat mitigation intensities, two cooling scenarios were selected in the changing environment simulation. Travelers can also reduce their heat exposure by changing their travel behavior, which is rerouting to a cooler path with some extra distance.

4.2.3.1. Simulation 2 - Changing the Built Environment

Changing the built environment with more shading, and cooling pavement may potentially reduce the radiant effects on travelers. The built environment transformation

assumes corridors can cool down to a temperature equivalent to the coolest roadways in the same local climate zones (LCZs). LCZs are classifications of the urban and rural landscape with similar structural and land cover properties (Stewart et al., 2013). In the current roadway network, Although the temperature on roadways fluctuates during the time of day, some corridors have a lower total and peak temperature in the network. The simulation assumes corridors temperature can be reduced to the coolest ones in the current network by changing their built environment configuration to those identified as the coolest. And corridors may be more likely to be transformed to the coolest ones identified in the same LCZ other than across LCZ since corridors within the same LCZ already share the similar structure and land cover properties.

Roadways with low temperature in the LCZs are selected as cool corridors. The selection of cool corridors embraces the following principles. First, LCZ data (Wang, et al., 2018) are introduced to find cool and uncooled corridors, and the cool corridors are selected for each LCZ. Secondly, two scenarios—the coolest 15% and the coolest 10%—are considered to resemble different cooling levels. Thirdly, the cool corridors are selected based on the total T_{MRT} between 8 am and 8 pm. The cool corridors selection excludes outliers identified with the 1.5xIQR rule where a numerical fence was built by taking 1.5 times the interquartile range.

After identifying the cool corridors, the rest of the roadway network are potential candidates for environmental transformation. Gradually increased the roadway transformation from the 1 km to all used non-cool corridors, miming the limited to eventually unlimited resources used in the environmental change. Environmental change

embraces the following assumptions. First, the non-cool corridors can only be cooled to the identified cool corridors in the same LCZ. Second, when corridors get selected for cooling, their T_{MRT} day is replaced by the T_{MRT} from the cool corridors located in the same LCZ. Third, the candidate non-cool roadways are chosen according to the link flow in the baseline simulation and prioritizing the most traveled links. Trip heat exposure is then calculated using the updated T_{MRT} in the network.

4.2.3.2. Simulation 3 - Changing Travel Behavior

In a heterogeneous local heat environment, where the temperature on the street could be impacted by the street-built environment, local inhabitants may choose a longer but cooler route to avoid excessive heat exposure. Simulating the behavior change is achieved by rerouting travelers on the temperature weighted network, A. With the origin (s), target (t), and the cost (ω_{ij}) for each edge (i, j) in A, consider the variables x_{ij}, the path choice follows Equation 4.1,

$$\min \sum_{ij \in A} \omega_{ij} x_{ij} \quad \text{subject to } x_{ij} \geq 0 \text{ and for all } i,$$

$$\sum_{j} x_{ij} - \sum_{j} x_{ji} = \begin{cases} 1, if\ i = s \\ -1, if\ i = t \\ 0, otherwise \end{cases} \qquad \text{Equation 4.1}$$

$$\omega_{ij} = \sum_{t \in H} (T_{MRT,ij,t})\, L_{ij}$$

where H is the time stamps T_{MRT} data offers, and L_{ij} is the length of edge ij. The shortest path is the collection of edges where x_{ij} equals to 1.

The rerouting process is carried out on the baseline simulation, and every time a section of the network is cooled.

4.3. Results

4.3.1. Baseline Simulation

The baseline simulation shows that most of the roadways in the Phoenix metro region are infrequently utilized for active trips. Only 44% (35,496 km) of roadway links was used at least once, and 6.5% (5,305 km) was used more than 100 times for active trips. The low utilization of the network by active trips matches the ABM input data that most are made by personal vehicles. Although the highest link flow in the network is over 7,000 times/day, occurring in downtown Phoenix, most roadways are used less than 100 times/day or have never been used (Figure 4.1). Considering the imbalance of usage within the network, cooling down the most traveled corridors could benefit more people and trips. The selection of hot corridors (see Appendix C) that used to be cooled down is based on the traffic flow on each link in the initial simulation.

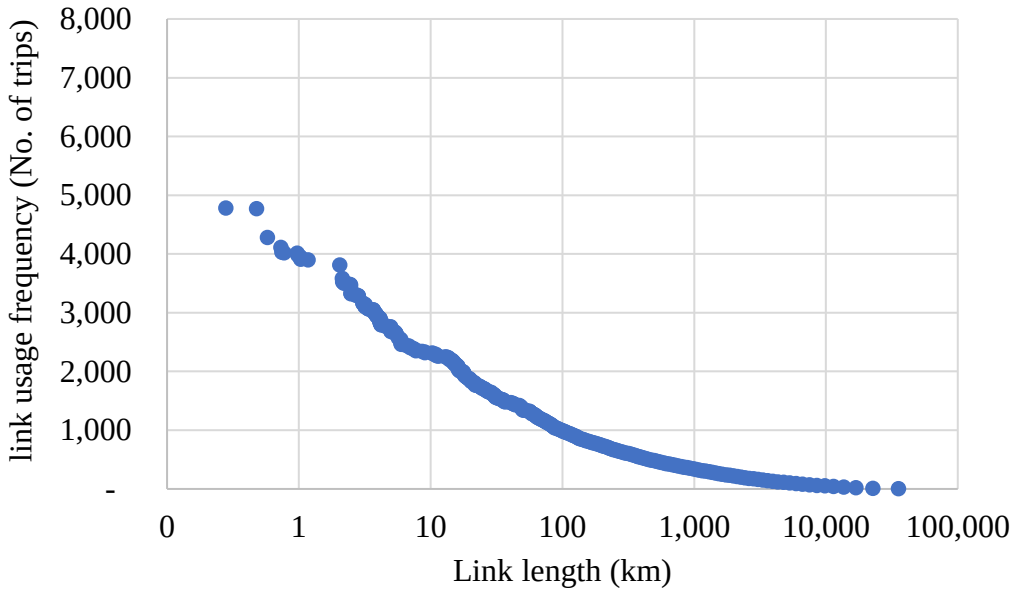

Figure 4.1. Link Length in the Network vs. the Link Usage Frequency

In the baseline simulation, the trips T_{MRT} exposure ranges between 22 to 65°C, with a median temperature of 52°C. Most of the active trips simulated experienced high T_{MRT}, and 20% of the trips were above 61.7°C.

4.3.2. Cool corridors environment

Over 94.6% of the roadways are in three LCZs: the open low-rise (LCZ 6), the large low-rise (LCZ 8), and the bare soil or sand climate zone (LCZ F) (Table 4.1). Compared to the non-cool corridors, those identified as the cool corridors have a higher tree and previous surface ratio, but a lower impervious ratio (Table 4.2). In the open high-rise, open midrise, and large low-rise climate zones, buildings create shade, as such, the cool corridors in these zones have a significantly higher amount of building ratio compared to the non-cool corridors. Cool corridors in cooling Scenario 1 (the coolest 10% corridors) have a lower T_{MRT} compared with Scenario 2 (the coolest 15% corridors). More efforts would be needed to cool the corridors from the lowest 15% to the lowest 10%, such as increasing tree planting, or impervious pavement.

Table 4.1. Current Environment for Corridors in Each LCZ

LCZ name	ratio of roadways in this LCZ	Built Environmental View Factors			
		Trees	Buildings	Impervious pavement	Pervious pavement
open low-rise (LCZ 6)	56.0%	13%	7%	37%	3%
large low-rise (LCZ 8)	27.4%	10%	8%	39%	2%
bare soil or sand (LCZ F)	11.2%	9%	5%	37%	4%
sparsely built (LCZ 9)	1.5%	14%	3%	32%	6%
open midrise (LCZ 5)	1.4%	16%	8%	36%	3%
low plants (LCZ D)	1.0%	7%	4%	38%	6%
open high-rise (LCZ 4)	0.2%	8.5%	28.5%	38.5%	0.6%

Table 4.2. Environment Difference Between the Cool and the Non-cool Corridors

LCZ type	(Mean of cool corridors - Mean of non-cool corridors) / mean of non-cool corridors							
	scenario 1: coolest 10%				scenario 2: coolest 15%			
	trees	buildings	Impervious pavement	Pervious pavement	trees	buildings	Impervious pavement	Pervious pavement
6	35%	-5%	-4%	31%	24%	-9%	-4%	30%
8	42%	16%	-4%	34%	29%	9%	-3%	26%
F	20%	-2%	-7%	22%	13%	-10%	-8%	36%
9	20%	-7%	-15%	32%	13%	-14%	-13%	29%
5	36%	49%	-9%	59%	28%	33%	-8%	45%
D	44%	3%	-4%	8%	16%	-1%	-6%	25%
4	7%	47%	-9%	22%	36%	35%	-10%	179%

4.3.3. Trips heat exposure reduction from changing environment and travel behavior

4.3.3.1. Trip Cooling Benefits from Changing Environment

As the total distance of cooled corridors increases, the number of trips cooled increases and the average trip temperature decreases (Figure 4.2). Of the 1.17 million active trips, 3.3 - 3.6% of the trips' heat exposure is reduced if converting the most traveled 10 km network to the identified cool corridors. 68 - 70% of the active trips can be cooled if changing all non-cool roadways to the identified cool corridor environment. The mean temperature reduction is insignificant (less than 0.05°C) for the short distance network to cool (less than 100 km), as the cooling benefit is averaged out among all active trips. However, if all the traveled corridors were cooled, trips would get an average 0.45 - 0.63°C benefit.

More trips cooled with aggressive (cooled to the coolest 10th percentile in the LCZ) changes to the built environment. The advantage of the intensifier cooling strategy—transforming the network to the coolest 10%—is significant when the total distance of corridors selected to transform is long. For instance, 483,000 trips get cooled, and an average of 0.113°C heat is reduced for active trips if transforming 1,000 km corridors to the coolest 15% in the network. An extra 17,000 trips could reduce exposure if the network is transformed to the coolest 10%, and active trips' heat exposure could be reduced by an average of 0.143°C.

Increasing the length of corridors to transform is more effective than transforming the built environment into a cooler scenario when the roadway transformation happens in a short-distance network. For example, by changing the most traveled 10 km corridors to the 10% coolest in the network, 40,400 trips get cooled, and all trips' heat exposure is reduced by an average of 0.005°C. Meanwhile, 22,800 more trips get cooled when changing the 20 km corridors to the 15% coolest in the network, and active trips' heat exposure is chilled by an average of 0.006°C.

Some early morning and late day trips experience warmer temperatures when cooling the built environment. The complex interactions of features in the built environment produce temperature effects that vary over time of day but result in net cooling over the day. The cool corridors are chosen based on the lowest temperature during the daytime, which have higher temperatures after sunset. As cool corridors typically have more trees than non-cool corridors (Table 4.2), the tree canopies along the walkway prevent the heat accumulated on the ground from releasing into the atmosphere

after sunset. Changing the environment to cooler, trips starting between 6:00 to 18:00 are more likely to get the cooling benefit (Figure 4.4), while trips after sunset may likely get higher exposure. More trips are cooled than getting warmed up, especially during the time with the hottest T_{MRT} of the day—10:00 to 14:00.

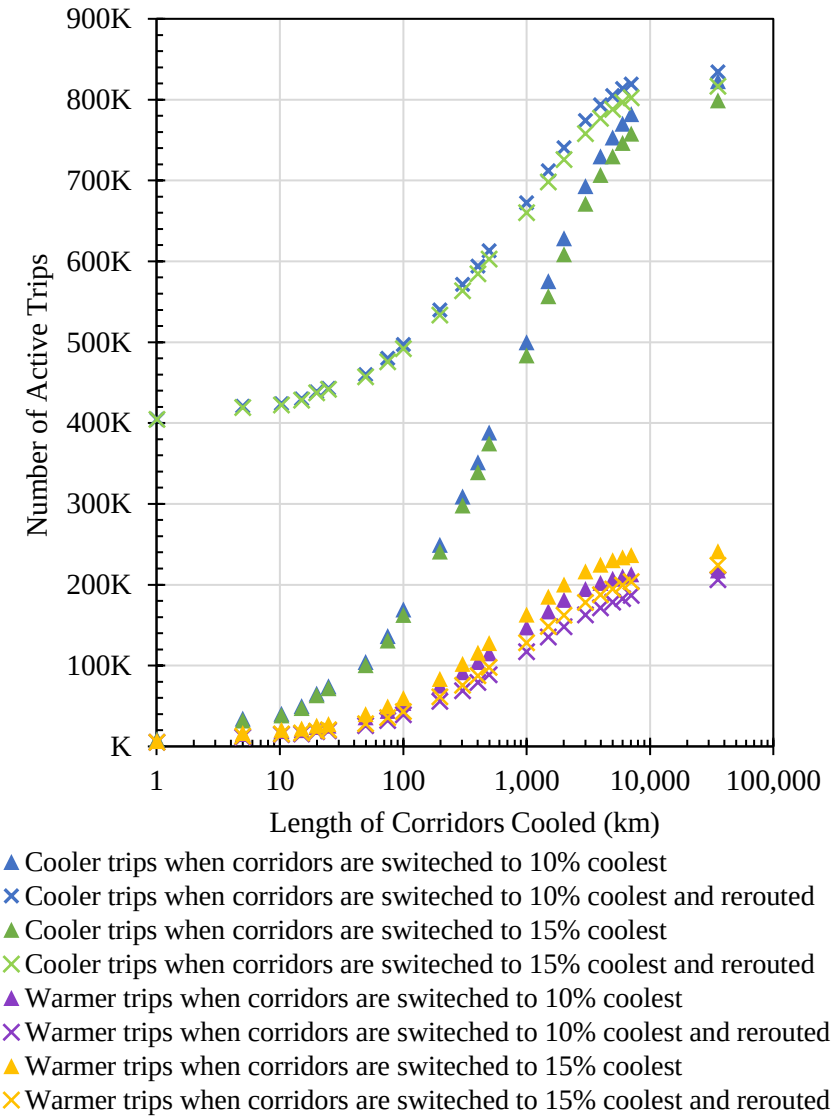

Figure 4.2. The Number of Active Trips Cooled/warmed by Changing Environment and Travel Behavior

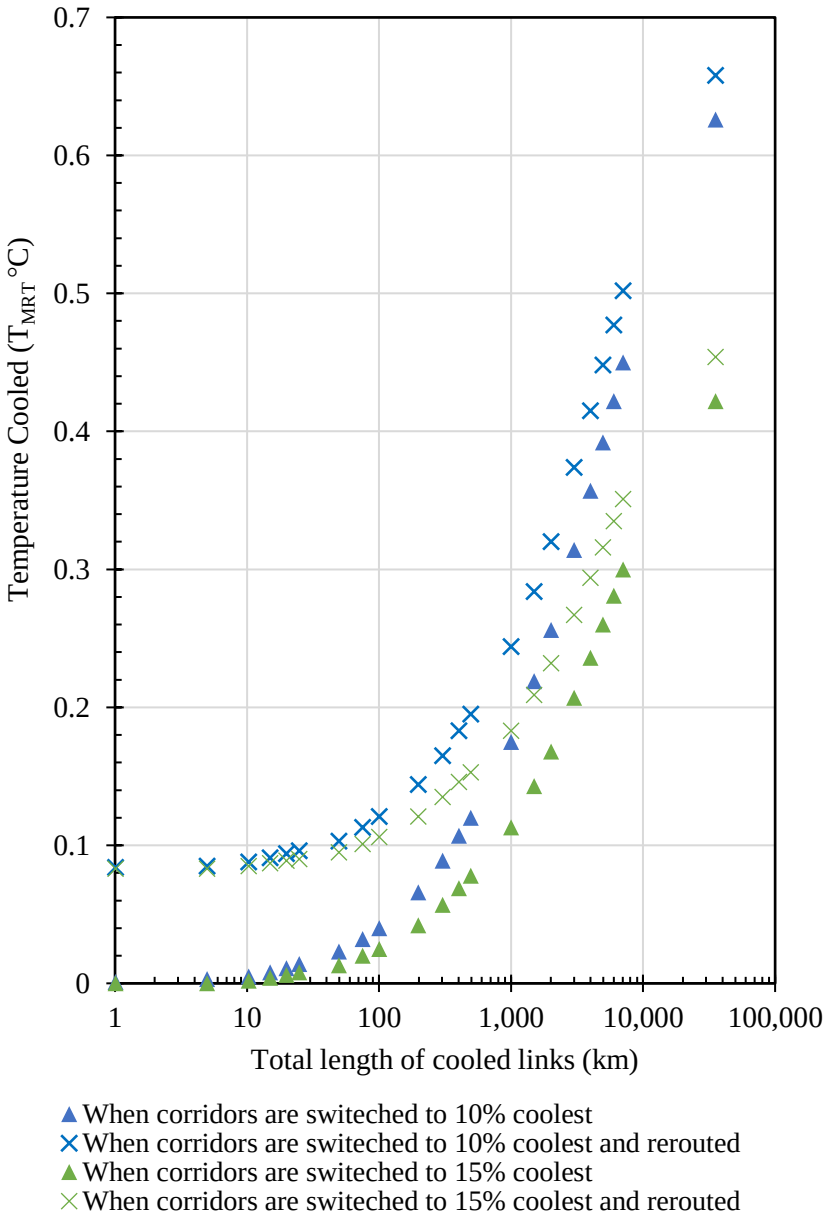

Figure 4.3. The Average Heat Exposure Reduced by Changing Environment and Travel Behavior

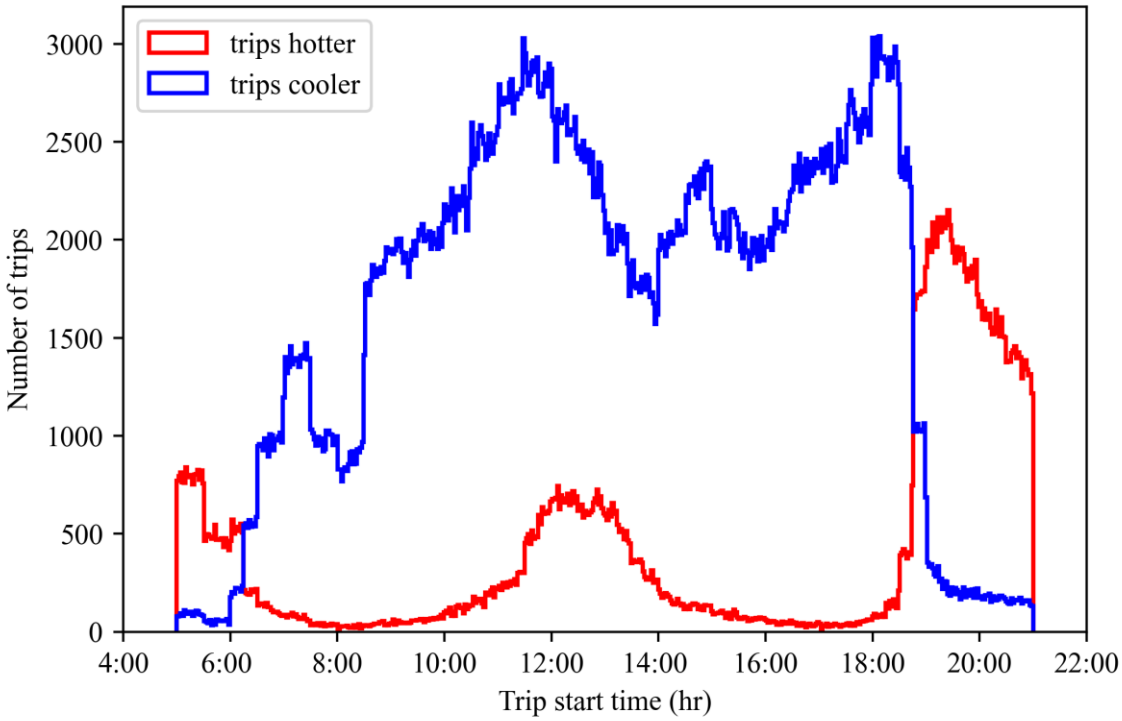

Figure 4.4. The Time Active Trips Get Cooled/Warmed by Changing Environment

4.3.3.2. Benefit from Changing Behavior

When travelers are rerouted in the cooled built environment, significant additional exposure reductions occur especially when the most heavily trafficked corridors are targeted. Rerouting trips to a cooler but longer path on the original network could reduce trips' heat exposure by an average of 0.08°C and cool 34% of the active trips. Switching the network to a cooler environment can potentially attract even more agents to detour from the shortest path to have heat mitigation. By switching the network to the coolest 10% or 15%, a significant increase in the number of trips cooled down from rerouting can be seen in Figure 4.2. And letting people reroute to the cooler path is more important than changing the corridors to the coolest ones in the network. As shown in Figure 4.2, more trips cooled by rerouting on the network cooled to the coldest 15% network (more intense

cooling) than not rerouting on the more intensely cooled network where corridors are switched to the 10% coolest.

The cooling benefit from rerouting is especially promising when cooling down a short network distance (Figure 4.3). For instance, cooling the most traveled 10 km corridors in the network, 36.1 - 36.3% of trips get cooler if agents can reroute in the transformed environment, which is ten times more than not rerouting but just changing the environment alone. And the heat exposure of active trips was reduced by an additional 0.08°C compared to not rerouting in the cooled network (Figure 4.2).

However, the bonus from rerouting people into a cooler path decreases as the length of the corridor cooled increases. As the total distance of corridors cooling down increases, the temperature within one LCZ becomes homogeneous as the simulation assumes all hot corridors will cool down to the cool corridor level. In this cooled homogeneous network, trips tend to stay on the shortest distance route. For instance, 94% of the cooled trips benefited from rerouting in a 10 km corridor cooled network, if agents can reroute (Figure 4.4). Meanwhile, rerouting agents in a network with 1,000 km cooled corridors, among the 0.66 - 0.67 million heat mitigated trips, 44 - 47% of them benefit from changing paths while the rest have their shortest path as the coolest (Figure 4.4). And ultimately, if all traveled roadways are shifted to cool corridors, only 22 - 25% of the trips are cooled from rerouting.

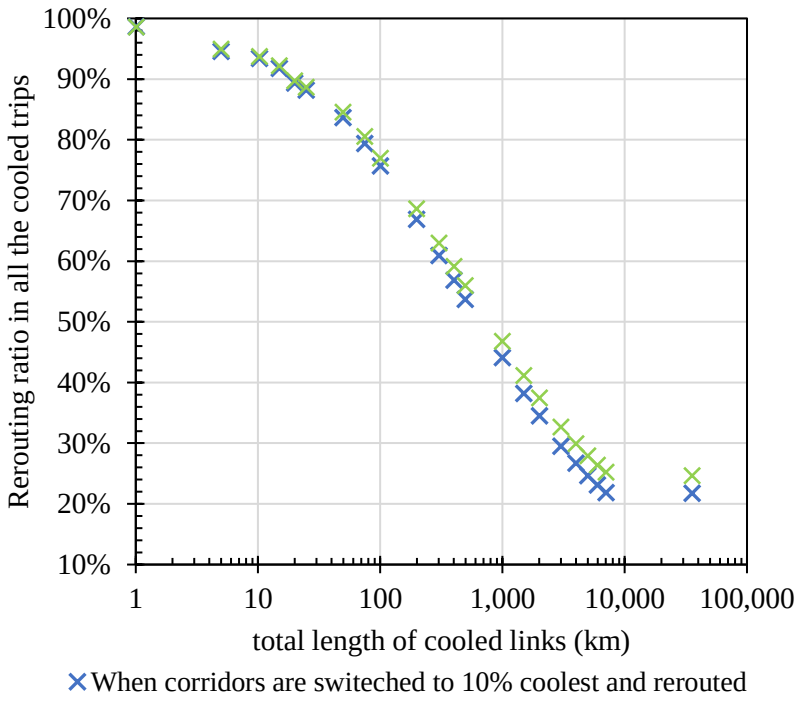

Figure 4.5. The Ratio of Trips Cooled by Rerouting Under Different Cooled Networks

4.3.3.3. Marginal Benefits from Changing Environment and Behavior

The marginal exposure benefit (as both built environment and travel behavior change) decreases as more of the network is cooled, revealing that limited resources should be prioritized on heavily traveled corridors. The marginal benefit of changing the environment and travel behavior, shown in Figure 4.6, is the number of trips that cooled down for every kilometer of additional length of roadways transformed. The marginal benefits of both changing environments, and rerouting, quickly diminished as the total length of corridors cooled increased. When the total length of cooled corridors is below 15 km, the marginal benefits for changing the environment and behavior are above 1,000 trips/km. When the total length of cooled corridors is above 1,500 km, the marginal benefits quickly drop to below 100 trips/km. Ultimately, the marginal benefit gets to 1

trip/km when all corridors transform into a cool environment. The diminished marginal benefit curve shows that switching long-distance corridors to cool may not be financially sustainable since the marginal benefit from investment is low, and the monetary and resources used to change the hot corridors to cooler might be high.

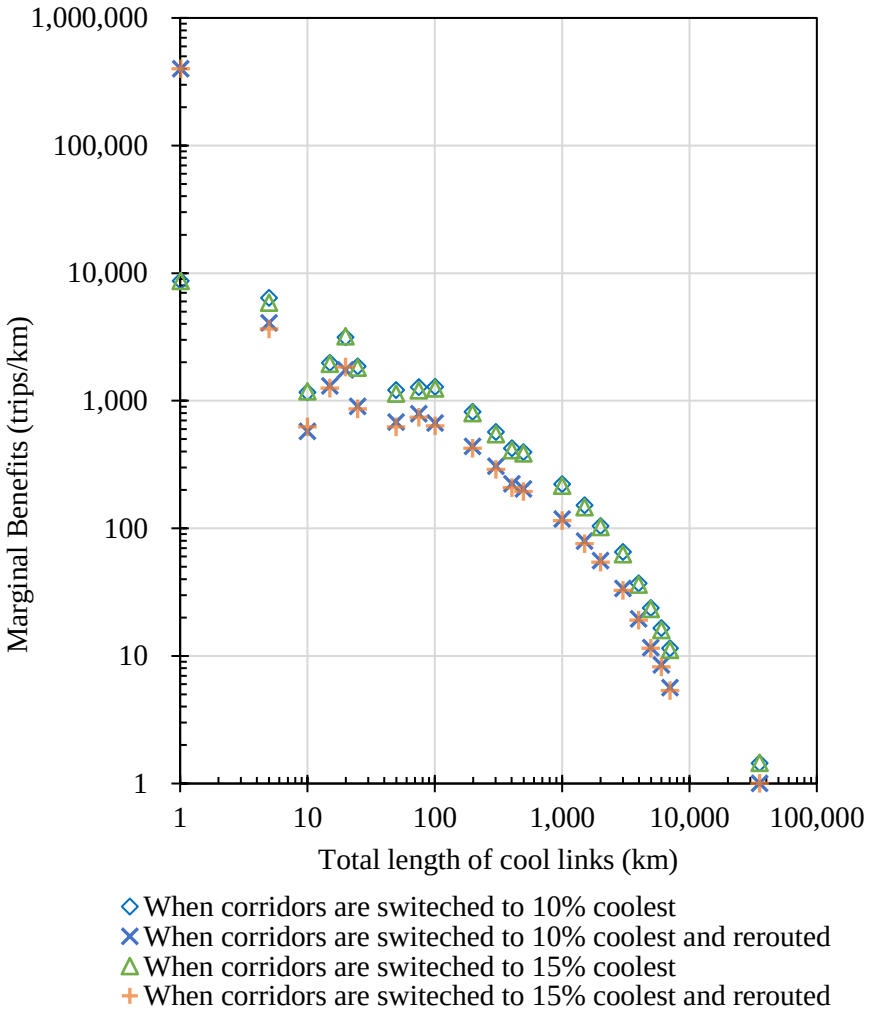

Figure 4.6 Marginal Benefits of Changing Environment and Travel Behavior

4.3.3.4. Heat Exposure Mitigation of the Very Hot Trips

In the baseline simulation, 20% of active trips were estimated to experience over 61.7°C T_{MRT} degree heat exposure. Using the 61.7°C T_{MRT} as a threshold to define the

very hot trips, changing the built environment and travel behavior can reduce the ratio of very hot trips from 20% in the baseline simulation, to 17.3 to 18.5% (Figure 4.7) when all corridors are cooled. However, if just switching the built environment for a short distance of the network, trips can hardly get cooled to a temperature below the high exposure threshold. Combining rerouting with a cooled environment can create more opportunities for hot trips to get cooled under the high exposure threshold (Figure 4.7). For instance, when switching 10 km corridors to cool corridors, around 19.5% trips are very hot when agents could reroute, and around 20% of the trips are very hot if agents are not rerouting. From Figure 4.6, when the total length of corridors cooled down is less than 1,000 km, the rerouting on the less cooled network can be more effective in mitigating very hot exposures than just changing the network to a more intensely cooled environment but not letting people reroute.

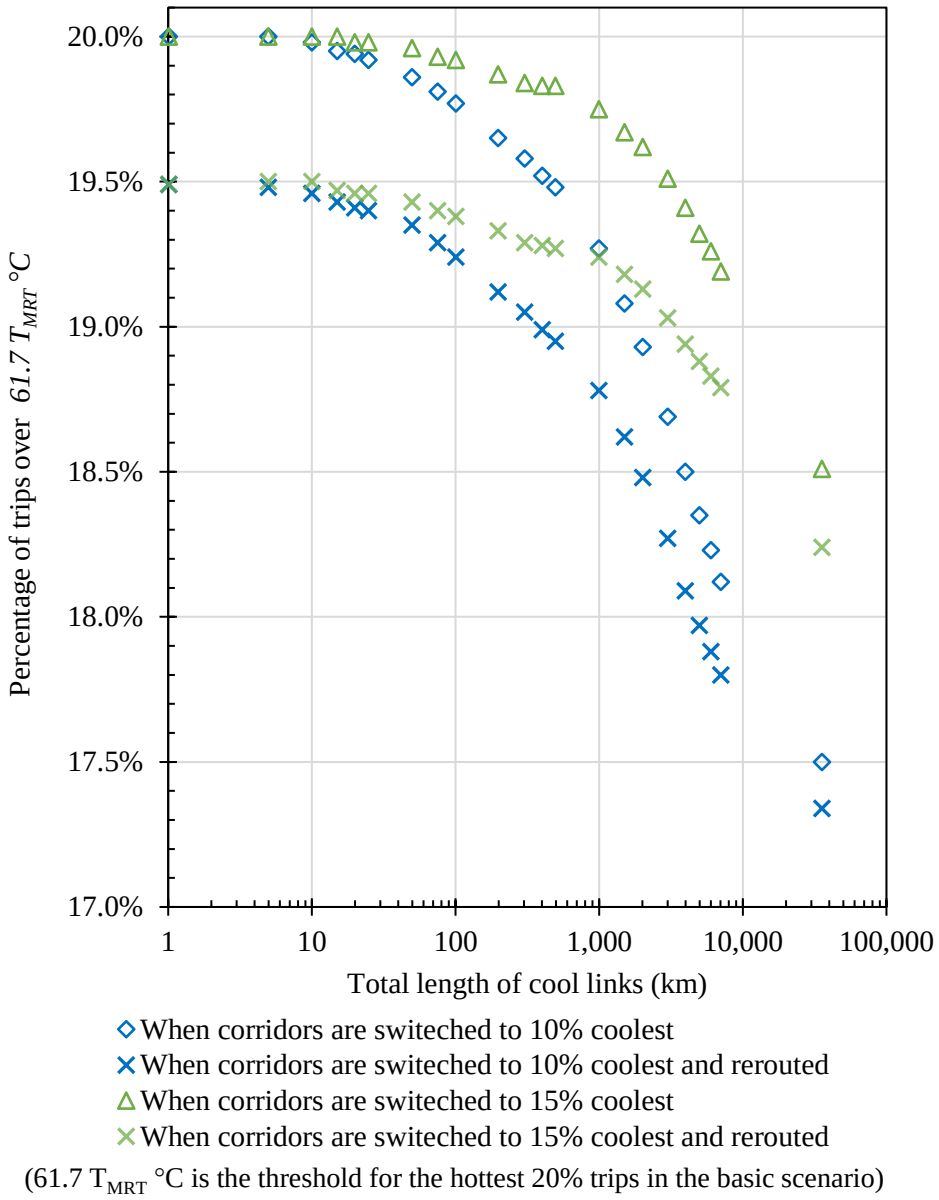

Figure 4.7. Cooling of the Hottest Trips. Hottest Trips Are Defined As Over 61.7°C T_{MRT}

4.4. Conclusion and Discussion

This study tests out the effectiveness of the designed simulation platform—Icarus—in assessing personal heat exposure in changing environments and behavior settings. The analysis provides a prototype for dynamically analyzing the heat mitigation

from changing the built environment and travel behavior. The results show the personal heat exposure reducing benefit from changing the built environment and travel behavior. The Phoenix metro area is heavily car-dependent, with many opportunities to shift drivers to active trips and meet sustainability goals. However, the extreme temperature may threaten outdoor travelers during hot summer days.

4.4.1. Balancing Between Changing Environment and Travel Behavior

Changing the built environment and travel behavior could reduce the simulated agents heat exposure, especially for active trips happening at the hottest time of the day. With the limited municipal budget for improving the corridors (City of Phoenix, 2021), balancing the difference in cooling intensity, cooling roadway length, and travel behavior change could significantly affect residents' heat exposure mitigation.

As active trips do not use the majority of roadways in the city, changing the built environment should consider the current infrastructure usage. Knowing the popularly traveled corridors before changing the built environment to cooler is vital as more people and trips could benefit from cooling down the most traveled pathways. Changing the short distance of the network to cool might be closer to people travel route choice in real-life, as transforming the built environment requires monetary investment for tree planting, previous pavement, or shading construction. As the city plans to equip the city residents with more heat mitigation infrastructures, increasing the awareness of the cooling corridors (both currently existing and future designed) is crucial. The municipal budget for improving the corridors to cooler is mainly limited to a short distance of network improvement. For short-distance network environmental change, rerouting on

those corridors creates more heat mitigation benefits than just changing the built environment. And if the budget is limited to transform a short distance of the network, increasing the length of corridors cooled down creates more benefits than putting all investment into a shorter distance corridor and making it the coolest. Even if the city has an unlimited budget to cool down the roadways, it's not ideal for cooling down the whole city network. As most of the street networks were only used by active travelers less than 100 times per day, the marginal benefits of every kilometer cooled quickly reduced to less than a hundred trips.

Besides reducing personal heat exposure for outdoor travelers, changing built environment, and encouraging people using the cooled roadways could bring sustainability benefits and increasing the quality of life. The Phoenix metro area has historically been heavily car-dependent, and there is a significant potential to motivate residents of the region to shift to low emission active trips. In addition, shifting away from car driving can reduce the impact of inflation of rising gas price (Harris, 2022).

4.4.2. Limitations

The simulation contains several limitations despite the meaningful findings on personal heat exposure mitigation. First, the personal heat exposure in the model only considers the temperature exposure, which is the heat stress from the environment, but neglects individual strain. The personal heat strain is resulted from the physiological responses to the heat stress (ACGIH 2019). Factors such as the acclimation, clothing, gender, age, and health conditions all affect the personal heat strain (ACGIH 2019; Glass et al., 2015). Taking such sociological matrices into consideration would be essential to

understand the people's resilience when facing the heat hazard and could be the future feature of the Icarus. Mechanistic models, which simulate human physiological and thermoregulation – considering individual activities, gender, race, and age – would be valuable tools for estimating personal heat strain (Glass et al., 2015).

Other limitations come with the uncertainty of the temperature assessment. Although T_{MRT} has a higher resolution compared to other temperature measures, the coverage of T_{MRT} data used in this study is still limited to the roadways where Google Street View presents-which means with car access. However, many pedestrian-accessible trails and sidewalks don't have the simulated T_{MRT} and Google Street View shading ratio data. Future studies could incorporate the updated T_{MRT} data after its release.

CHAPTER 5

SUMMARY AND FUTURE WORK

This dissertation contribute to expanding the current transportation infrastructure vulnerability assessment method by: i) introducing the post-fire debris flow risk into understanding the roadways network's vulnerability under current and climate changing future conditions; ii) incorporating the transportation system users into estimating the traveler heat vulnerability; and iii) testing out potential heat mitigation from changing the built environment and travel behavior.

The current assessment methods ignore the user vulnerability (Tylor, 2008) and are limited to the hazards that are spatially coincidental with the physical infrastructures. The spatial coincidence method used in the current vulnerability assessment was insufficient to capture the complexity of transportation infrastructure vulnerability to climatic perturbations. First, the perturbation could be a combined result of different climatic threats. For example, the post-fire debris flow studied in chapter two is a combined result of the fire and rainfall working together. Vegetation, soil characteristics, and geological features all play a role in the post-fire debris flow development. Spatially overlaying the fire or rainfall map over the transportation network could miss leading the analysis of the vulnerable locations on the physical infrastructure network. Then, the perturbations threaten the infrastructure users rather than the physical structure. Extreme heat studied in the third and fourth chapters falls in this category. The threat of heat on the outdoor travelers health and life is more critical than the infrastructure damage, although the physical infrastructure does exist, such as shortened service life of asphalt

pavement. And the built environment shapes the environmental temperature profile along the transportation network, affecting outdoor travelers heat exposure. This dissertation advanced the vulnerability assessment by addressing the complexity of the concurrent climatic hazards and the interactions between infrastructure and its users.

5.1. Summaries

This dissertation expands the current vulnerability assessment method by addressing the environmental hazard and coupling the infrastructure to users. Chapter 2 presents a novel approach to evaluating the vulnerability of roadways to the post-fire debris flow, considering current and climate change impacts on fire and rainfall risks. Chapter 3 and chapter 4 test out the possibility of coupling the transportation infrastructure with its users to estimate the vulnerability of travelers to heat. Chapter 3 proposes a computational framework and module that leverages the activity-based transportation model, infrastructure network data, and the environmental temperature profile to estimate personal heat exposure for city dwellers. It further tests out the city travelers heat exposure on a hot summer day using a case study in the city of Phoenix. Chapter 4 continues the work in chapter 3 to test the heat mitigation potentials from changing the built environment and travel behavior.

- Summary of Chapter 2: Post-wildfire debris flows represent a major hazard for transportation infrastructure. The location and intensity of post-fire debris movements are hard to predict, and threats could last for several years until the watershed is restored to pre-fire conditions. This situation might worsen as climate change forecasts predict increasing numbers of wildfire-burnt areas and

extreme precipitation intensity. Using California as a case study, transportation infrastructure vulnerability to post-fire debris flow is assessed considering geologic conditions, vegetation conditions, precipitation, fire risk, and roadway importance under current and future climate scenarios. The results show significant but uneven statewide increases in the number of vulnerable roadways from the present to future emissions scenarios. Under current climate conditions, 0.97% of roadways are highly vulnerable because they are critical to the network, and a common rainfall event (i.e., a once every 10-year storm) can result in a 90% likelihood of debris flow. In the climate-changing future, the ratio of vulnerable roadways is expected to increase 92% to 131% in the RCP 4.5 emission scenario and 251% to 327% in the RCP 8.5 emission scenario. The vulnerability assessment results are positioned to: 1) identify, reinforce, and fortify highly vulnerable roadways, 2) prioritize watershed fire mitigation, and 3) guide future infrastructure site selection.

- Summary of Chapter 3: In cities under extreme heat, travelers are susceptible to extreme environmental temperatures. A personal heat exposure simulation platform, Icarus, was built in Python. Icarus is applied to the Phoenix metropolitan region as a case study using three different temperature measurements: air temperature (T_{air}), mean radiant temperature (T_{MRT}), and wet bulb globe temperature (T_{WBGT}). The case study shows that travel patterns (such as trip duration and the trip start time) for different demographic groups affect personal and population heat exposure. Different temperature measures also

resulted in widely varying estimates of personal heat exposure. Using T_{air} and T_{WBGT}, active trips between 12:50 to 17:50 experienced high heat exposure. However, trips that started between 10:30-14:10 had very high T_{MRT} heat exposure. Personal heat exposure calculated with T_{air} indicates people under 20 are more likely to take very hot trips. Personal heat exposure calculated with T_{MRT} identifies more trips among people older than 20 under high temperature, especially for seniors over 65. Only 11% of all active trips are identified as violating the WBGT work and rest table, and people older than 65 are barely at risk when calculating exposure using T_{WBGT}. Different temperature measures also result in the diverse locations of very hot trips. The corridors with a high ratio of very hot trips (over 50% of the link flow is from very hot trips) are evenly distributed across the whole city when calculating exposure with T_{air}. However, when the exposure is calculated using T_{MRT}, the very hot trips are concentrated near the downtown, commercial district, and major corridors. Trips violating the WBGT work/rest table are also concentrated in downtown phoenix and the major arterials.

- Summary of Chapter 4: Climate change is projected to increase the temperature in cities. For cities like Phoenix, where residents are heavily car-dependent, motivating people to use active trips can mitigate GHG emissions and introduce health benefits. However, the extreme heat during the summer can threaten the travelers health. Heat mitigation strategies such as changing the built environment and travel behavior were compared using Icarus for the city of Phoenix. Baseline,

changing built environment, and changing travel behavior simulations were conducted to compare the heat mitigation benefits. The baseline simulation was conducted to describe the personal heat exposure in the current environment. The changing built environment simulation assumes the street thermal temperature can be reduced by transforming the corridor environment to the cool corridor level. And changing travel behavior simulation assumes people would detour to a longer distance but a cooler route to get heat mitigation benefit. Results show that changing the built environment and travel behavior can both reduce personal heat exposure. Encouraging changing behavior on the environmentally cooled network could produce extra cooling benefits compared to changing the environment alone. The marginal benefits of heat mitigation from environmental and behavioral change decrease when adding more roadways to cool down. The hottest 20% of trips in the baseline scenario experienced a T_{MRT} above 61.7°C. After changing the built environment to cooler and rerouting people to cooler routes, the ratio of trips above 61.7°C threshold reduced to below 18.5%.

Each chapter provides scalable methods and practical results that can be used to help decision-making. For instance, the delivered roadway post-fire debris flows vulnerability result in chapter 2 has been used by The California Nature Conservancy to identify the potential locations of wildlife corridors and crossings. The city of Phoenix is using the personal heat exposure results from chapter 3 in their tree planting planning and heat mitigation planning. The framework and models built in this dissertation are also

scalable to other locations and larger geographic areas. For instance, researchers at Colorado State University are scaling the Post-fire Debris Flow models in chapter 3 to the whole United States.

5.2. Limitations

Despite the novelties brought by each chapter that expands the vulnerability assessment method, this dissertation contains limitations. In chapter 2, the likelihood of post-fire debris flow was assessed, but the magnitude of the debris flow was not included in the analysis. The likelihood and quantity of the debris flow are the two major matrices the post-fire debris flow early warning system uses (USGS, 2018). Chapter 2 initially included the debris flow volume calculation using Cannon et al.(2010). However, the model needs variables such as fire burned severity which can only be obtained after the fire has already happened. The debris flow volume calculation was eventually removed from the method. Besides, chapter 2 only included the major highway and arterials in the analysis and didn't consider the service road in the mountainous region. The service roads may be more susceptible to the post-fire debris flow considering their geographical locations. These roadways were not included in the analysis because the dataset was too big to carry out the betweenness centrality calculations. Another limitation is the criticality of the roadway network in the climate change future was assumed to be the same as the current situation.

In chapter 3, Icarus simplified the routing behavior by assuming the travelers would use the shortest distance path. However, the traveler walking or biking path choice is affected by safety, preference, or street perceptions and conditions (Marshall &

Garrick, 2010; Titze et al., 2012). Besides the shortest path routing for active trips, the simulation didn't consider the heat exposure from public transportation, car driving, and ride-sharing due to the lack of information on the in-vehicle temperature. Different temperature metrics tested the sensitivity of personal heat exposure to the temperature matrix but complicated the result interpretation, as the high heat stress population and locations depend on the metric used for analysis. And more research needs to be done to identify the temperature metrics most suitable for personal heat exposure study.

In chapter 3 and chapter 4, the personal heat exposure only considers the environmental temperature—heat stress but does not examine the personal heat strain. Heat strain is the personal physiological response to heat stress. Acclimation, clothing, gender, age, and health conditions affect the personal heat strain (ACGIH 2019; Glass et al., 2015). Considering the heat strain could be essential for understanding city residents resiliency to heat stress.

5.3. Future Directions

The expansion of the vulnerability assessment is useful but also brings with its conundrums. While the toolset for assessing transportation vulnerability is expanding, stakeholders and decision-makers lack the guidance to choose the appropriate tool under different circumstances. The different interpretations of vulnerability leave the practice depending on the particular interpretation (O'Brien et al., 2007). More work needs to be done to summarize playbooks for the infrastructure stakeholders to better incorporate and understand vulnerability in the decision-making process.

The future study, the transportation infrastructure vulnerability assessment should consider the resilience of the social, ecological, and technological systems (SETs). Vulnerability is defined as the 'propensity or predisposition to be adversely affected and encompasses a variety of concepts and elements, including sensitivity or susceptibility to harm and lack of capacity to cope and adapt' (IPCC 2022). The 'capacity to cope and adapt' could be interpreted as 'resilience', although the latter has a broader definition. In social and ecological studies, vulnerability has a long history of incorporating adaptability—one aspect of resiliency (Woods, 2005)—in the assessment. Individuals or social groups' endorsement and economic capacity are commonly used to measure adaptability or resilience. Transportation vulnerability studies also acknowledge vulnerability rooted in the lack of the capability to adapt. However, the resilience of infrastructures was either not included in the analysis (Berdic, 2002; Adger 2003) or simplified as the connective analysis inherited from the graph theory (Demirel et al., 2015; Kermanshah & Derrible, 2016; Murray et al., 2008; Taylor, 2017). The absence of resilience in vulnerability analysis might be rooted in the fail-safe design mindset, which focuses on the physical assets and assumes infrastructures will be rigid when perturbation happens. However, when facing unexpected climate perturbations, the resiliency of the social-ecological system would mitigate the vulnerability of the physical infrastructure. Thus, the future research agenda should include the SETs resiliency for infrastructure vulnerability assessment.

REFERENCES

ACGIH. (2019). TLVs and BEIs: Based on the documentation of the threshold limit values for chemical substances and physical agents & biological exposure indices. ACGIH.

Adger, W. N. (2006). Vulnerability. Global Environmental Change, 16(3), 268–281. https://doi.org/10.1016/j.gloenvcha.2006.02.006

Aminipouri, M., Knudby, A. J., Krayenhoff, E. S., Zickfeld, K., & Middel, A. (2019). Modelling the impact of increased street tree cover on mean radiant temperature across Vancouver's local climate zones. Urban Forestry and Urban Greening, 39(July 2018), 9–17. https://doi.org/10.1016/j.ufug.2019.01.016

Anderson, G. B., & Bell, M. L. (2011). Heat Waves in the United States: Mortality Risk during Heat Waves and Effect Modification by Heat Wave Characteristics in 43 U.S. Communities. Environmental Health Perspectives, 119(2), 210–218. https://doi.org/10.1289/ehp.1002313

Aniello, C., Morgan, K., Busbey, A., & Newland, L. (1995). MAPPING MICRO-URBAN HEAT ISLANDS USING LANDSAT TM AND A GIS. In Computers & Geoscience.~ (Vol. 21, Issue 8, pp. 965–969).

Bao, J., Li, X., & Yu, C. (2015). The Construction and Validation of the Heat Vulnerability Index, a Review. International Journal of Environmental Research and Public Health, 12(7), 7220–7234. https://doi.org/10.3390/ijerph120707220

Berdica, K. (2002). An introduction to road vulnerability:what has been done, is done and should be done. Transport Policy, 117–127.

Bernhard, M. C., Kent, S. T., Sloan, M. E., Evans, M. B., McClure, L. A., & Gohlke, J. M. (2015). Measuring personal heat exposure in an urban and rural environment. Environmental Research, 137, 410–418. https://doi.org/10.1016/j.envres.2014.11.002

Bonnin, G. M., Martin, D., Lin, B., Parzybok, T., Yekta, M., & Riley, D. (2006). Precipitation-Frequency Atlas of the United States Volume 6 Version 2.3: California.

Budd, G. M. (2008). Wet-bulb globe temperature (WBGT)—Its history and its limitations. Journal of Science and Medicine in Sport, 11(1), 20–32. https://doi.org/10.1016/j.jsams.2007.07.003

Cal-Adapt. (2017). About Cal-Adapt—Cal-Adapt API Docs 1.0 documentation. Cal-Adapt API Docs. https://berkeley-gif.github.io/caladapt-docs/index.html

California Energy Comission. (2021). Wildfire-Explore wildfire scenario projections for area burned and estimated decadal wildfire probabilities for California. Cal-Adapt. https://cal-adapt.org/tools/wildfire/

Camp, J., Abkowitz, M., Hornberger, G., Benneyworth, L., & Banks, J. C. (2013). Climate Change and Freight-Transportation Infrastructure: Current Challenges for Adaptation. Journal of Infrastructure Systems, 19(4), 363–370. https://doi.org/10.1061/(ASCE)IS.1943-555X.0000151

Cannon, S. H., Gartner, J. E., Wilson, R. C., Bowers, J. C., & Laber, J. L. (2008). Storm rainfall conditions for floods and debris flows from recently burned areas in

southwestern Colorado and southern California. Geomorphology, 96(3–4), 250–269. https://doi.org/10.1016/j.geomorph.2007.03.019

Chester, M. V., & Allenby, B. (2019). Infrastructure as a wicked complex process. Elementa Science of Anthropocene, 7(1), 21. https://doi.org/10.1525/elementa.360

Chester, M. V., Markolf, S., & Allenby, B. (2019). Infrastructure and the environment in the Anthropocene. Journal of Industrial Ecology, 23(5), 1006–1015. https://doi.org/10.1111/jiec.12848

Chester, M. V., Underwood, B. S., & Samaras, C. (2020). Keeping infrastructure reliable under climate uncertainty. Nature Climate Change, 10(6), 488–490. https://doi.org/10.1038/s41558-020-0741-0

Chow, W. T. L., Chuang, W.-C., & Gober, P. (2012). Vulnerability to Extreme Heat in Metropolitan Phoenix: Spatial, Temporal, and Demographic Dimensions. The Professional Geographer, 64(2), 286–302. https://doi.org/10.1080/00330124.2011.600225

Church, R. L., Scaparra, M. P., & Middleton, R. S. (2004). Identifying Critical Infrastructure: The Median and Covering Facility Interdiction Problems. Annals of the Association of American Geographers, 94(3), 491–502. https://doi.org/10.1111/j.1467-8306.2004.00410.x

City of Mesa. (2014). Mesa 2040 General Plan. City of Mesa. https://www.mesaaz.gov/home/showdocument?id=12298

Cohn, P. J., Carroll, M. S., & Kumagai, Y. (2006). Evacuation behavior during wildfires: Results of three case studies. Western Journal of Applied Forestry, 21(1), 39–48. https://doi.org/10.1093/wjaf/21.1.39

Cova, T. J., Theobald, D. M., Norman, J. B., & Siebeneck, L. K. (2013). Mapping wildfire evacuation vulnerability in the western US: The limits of infrastructure. GeoJournal, 78(2), 273–285. https://doi.org/10.1007/s10708-011-9419-5

Crank, P. J., Middel, A., Wagner, M., Hoots, D., Smith, M., & Brazel, A. (2020). Validation of seasonal mean radiant temperature simulations in hot arid urban climates. Science of The Total Environment, 749, 141392. https://doi.org/10.1016/j.scitotenv.2020.141392

Davidson, W., Vovsha, P., Freedman, J., & Donnelly, R. (2010). CT-RAMP Family of Activity-Based Models. Australasian Transport Research Forum 2010 Proceedings, Canberra, Australia.

De Graff, J. V., Shelmerdine, B., Gallegos, A., & Annis, D. (2015). Uncertainty associated with evaluating rockfall hazard to roads in burned areas. Environmental and Engineering Geoscience, 21(1), 21–33. https://doi.org/10.2113/gseegeosci.21.1.21

Demirel, H., Kompil, M., & Nemry, F. (2015). A framework to analyze the vulnerability of European road networks due to Sea-Level Rise (SLR) and sea storm surges. Transportation Research Part A: Policy and Practice, 81, 62–76. https://doi.org/10.1016/j.tra.2015.05.002

Dijst, M., Böcker, L., & Kwan, M. P. (2013). Exposure to weather and implications for travel behaviour: Introducing empirical evidence from Europe and Canada. Journal of Transport Geography, 28, 164–166. https://doi.org/10.1016/j.jtrangeo.2013.01.004

Dowds, J., Sentoff, K., Sullivan, J. L., & Aultman-Hall, L. (2017). Impacts of Model Resolution on Transportation Network Criticality Rankings. Transportation Research Record: Journal of the Transportation Research Board, 2653(1), 93–100. https://doi.org/10.3141/2653-11

Eisenman, D. P., Wilhalme, H., Tseng, C.-H., Chester, M., English, P., Pincetl, S., Fraser, A., Vangala, S., & Dhaliwal, S. K. (2016). Heat Death Associations with the built environment, social vulnerability and their interactions with rising temperature. Health & Place, 41, 89–99. http://dx.doi.org/10.1016/j.healthplace.2016.08.007

Elliott, J. G., Smith, M. E., Friedel, M. J., Stevens, M. R., Bossong, C. R., Litke, D. W., Parker, R. S., Costello, C., Wagner, J., Char, S. J., Bauer, M. A., & Wilds, S. R. (2004). Analysis and mapping of post-fire hydrologic hazards for the 2002 Hayman, Coal Seam, and Missionary Ridge Wildfires, Colorado. US Geological Scientific Investigations Report, 5300, 1–109.

Epstein, Y., & Moran, D. S. (2006). Thermal Comfort and the Heat Stress Indices. Industrial Health, 44(3), 388–398. https://doi.org/10.2486/indhealth.44.388

FlLOW Project. (2016). The Role of Walking and Cycling in Reducing Congestion: A Porfolio of Measures. http://www.h2020-flow.eu.

Ford, J. D., Pearce, T., McDowell, G., Berrang-Ford, L., Sayles, J. S., & Belfer, E. (2018). Vulnerability and its discontents: The past, present, and future of climate change vulnerability research. Climatic Change, 151(2), 189–203. https://doi.org/10.1007/s10584-018-2304-1

FRAP. (2017). Statewide map of wildland Fire Threat data. https://frap.fire.ca.gov/mapping/gis-data/

Fraser, A. M., Chester, M. V., & Underwood, B. S. (2020). Wildfire risk, post-fire debris flows, and transportation infrastructure vulnerability vulnerability. Sustainable and Resilient Infrastructure, 00(00), 1–13. https://doi.org/10.1080/23789689.2020.1737785

Gartner, J. E., Cannon, S. H., Santi, P. M., & Dewolfe, V. G. (2008). Empirical models to predict the volumes of debris flows generated by recently burned basins in the western U.S. Geomorphology, 96(3–4), 339–354. https://doi.org/10.1016/j.geomorph.2007.02.033

Glass, K., Tait, P. W., Hanna, E. G., & Dear, K. (2015). Estimating Risks of Heat Strain by Age and Sex: A Population-Level Simulation Model. International Journal of Environmental Research and Public Health, 12(5), 5241–5255. https://doi.org/10.3390/ijerph120505241

Grubesic, T. H., Matisziw, T. C., Murray, A. T., & Snediker, D. (2008). Comparative approaches for assessing network vulnerability. International Regional Science Review, 31(1), 88–112. https://doi.org/10.1177/0160017607308679

Hagberg, A. A., Schult, D. A., & Swart, P. J. (2008). Exploring Network Structure, Dynamics, and Function using NetworkX. 11–16.

Hajat, S., & Kosatky, T. (2010). Heat-related mortality: A review and exploration of heterogeneity. Journal of Epidemiology & Community Health, 64(9), 753–760. https://doi.org/10.1136/jech.2009.087999

Hamer, M., & Chida, Y. (2008). Active commuting and cardiovascular risk: A meta-analytic review. Preventive Medicine, 46(1), 9–13. https://doi.org/10.1016/j.ypmed.2007.03.006

Harris, M. (2022, March 24). Want to Fight Inflation? Take the Bus. https://www.thenation.com/article/economy/inflation-bus-public-transit/

Hoehne, C. G., Hondula, D. M., Chester, M. V., Eisenman, D. P., Middel, A., Fraser, A. M., Watkins, L., & Gerster, K. (2018). Heat exposure during outdoor activities in the US varies significantly by city, demography, and activity. Health and Place, 54(July), 1–10. https://doi.org/10.1016/j.healthplace.2018.08.014

Hoffmann, S. (2021). osmium: Python bindings for libosmium, the data processing library for OSM data (3.2.0) [C++, Python]. https://osmcode.org/pyosmium

Hollnagel, E. (2009). The four cornerstones of resilience engineering (p. Chapter 6-pages 117-134). Ashgate.

Hollnagel, E., Woods, D. D., & Leveson, N. (2006). Resilience Engineering: Concepts and Precepts. Ashgate Publishing, Ltd.

Hondula, D., & Davis, R. (2012). P-414: The Characteristics of Places within Seven U.S. cities where the Mortality Rate is Highest during Extreme Heat Events. Epidemiology, 23(5S). https://doi.org/10.1097/01.ede.0000417413.00991.f9

Hondula, D. M., Georgescu, M., & Balling, R. C. (2014). Challenges associated with projecting urbanization-induced heat-related mortality. Science of The Total Environment, 490, 538–544. https://doi.org/10.1016/j.scitotenv.2014.04.130

Hondula, D. M., & Kuras, E. R. (2021). Novel metrics for relating personal heat exposure to social risk factors and outdoor ambient temperature. Environment International, 146. https://doi.org/10.1016/j.envint.2020.106271

Ibrahim, S., Ammar, R., Rajasekaran, S., Lownes, N., Wang, Q., & Sharma, D. (2011). An efficient heuristic for estimating transportation network vulnerability. Proceedings - IEEE Symposium on Computers and Communications, 1092–1098. https://doi.org/10.1109/ISCC.2011.5983988

Ice, G. G., Neary, D. G., & Adams, P. W. (2004). Effects of Wildfire on Soils and Watershed Processes. Journal of Forestry, 102(6), 16–20. https://doi.org/10.1093/JOF/102.6.16

Iverson, S. A., Gettel, A., Bezold, C. P., Goodin, K., McKinney, B., Sunenshine, R., & Berisha, V. (2020). Heat-Associated Mortality in a Hot Climate: Maricopa County, Arizona, 2006-2016. Public Health Reports, 135(5), 631–639. https://doi.org/10.1177/0033354920938006

Johnson, T. R., Langstaff, J. E., Graham, S., Fujita, E. M., & Campbell, D. E. (2018). A multipollutant evaluation of APEX using microenvironmental ozone, carbon

monoxide, and particulate matter (PM2.5) concentrations measured in Los Angeles by the exposure classification project. Cogent Environmental Science, 4(1), 1453022. https://doi.org/10.1080/23311843.2018.1453022

Kántor, N., & Unger, J. (2011). The most problematic variable in the course of human-biometeorological comfort assessment—The mean radiant temperature. Open Geosciences, 3(1), 90–100. https://doi.org/10.2478/s13533-011-0010-x

Karner, A., Hondula, D. M., & Vanos, J. K. (2015). Heat exposure during non-motorized travel: Implications for transportation policy under climate change. Journal of Transport & Health, 2(4), 451–459. https://doi.org/10.1016/j.jth.2015.10.001

Kean, J. W., & Staley, D. M. (2018, June 23). Emergency Assessment of Post-Fire Debris-Flow Hazards. https://www.usgs.gov/natural-hazards/landslide-hazards/science/emergency-assessment-post-fire-debris-flow-hazards?qt-science_center_objects=0#qt-science_center_objects

Kean, J. W., Staley, D. M., Lancaster, J. T., Rengers, F. K., Swanson, B. J., Coe, J. A., Hernandez, J. L., Sigman, A. J., Allstadt, K. E., & Lindsay, D. N. (2019). Inundation, flow dynamics, and damage in the 9 January 2018 Montecito debris-flow event, California, USA: Opportunities and challenges for post-wildfire risk assessment. Geosphere, 15(4), 1140–1163. https://doi.org/10.1130/GES02048.1

Kermanshah, A., & Derrible, S. (2016). A geographical and multi-criteria vulnerability assessment of transportation networks against extreme earthquakes. Reliability Engineering and System Safety, 153, 39–49. https://doi.org/10.1016/j.ress.2016.04.007

Kim, Y., Eisenberg, D. A., Bondank, E. N., Chester, M. V., Mascaro, G., & Underwood, B. S. (2017). Fail-safe and safe-to-fail adaptation: Decision-making for urban flooding under climate change. Climatic Change, 145(3–4), 397–412. https://doi.org/10.1007/s10584-017-2090-1

Kovats, R. S., & Hajat, S. (2008). Heat Stress and Public Health: A Critical Review. Annual Review of Public Health, 29, 41–55. https://doi.org/10.1146/annurev.publhealth.29.020907.090843

Kuras, E. R., Hondula, D. M., & Brown-Saracino, J. (2015). Heterogeneity in individually experienced temperatures (IETs) within an urban neighborhood: Insights from a new approach to measuring heat exposure. International Journal of Biometeorology, 59(10), 1363–1372. https://doi.org/10.1007/s00484-014-0946-x

Kuras, E. R., Richardson, M. B., Calkins, M. M., Ebi, K. L., Hess, J. J., Kintziger, K. W., Jagger, M. A., Middel, A., Scott, A. A., Spector, J. T., Uejio, C. K., Vanos, J. K., Zaitchik, B. F., Gohlke, J. M., & Hondula, D. M. (2017). Opportunities and challenges for personal heat exposure research. Environmental Health Perspectives, 125(8). https://doi.org/10.1289/EHP556

Lawrimore, J., Ray, R., Applequist, S., Korzeniewski, B., & Menne, M. J. (2016). Global Summary of the Month (GSOM), Version 1 [Data set]. NOAA National Centers for Environmental Information. https://doi.org/10.7289/V5QV3JJ5

Li, J., & Ozbay, K. (2012). Evaluation of Link Criticality for Day-to-Day Degradable Transportation Networks. Transportation Research Record: Journal of the

Transportation Research Board, 2284(1), 117–124. https://doi.org/10.3141/2284-14

Lukasczyk, J., Middel, A., & Maciejewski, R. (2016). Synthetic Fisheye Images for Urban Climate Applications: Exploring Personalized Comfort Routing. SigSpatial, San Francisco Bay Area. https://doi.org/10.475/123 4

MacArthur, J., Mote, P., Ideker, J., Figliozzi, M., & Lee, L. (2012). Climate Change Impact Assessment for Surface Transportation in the Pacific Northwest and Alaska. https://www.wsdot.wa.gov/research/reports/fullreports/772.1.pdf

MacDonald, L. H., & Larsen, I. J. (2008). Runoff and Erosion from Wildfires and Roads: Effects and Mitigation (pp. 145–167).

Maricopa County Assessor's Office. (2018). Maricopa County Parcel Data. https://maps.mcassessor.maricopa.gov/

Maricopa County Public Health. (2017). Heat-Associated Death in Maricopa County, AZ. Maricopa County Public Health.

Maricopa County Public Health. (2020). Heat-Associated Death in Maricopa County, AZ (p. 73). Maricopa County Public Health.

Markolf, S. A., Hoehne, C., Fraser, A., Chester, M. V., Underwood, B. S., Markolf, A. S., Hoehne, C., Fraser, A., Chester, V. M., Underwood, B. S., Markolf, S. A., Hoehne, C., Fraser, A., Chester, M. V., & Underwood, B. S. (2019). Transportation resilience to climate change and extreme weather events – Beyond risk and robustness. Transport Policy, 74(November 2018), 174–186. https://doi.org/10.1016/j.tranpol.2018.11.003

Marshall, W. E., & Garrick, N. W. (2010). Effect of Street Network Design on Walking and Biking. Transportation Research Record, 2198(1), 103–115. https://doi.org/10.3141/2198-12

Mattsson, L. G., & Jenelius, E. (2015). Vulnerability and resilience of transport systems—A discussion of recent research. Transportation Research Part A: Policy and Practice, 81, 16–34. https://doi.org/10.1016/j.tra.2015.06.002

McGregor, G. R., & Vanos, J. K. (2018). Heat: A primer for public health researchers. Public Health, 161, 138–146. https://doi.org/10.1016/j.puhe.2017.11.005

Mesa. (2014). 2040 General Plan. City of Mesa.

Meyer, M. D. (2008). Design Standards for U.S. Transportation Infrastructure: The Implications of Climate Change. https://rosap.ntl.bts.gov/view/dot/17365

Middel, A., Häb, K., Brazel, A. J., Martin, C. A., & Guhathakurta, S. (2014). Impact of urban form and design on mid-afternoon microclimate in Phoenix Local Climate Zones. Landscape and Urban Planning, 122, 16–28. https://doi.org/10.1016/j.landurbplan.2013.11.004

Middel, A., & Krayenhoff, E. S. (2019). Micrometeorological determinants of pedestrian thermal exposure during record-breaking heat in Tempe, Arizona: Introducing the MaRTy observational platform. Science of The Total Environment, 687, 137–151. https://doi.org/10.1016/j.scitotenv.2019.06.085

Middel, A., Lukasczyk, J., & Maciejewski, R. (2017). Sky View Factors from Synthetic Fisheye Photos for Thermal Comfort Routing—A Case Study in Phoenix, Arizona. Urban Planning, 2(1), 19–30. https://doi.org/10.17645/up.v2i1.855

Milošević, D. D., Bajšanski, I. V., & Savić, S. M. (2017). Influence of changing trees locations on thermal comfort on street parking lot and footways. Urban Forestry and Urban Greening, 23, 113–124. https://doi.org/10.1016/j.ufug.2017.03.011

Minnesota Department of Transportation. (2021). Prescribed Fire—Roadside Vegetation Management. https://www.dot.state.mn.us/roadsides/vegetation/fire.html

Molly Mowery, Anna Read, Kelly Johnston, Tareq Wafaie, Mowery, M., Read, A., Johnston, K., Wafaie, T., Molly Mowery, Anna Read, Kelly Johnston, & Tareq Wafaie. (2019). Planning the wildland-urban interface (No. 9781611902020). https://www.planning.org/publications/report/9174069/

Morton, D. C., Roessing, M. E., Camp, A. E., & Tyrrell, M. L. (2003). Assessing the Environmental, Social, and Economic Impacts of Wildfire. Yale University School of Forestry and Environmental Studies Global Institute of Sustainable Forestry.

Murray, A. T., Matisziw, T. C., & Grubesic, T. H. (2008). A Methodological Overview of Network Vulnerability Analysis. Growth and Change, 39(4), 573–592. https://doi.org/10.1111/j.1468-2257.2008.00447.x

NASA. (2021). How does climate change affect precipitation? NASA Global Precipitation Measurement Mission. https://gpm.nasa.gov/resources/faq/how-does-climate-change-affect-precipitation

National Cancer Institute. (2002). Metabolic Equivalent of Task Values for Activities in American Time Use Survey and 2002 Census Occupational Classification

System. https://epi.grants.cancer.gov/physical/met/atus-met.php?major[]=17&keywords=&metval_min=&metval_max=

Nazelle, A. de, Morton, B. J., Jerrett, M., & Crawford-Brown, D. (2010). Short trips: An opportunity for reducing mobile-source emissions? Transportation Research Part D: Transport and Environment, 15(8), 451–457. https://doi.org/10.1016/j.trd.2010.04.012

O'Neill, B. C., Oppenheimer, M., Warren, R., Hallegatte, S., Kopp, R. E., Pörtner, H. O., Scholes, R., Birkmann, J., Foden, W., Licker, R., Mach, K. J., Marbaix, P., Mastrandrea, M. D., Price, J., Takahashi, K., van Ypersele, J.-P., & Yohe, G. (2017). IPCC reasons for concern regarding climate change risks. Nature Climate Change, 7(1), 28–37. https://doi.org/10.1038/nclimate3179

Onishi, A., Cao, X., Ito, T., Shi, F., & Imura, H. (2010). Evaluating the potential for urban heat-island mitigation by greening parking lots. Urban Forestry and Urban Greening, 9(4), 323–332. https://doi.org/10.1016/j.ufug.2010.06.002

OpenStreetMap Contributors. (2015). OpenStreetMap. OpenStreetMap. https://www.openstreetmap.org/

OSHA. (2015). OSHA Technical Manual (OTM)—Section III: Chapter 4 | Occupational Safety and Health Administration. https://www.osha.gov/otm/section-3-health-hazards/chapter-4

OSM. (2019). Planet dump. OpenStreetMap Contributors. https://planet.openstreetmap.org/

Paulson, F. (2020, July 27). What is the Top Speed of an Electric Bike? OCLU Blog. https://oclu.com/blog/top-speed-electric-bike/

Perkins-Kirkpatrick, S. E., & Gibson, P. B. (2017). Changes in regional heatwave characteristics as a function of increasing global temperature. Scientific Reports, 7(1), 12256. https://doi.org/10.1038/s41598-017-12520-2

Phoenix. (2021). Climate Action Plan. City of Phoenix.

Pierce, D. W., Kalansky, J. F., & Cayan, D. R. (2018a). Climate, Drought, and Sea Level Rise Scenarios for California's Fourth Climate Change Assessment (Issue August 2018). https://www.energy.ca.gov/sites/default/files/2019-11/Projections_CCCA4-CEC-2018-006_ADA.pdf

Pierce, D. W., Kalansky, J. F., & Cayan, D. R. (2018b). Extreme Precipitation. Cal-Adapt. https://cal-adapt.org/tools/extreme-precipitation/

Pörtner, H.-O., Roberts, D. C., Tignor, M. M. B., Poloczanska, E. S., Mintenbeck, K., Alegría, A., Craig, M., Langsdorf, S., Löschke, S., Möller, V., Okem, A., & Rama, B. (Eds.). (2022). Climate Change 2022: Impacts, Adaptation and Vulnerability. Contribution of Working Group II to the Sixth Assessment Report of the Intergovernmental Panel on Climate Change.

Qin, Y., & Hiller, J. E. (2014). Understanding pavement-surface energy balance and its implications on cool pavement development. Energy and Buildings, 85, 389–399. https://doi.org/10.1016/j.enbuild.2014.09.076

Radeloff, V. C., Helmers, D. P., Kramer, H. A., Mockrin, M. H., Alexandre, P. M., Bar Massada, A., Butsic, V., Hawbaker, T. J., Martinuzzi, S., Syphard, A. D., &

Stewart, S. I. (2017). Forest Service Research Data Archive. In The 1990-2010 wildland-urban interface of the conterminous United States—Geospatial data. 2nd Edition. Fort Collins, CO: Forest Service Research Data Archive. https://doi.org/10.2737/RDS-2015-0012-2

Reid, C. E., O, 'Neill Marie S., Gronlund, C. J., Brines, S. J., Brown, D. G., Diez, -Roux Ana V., & Schwartz, J. (2009). Mapping Community Determinants of Heat Vulnerability. Environmental Health Perspectives, 117(11), 1730–1736. https://doi.org/10.1289/ehp.0900683

Saelens, B. E., Sallis, J. F., & Frank, L. D. (2003). Environmental correlates of walking and cycling: Findings from the transportation, urban design, and planning literatures. Annals of Behavioral Medicine, 25(2), 80–91. https://doi.org/10.1207/S15324796ABM2502_03

Schwartz, G. E., & Alexander, R. B. (1995). Soils data for the conterminous United States derived from the NRCS State Soil Geographic (STATSGO) data base. https://water.usgs.gov/GIS/metadata/usgswrd/XML/ussoils.xml

Seidl, T., Russomanno, T. G., Stöckl, M., & Lames, M. (2021). Assessment of Sprint Parameters in Top Speed Interval in 100 m Sprint—A Pilot Study Under Field Conditions. Frontiers in Sports and Active Living, 3. https://www.frontiersin.org/article/10.3389/fspor.2021.689341

Staley, D. M., Negri, J. A., Kean, J. W., Laber, J. L., Tillery, A. C., & Youberg, A. M. (2017). Prediction of spatially explicit rainfall intensity – duration thresholds for

post- fire debris- flow generation in the western United States. Geomorphology, 278, 149–162. https://doi.org/10.1016/j.geomorph.2016.10.019

Staley, D. M., Tillery, A. C., Kean, J. W., McGuire, L. A., Pauling, H. E., Rengers, F. K., & Smith, J. B. (2018). Estimating post-fire debris-flow hazards prior to wildfire using a statistical analysis of historical distributions of fire severity from remote sensing data. International Journal of Wildland Fire, 27(9), 595–608. https://doi.org/10.1071/WF17122

State of Arizona. (2018). Arizona State and County Population Projections, 2018-2055: Methodology Report (p. 31). https://www.azcommerce.com/media/1544715/pop-prj-state-county-2018methodology.pdf

Steffen, W., Broadgate, W., Deutsch, L., Gaffney, O., & Ludwig, C. (2015). The trajectory of the Anthropocene: The Great Acceleration. The Anthropocene Review, 2(1), 81–98. https://doi.org/10.1177/2053019614564785

Stewart, I. D., Oke, T. R., & Krayenhoff, E. S. (2014). Evaluation of the 'local climate zone' scheme using temperature observations and model simulations. International Journal of Climatology, 34(4), 1062–1080. https://doi.org/10.1002/joc.3746

Stocker, T. F., Qin, D., Plattner, G.-K., Tignor, M. M. B., Allen, S. K., Boschung, J., Nauels, A., Xia, Y., Bex, V., & Midgley, P. M. (2014). Climate Change 2013—The Physical Science Basis. Cambridge University Press. https://www.google.com/books/edition/Climate_Change_2013_The_Physical_Sci

ence/o4gaBQAAQBAJ?hl=en&gbpv=1&dq=stocker+2013+physical+&pg=PR1&printsec=frontcover

Stull, R. (2011). Wet-Bulb Temperature from Relative Humidity and Air Temperature. Journal of Applied Meteorology and Climatology, 50(11), 2267–2269. https://doi.org/10.1175/JAMC-D-11-0143.1

Sutherland, A. (2015, August 17). Wet Bulb Globe Temperature: What It Is and How To Use It | Weather and Agriculture: A Plains Perspective. http://blog.mesonet.org/agriculture/wet-bulb-globe-temperature-what-it-is-and-how-to-use-it/

Tan, Z., Lau, K. K. L., & Ng, E. (2017). Planning strategies for roadside tree planting and outdoor comfort enhancement in subtropical high-density urban areas. Building and Environment, 120, 93–109. https://doi.org/10.1016/j.buildenv.2017.05.017

Taylor, M. (2017). Vulnerability analysis for transportation networks (First edition.). Elsevier.

Tempe. (2019). Climate Action Plan. City of Tempe.

Thornton, P. E., Shrestha, R., Thornton, M., Kao, S.-C., Wei, Y., & Wilson, B. E. (2021). Gridded daily weather data for North America with comprehensive uncertainty quantification. Scientific Data, 8(1), 190. https://doi.org/10.1038/s41597-021-00973-0

Thornton, P. E., Thornton, M. M., & Vose, R. S. (2016). Daymet: Annual Tile Summary Cross-Validation Statistics for North America, Version 3. https://daac.ornl.gov/cgi-bin/dsviewer.pl?ds_id=1348

Titze, S., Krenn, P., & Oja, P. (2012). Developing a bikeability index to score the biking-friendliness of urban environments. Journal of Science and Medicine in Sport, 15, S29–S30. https://doi.org/10.1016/j.jsams.2012.11.071

Tudor-Locke, C., Johnson, W. D., & Katzmarzyk, P. T. (2009). Accelerometer-Determined Steps per Day inUS Adults. Medicine & Science in Sports & Exercise, 41(7), 1384–1391. https://doi.org/10.1249/MSS.0b013e318199885c

US Census Bureau. (2022, January 24). 2020 Census. Census.Gov. https://www.census.gov/2020census

USGS. (2017). Unites States geological Survey, The National Map, 3D Elevation Program. https://www.usgs.gov/core-science-systems/national-geospatial-program/national-map

USGS. (2018, June 23). Early Warning System. https://www.usgs.gov/natural-hazards/landslide-hazards/science/early-warning-system?qt-science_center_objects=0#qt-science_center_objects

Valentin, V., & Stormont, J. (2019). Evaluating Post-Wildfire Flood Impacts on Transportation Infrastructure for Mitigation Planning. https://static1.squarespace.com/static/526c7a98e4b023d8f09390ed/t/5e0a72f98863c530b1ef2473/1577743118017/SPTC15.1-50-F-Valentin+Final+Report+123019.pdf

Vanos, J. K., Rykaczewski, K., Middel, A., Vecellio, D. J., Brown, R. D., & Gillespie, T. J. (2021). Improved methods for estimating mean radiant temperature in hot and

sunny outdoor settings. International Journal of Biometeorology, 65(6), 967–983. https://doi.org/10.1007/s00484-021-02131-y

Vennapusa, P., White, D., & Miller, K. (2013). Western Iowa Missouri River Flooding—Geo-Infrastructure Damage Assessment, Repair, and Mitigation Strategies. www.ceer.iastate.edu

Verdin, K. L., Dupree, J. A., & Elliott, J. G. (2012). Probability and Volume of Potential Postwildfire Debris Flows in the 2012 Waldo Canyon Burn Area near Colorado Springs, Colorado: U.S. Geological Survey Open-File Report 2012-1158. 8p.

Viger, R. J., Rea, A., Simley, J. D., & Hanson, K. M. (2016). NHDPlusHR: A National Geospatial Framework for Surface-Water Information. JAWRA Journal of the American Water Resources Association, 52(4), 901–905. https://doi.org/10.1111/1752-1688.12429

Vovsha, P., Freedman, J., Livshits, V., & Sun, W. (2011). Design Features of Activity-Based Models in Practice Coordinated Travel–Regional Activity Modeling Platform. Transportation Research Record: Journal of the Transportation Research, 300, 19–27. https://doi.org/10.3141/2254-03

Westerling, A. L. (2018). Wildfire simulations for California's fourth climate change assessment: Projecting changes in extreme wildfire events with a warming climate. In California's Fourth Climate Change Assessment, California Energy Comission (pp. 1–29). http://www.climateassessment.ca.gov/techreports/docs/20180827-Projections_CCCA4-CEC-2018-014.pdf

Westerling, A. L., Bryant, B. P., Preisler, H. K., Holmes, T. P., Hidalgo, H. G., Das, T., & Shrestha, S. R. (2011). Climate change and growth scenarios for California wildfire. Climatic Change, 109(SUPPL. 1), 445–463. https://doi.org/10.1007/s10584-011-0329-9

Whitehouse, T. (2019, August 6). What is a good average speed on a road bike? Road Bike Basics. https://roadbikebasics.com/average-speed-on-road-bike/

Wolshon, B., & Marchive, E. (2007). Emergency Planning in the Urban-Wildland Interface: Subdivision-Level Analysis of Wildfire Evacuations. Journal of Urban Planning and Development, 133(1), 73–81. https://doi.org/10.1061/(ASCE)0733-9488(2007)133:1(73)

Woods, D. D. (2015). Four concepts for resilience and the implications for the future of resilience engineering. Reliability Engineering and System Safety, 141, 5–9. https://doi.org/10.1016/j.ress.2015.03.018

Wu, T. C. (2001). Application of Remote Sensing for the Prediction, Monitoring, and Assessment of Hazard and Disasters that Impact Transportation.

Xiao, T. Q., Jatowt, A., Wang, Z., Si, R., Zhang, H., Liu, X., Shibasaki, R., Song, X., & Kim, K. (2020). CoolPath: An Application for Recommending Pedestrian Routes with Reduced Heatstroke Risk. In S. Di, M. Z. Fang, & K.-J. Li (Eds.), Web and wireless geographical information systems. Springer. http://www.springer.com/series/7409

Yang, S., Hu, F., Thompson, R. G., Wang, W., Li, Y., Li, S., & Ni, W. (2018). Criticality ranking for components of a transportation network at risk from tropical cyclones.

International Journal of Disaster Risk Reduction, 28, 43–55. https://doi.org/10.1016/j.ijdrr.2018.02.017

Yoo, E., Rudra, C., Glasgow, M., & Mu, L. (2015). Geospatial Estimation of Individual Exposure to Air Pollutants: Moving from Static Monitoring to Activity-Based Dynamic Exposure Assessment. Annals of the Association of American Geographers, 105(5), 915–926. https://doi.org/10.1080/00045608.2015.1054253

Zhang, X., Miller-Hooks, E., & Denny, K. (2015). Assessing the role of network topology in transportation network resilience. Journal of Transport Geography, 46, 35–45. https://doi.org/10.1016/j.jtrangeo.2015.05.006

APPENDIX A

ABM ACTIVITY TYPE AND ICARUS PARCEL TYPE ASSIGNMENT

Activity Description From ABM	**Parcel Assignment in Simulation**
Home	residential
Workplace	non-residential
University	non-residential
School	non-residential
Escorting	non-residential
School escort	non-residential
Pure escort (as main purpose of the tour)	non-residential
Ridesharing (as a stop on commuting tours)	non-residential
Other escort (not by same household members)	non-residential
Shopping	non-residential
Other maintenance	non-residential
Eating out	non-residential
Breakfast	non-residential
Lunch	non-residential
Dinner	non-residential
Visiting relatives or friends	non-residential
Other discretionary	non-residential
Special event	non-residential
At work	non-residential
At work business	non-residential
At work lunch	non-residential
At work other	non-residential
Work-related business	non-residential

Activity Description From ABM	Parcel Assignment in Simulation
ASU related trip to ASU MAZs	non-residential

APPENDIX B

PARCEL AC ASSUMPTIONS

Non-residential Parcel Type	AC	Non-residential Parcel Type	AC
Apartment	Yes	Clubhouse	Yes
Apartment Garages/Out Building, Multiple Res (Low Rise)	Yes	Cocktail Lounge	Yes
Arcade Building	Yes	Cold Storage Facility	Yes
Arena Shelter	Yes	Cold Storage, Farm	Yes
Auditorium	Yes	College (Entire)	Yes
Automobile Showroom	Yes	Community Center	Yes
Automotive Center	Yes	Community Shopping Center	Yes
Bank	Yes	Computer Center	Yes
Banquet Hall	Yes	Convalescent Hospital	Yes
Bar/Tavern	Yes	Convenience Market	Yes
Barber Shop	Yes	Cotton Gin	Yes
Barn, General Purpose	No	Country Club	Yes
Barn, Special Purpose	No	Covered Storage, Commercial/In, Storage Warehouse	Yes
Bed and Breakfast Inn	Yes	Dairy	Yes
Bowling Center	Yes	Day Care Center	Yes
Broadcasting Facility	Yes	Dental Office/Clinic	Yes
Car Wash - Automatic	No	Dining Atrium	Yes
Car Wash - Canopy	No	Discount Store	Yes
Car Wash - Drive Thru	No	Discount Warehouse Store	Yes
Car Wash - Self Serve	No	Dispensary	Yes
Central Bank	Yes	Distribution Warehouse	Yes
Church	Yes	Dormitory	Yes
Citrus Trees, Permanent Crops	No	Drug Store	Yes

Non-residential Parcel Type	AC	Non-residential Parcel Type	AC
Classroom (College)	Yes	Elderly Assist. Multi. Res.	Yes
Elementary School (Entire)	Yes	Greenhouse, Hoop, Arch-Rib, Me	No
Equipment (Shop) Building	Yes	Greenhouse, Hoop, Arch-Rib, Sm	No
Equipment Shed	No	Greenhouse, Modified Hoop, Lar	No
Farm Commodity Storage Shed	No	Greenhouse, Modified Hoop, Sma	No
Farm Implement Building	Yes	Greenhouse, Straight-Wall, Lar	No
Farm Implement Shed	No	Greenhouse, Straight-Wall, Sma	No
Farm Sun Shade Shelter	No	Group Care Home	Yes
Farm Utility Arch-rib, Quon.	Yes	Guest Cottage	Yes
Farm Utility Building	Yes	Gymnasium (School)	Yes
Farm Utility Shelter	Yes	Handball-Racquetball Club	Yes
Farm Utility Storage Shed	No	Health Club	Yes
Fast Food Restaurant	Yes	High School (Entire)	Yes
Fieldhouse	Yes	Home For The Elderly	Yes
Fine Arts & Crafts Building	Yes	Horse Arena	Yes
Fire Station (Staff)	Yes	Hospital	Yes
Fitness Center	Yes	Hotel, Full Service	Yes
Flathouse	Yes	Hotel, Limited Service	Yes
Fraternal Building	Yes	Industrial Engineering	Yes
Freestall Barn	Yes	Industrial Flex Building	Yes
Fruit Packing Barn	Yes	Industrials, Heavy Mftg.	Yes
Golf Cart Storage Building	No	Industrials, Light Mftg.	Yes
Golf Course - Non-Statutory	No	Jail - Correctional Facility	Yes
Golf Course - Statutory	No	Jail - Police Station	Yes

Non-residential Parcel Type	AC	Non-residential Parcel Type	AC
Golf Starter Booth	No	Junior High School (Entire)	Yes
Governmental Building	Yes	Kennels	Yes
Greenhouse, Hoop, Arch-Rib, La	No	Labor Dormitory	Yes
Laboratory	Yes	Neighborhood Shopping Ctr	Yes
Laundry Building, Laundromat	Yes	Office Building	Yes
Lean-to, Farm Utility	No	Outpatient Surgical Center	Yes
Library, Public	Yes	Parking Level	Yes
Loft	Yes	Parking Structure	No
Log Home	Yes	Passenger Terminal	Yes
Lt. Commercial Arch-rib, Quon	Yes	Pavilion	No
Lt. Commercial Utility Build.	Yes	Post Office, Branch	Yes
Lumber Storage Shed, Horz.	Yes	Post Office, Main	Yes
Mall Anchor Department Store	Yes	Poultry House, Cage Op., Yes Sto	Yes
Market	Yes	Recreational Enclosure	Yes
Material Shelter	Yes	Rectory	Yes
Material Storage Building	Yes	Regional Discount Shopping Cen	Yes
Material Storage Shed	No	Regional Shopping Center	Yes
Medical Office	Yes	Residential Garage - Attached	No
Mega Warehouse	Yes	Residential Garage - Built-in	No
Mega Warehouse Discount Store	Yes	Residential Garage - Detached	No
Mini-Lube Garage	No	Restaurant	Yes
Mini-Mart Convenience Store	Yes	Restroom Building,	No
Mini-Warehouse	Yes	Retail Store, Commercial Yard Improvements	Yes

Non-residential Parcel Type	AC	Non-residential Parcel Type	AC
Mobile Home Recreational Vehicle	No	Retirement Community Complex	Yes
Mobile Home Yard Imps	Yes	Senior Center	Yes
Mortuary	Yes	Service Garage Shed	Yes
Motel	Yes	Service Repair Garage	Yes
Multiple Res. (Sen. Citizen)	Yes	Service Station, Service Station, Full Service	No
Museum	Yes	SF Mobile Home Room Addition	
Single Family Res. Multi-Story, Factory/Site Built Home, Specialty Home, A - Frame House, Earth Sheltered Home, Mobile Home Room Addition, Single-Family Residence, Residential Yard Improvements, SF Mobile Home Yard Improvement, Mobile Home Yard Improvements	Yes	Theater - Cinema	Yes
Shed Office Structure	Yes	Town House, End Unit	Yes
Site Improvements	No	Transit Warehouse	No
Skating Rink, Ice	Yes	Travel Trailer - Permanently A, Mobile Office - Not Affixed, Mobile Home-Permanently Affixed, Park Model - Permanently Affix, Mobile Home - Not Affixed	No
Skating Rink, Roller	Yes	Truck Stop	Yes
Snack Bar	Yes	Underground Parking Structure	Yes
Stable	Yes	Veterinary Hospital	Yes
Stable, High-value	Yes	Visitor Center	Yes
Storage Garage	No	Vocational School	Yes
Storage Hangar	Yes	Warehouse Food Store	Yes

Non-residential Parcel Type	AC	Non-residential Parcel Type	AC
Supermarket	Yes	Warehouse Showroom Store	Yes
T-Hangar	Yes		

APPENDIX C

SELECTION OF CORRIDORS IN THE SIMULATION

Minimum link flow	Corridors Cooled Length (kilometers)
1	35495.6
75	7036.79
89	5995.95
106	4976.78
129	3984.93
162	3000.2
218	2007
264	1497.6
337	998.2
480	495.8517
530	402.6022
610	302.544
740	198.1815
990	100.3986
1140	74.87057
1350	49.67661
1710	24.81074
1860	19.91349
2150	14.97153
2310	10.28418
2700	4.988248
3950	1.010235
4810	0.089709

7030	0.026387